Earth-Science Reviews 212 (2021) 103444

Contents lists available at ScienceDirect

Earth-Science Reviews

journal homepage: www.elsevier.com/locate/earscirev

Review Article

Tracing volcanic emissions from the Central Atlantic Magmatic Province in the sedimentary record

Sofie Lindström [a,*], Sara Callegaro [b], Joshua Davies [c], Christian Tegner [d], Bas van de Schootbrugge [e], Gunver K. Pedersen [a], Nasrrddine Youbi [f,g,h], Hamed Sanei [d], Andrea Marzoli [b]

[a] Stratigraphy Department, Geological Survey of Denmark and Greenland, Øster Voldgade 10, DK-1350 Copenhagen K, Denmark
[b] Department of Land, Environment, Agriculture and Forestry, University of Padova, via dell'Università 16, 35020 Legnaro, Italy
[c] Département des Sciences de la Terre et de l'Atmosphère, Université du Québec à Montréal, Montréal, QC H2X3Y7, Canada
[d] Department of Geoscience, Aarhus University, Hoegh-Guldbergs Gade 2, DK-8000 Aarhus C, Denmark
[e] Department of Earth Sciences, Marine Palynology and Paleoceanography, Utrecht University, Princetonlaan 8, 3584 CB Utrecht, the Netherlands
[f] Department of Geology, Faculty of Sciences-Semlalia, Cadi Ayyad University, Marrakesh, Morocco
[g] Mohammed VI Polytechnic University, Geology and Sustainable Mining Department, Ben Guerir 43150, Morocco
[h] Faculty of Geology and Geography, Tomsk State University, Tomsk, Russia

ARTICLE INFO

Keywords:
Triassic–Jurassic boundary
Volcanism
C-isotope
Mercury
Iridium
PAH

ABSTRACT

The end-Triassic mass extinction (ETME) is thought to have been caused by voluminous, pulsed volcanic activity of the Central Atlantic Magmatic Province (CAMP). Over the last decades, various geochemical signals and proxy records, including $\delta^{13}C$, pCO_2, iridium and other platinum-group elements, mercury, polycyclic aromatic hydrocarbons (PAH), charcoal and SO_2, have been directly or indirectly attributed to CAMP magmatism. Here, we compile these various records in a stratigraphic framework to present a cohesive chain of events for the CAMP and the end-Triassic mass extinction. Mercury and iridium anomalies in sediments indicate that CAMP activity commenced prior to the onset of the marine extinctions (as marked by the last occurrence of the Triassic ammonoid *Choristoceras marshi* or closely related species), and a negative $\delta^{13}C$ excursion in organic matter (the Marshi CIE). This CIE may be explained by input of light carbon to the atmosphere from CAMP lavas of the Tiourjdal and Prevalent groups. Pedogenic carbonate below and above the Prevalent group in North America indicates a more than twofold increase in atmospheric pCO_2. Subsequent n-alkane C-isotopes, and stomatal pCO_2 data seem to indicate a temporary cooling after the Marshi CIE, which is consistent with climate models incorporating volcanic emissions of both CO_2 and SO_2. Records of excess iridium and Hg/TOC indicate intensified magmatism during the extinction interval. Tectonic and perhaps epeirogenic (i.e. doming due to rise of magma) activity is suggested by the occurrence of multiple and widespread seismites in Europe. Atmospheric pCO_2 proxies indicate global warming, which culminated contemporaneously with the Spelae CIE. Global warming is corroborated by increased wildfire activity testified by charcoal and pyrolytic PAH records. Increased isotopic ratios of Os and Sr from sections that record global ocean signatures suggest increased weathering of continental crust likely due to climatic changes. Just prior to the increase in pCO_2 from stomatal proxy data, fossil plants exhibit SO_2-induced damage indicating excess sulfur dioxide deposition priot to and across the Triassic–Jurassic boundary. At the same time, increased ratios of heavy molecular PAHs (coronene/benzo(a)pyrene) in sediments suggest metamorphism of organic sediments also occurred across the Triassic–Jurassic boundary. These proxies may suggest that thermogenic release of light carbon and sulfur from sill intrusions in the Trans-Amazonian basins, where both evaporate- and organic-rich sediments are known to have been intruded, may have played an important role during the course of the ETME. Geochemical traces of magmatism, i.e. Ir and Hg, appear to have gradually disappeared during the Hettangian, suggesting that later phases of CAMP were less voluminous. Stomatal proxy data from Greenland and n-alkane C-isotope data from the UK, together with oxygen isotope data from carbonate fossils in the UK, may indicate that the global warming at the Spelae CIE was succeeded by another short-term cooling event. A gradual decrease in $\delta^{13}C$ culminated at the top-Tilmanni CIE,

* Corresponding author.
E-mail address: sli@geus.dk (S. Lindström).

https://doi.org/10.1016/j.earscirev.2020.103444
Received 7 December 2019; Received in revised form 22 October 2020; Accepted 17 November 2020
Available online 20 November 2020

marking the beginning of a long-term steady state with more negative C-isotope values than prior to the ETME. At this time, terrestrial ecosystems appear to have stabilized globally and ammonoids had begun to rediversify.

1. Introduction

Most of the so called "Big Five" mass extinctions of the Phanerozoic have been temporally linked to cataclysmic magmatic activity (e.g. Courtillot, 1999; Wignall, 2001; Bond and Wignall, 2014; Racki et al., 2018). For both the end-Permian and end-Triassic mass extinctions, flood basalt volcanism is generally considered the main cause of the biotic crises, through massive outgassing of greenhouse gases and other volatiles. Although this causality has been advocated by many authors, the exact chain of events and tempo for each of these crises remains poorly constrained. This is partly due to difficulties in tracing activity of flood basalt volcanism in the sedimentary record. Even prior to the availability of precise and accurate high-precision geochronology, flood basalt volcanism had been widely discussed as a possible causal mechanism for the end-Triassic mass extinction (ETME) (including e.g. Hallam and Wignall, 1999; Hesselbo et al., 2002; Pálfy et al., 2000; and Tanner et al., 2004). Recent advances in geochronological dating of the end-Triassic mass extinction (ETME) and of the contemporaneous large igneous province (LIP) - the Central Atlantic Magmatic Province (CAMP) (Marzoli et al., 1999, 2018, 2019; Pálfy et al., 2000; Schoene et al., 2010; Blackburn et al., 2013; Davies et al., 2017; Heimdal et al., 2018), has greatly improved correlations between fossil and sedimentary records and volcanic activity (Lindström et al., 2017b). The CAMP was emplaced in central Pangea (Fig. 1), and its remnants are found today on the four continents: South and North America, Africa and Europe, presently surrounding the Atlantic Ocean. CAMP magmatism was of tholeiitic basaltic composition. It preceded and likely initiated the break-up of the super-continent Pangea (Peace et al., 2020). The total surface area over which CAMP magmatic rocks are found exceeds 10 million km^2, while the estimated original volume of intrusive and extrusive magmatic rocks is ~ 2–4 million km^3 (Marzoli et al., 2018). CAMP thus ranks among the most voluminous and extensive Phanerozoic LIPs (Ernst, 2014; Ernst and Youbi, 2017). CAMP rocks are mainly represented by sills intruded into shallow continental sedimentary strata of dominantly Palaeozoic to Triassic age, and by dykes intruded in Archean to Mesozoic basement rocks, while preserved lava flows are relatively rare and limited to Triassic sedimentary basins in Morocco, Canada, USA, and Brazil.

During the past decade, advances in geochronology, especially in the reduction of laboratory Pb blanks for high precision U-Pb dating, has resulted in a much better calibration of the Triassic–Jurassic boundary (TJB) age and also much more precise and accurate ages for CAMP rocks and contemporaneous volcanic ash layers (Schoene et al., 2010; Blackburn et al., 2013; Wotzlaw et al., 2014; Davies et al., 2017; Marzoli et al., 2019). The base of the Jurassic is defined by the first occurrence of the ammonoid *Psiloceras spelae tirolicum* (Hillebrandt et al., 2013; Hillebrandt and Krystyn, 2009), and the age of the TJB has been estimated at 201.36 ± 0.17 Ma (Schoene et al., 2010; Wotzlaw et al., 2014) (Fig. 2).

A sharp negative carbon-isotope excursion (CIE) registered below the TJB and coincident with the onset of the mass extinction interval, has been interpreted to reflect large scale input of CO_2 or methane to the atmosphere-ocean system due to massive magmatism in the contemporaneous large igneous province, CAMP (Pálfy et al., 2001; Ward et al., 2001; Hesselbo et al., 2002; Ruhl and Kürschner, 2011; Hillebrandt et al., 2013; Capriolo et al., 2020). An amplitude of up to 6‰ has been recorded for this CIE in both organic and inorganic C-isotope records ($\delta^{13}C$; e.g. Hesselbo et al., 2002; van de Schootbrugge et al., 2008; Korte et al., 2009; Ruhl and Kürschner, 2011; Ruhl et al., 2011). Several authors have argued that volcanic CO_2 emissions alone could not have caused the carbon isotope excursion due to the large amount of isotopically-light carbon that would be required to produce a 6‰ negative shift, and considering the typical carbon isotopic composition of basaltic magmas ($\delta^{13}C$ ca. –5‰; Pálfy et al., 2001; Beerling and Berner, 2002; Ruhl et al., 2011; Paris et al., 2012; Barry et al., 2014; Bachan and Payne, 2016). Instead, either the release of methane from clathrates (Beerling and Berner, 2002; Ruhl et al., 2011) or from sediments heated by the intruding magmas has been suggested (Davies et al., 2017; Heimdal et al., 2018, 2019, 2020).

Considerable focus regarding the extinction has been placed on assessing the degree and impact of global warming, and subsequent ocean acidification (McElwain et al., 1999; Hautmann, 2004; Berner and Beerling, 2007; van de Schootbrugge et al., 2007; Steinthorsdottir et al., 2011; Ruhl et al., 2011; Ruhl and Kürschner, 2011; Greene et al., 2012). The most negative CIE has commonly been regarded as reflecting the primary trigger of the crisis (e.g. Hesselbo et al., 2002; Guex et al., 2004; Whiteside et al., 2007; Götz et al., 2009; Ruhl et al., 2011). However, C-isotope records across the TJ-interval generally show not just one, but multiple negative shifts indicating instability in the C-cycle (e.g. Hesselbo et al., 2002; Lindström et al., 2012; Yager et al., 2017; Fujisaki et al., 2018).

Difficulties in biostratigraphic correlations, related to provincialism

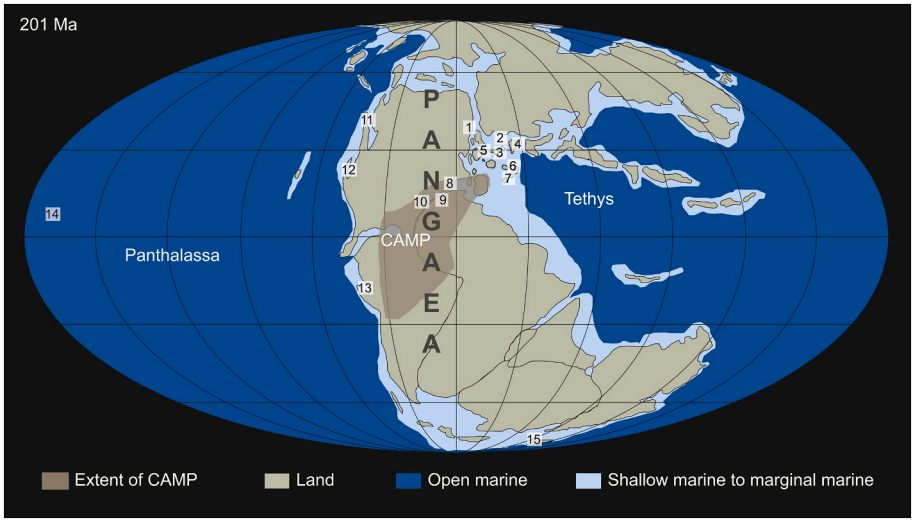

Fig. 1. Palaeogeographic map of Pangaea (after Blakey, 2014) with localities mentioned in the text: (1) Jameson Land, Greenland; (2) Danish Basin, Denmark; (3) North German Basin, Denmark and Germany; (4) Polish Trough, Poland; (5) Southwest Britain, United Kingdom; (6) Northern Calcareous Alps, Austria; (7) Csővár Basin, Hungary; (8) Fundy Basin, eastern Canada; (9) High Atlas and Argana basins, Morocco; (10) Newark Basin, USA; (11) Haida Gwaii, today located in western Canada, was during TJ-times part of the intra-oceanic terrane Wrangellia; (12) Nevada, USA; (13) Pucará Basin, Peru; (14) Southwest Japan; (15) North Island, New Zealand. The location of the Central Atlantic Magmatic Province (CAMP) is drawn after Marzoli et al. (2018).

in several fossil groups, have led many authors to rely on perturbations in the C-isotope record as a means of correlation. For decades, assessments of the timing and tempo of the ETME have been hampered by contrasting correlation and interpretation issues (see e.g. Fowell and Olsen, 1993 vs. Van Veen, 1995; Mander et al., 2008 vs. Radley et al., 2008; Whiteside et al., 2007, 2008; Marzoli et al., 2008). Several authors have pointed out that the marine invertebrate extinctions and terrestrial ecosystem changes took place prior to the most negative CIE, which was previously considered to reflect the trigger of the crisis (Bond and Wignall, 2008; Mander et al., 2008; Lindström et al., 2012, 2017b). Recently, Lindström et al. (2017b) presented a revised correlation for TJB successions, based on a combination of biostratigraphy and organic C-isotope records.

The new stratigraphic framework was based on the well-established ammonoid biostratigraphy combined with marine and terrestrial palynomorphs. The combination of biostratigraphic data including marine macrofossils, marine dinoflagellate cysts, and terrestrial spores and pollen, reduces correlation errors between successions from different types of depositional environments. Although at odds with the traditional correlation between the GSSP record at Kuhjoch and that of St. Audrie's Bay in the UK (e.g. Bonis et al., 2010b; Ruhl and Kürschner, 2011), it conclusively demonstrated that in NW Europe the marine mass extinction interval is contemporaneous with the deforestation interval of van de Schootbrugge et al. (2009). This has been further corroborated by additional chemo- and biostratigraphic studies of the Bonenburg section in Germany, in comparison with Kuhjoch and Stenlille (Schobben et al., 2019; Gravendyck et al., 2020), as well as several sections in Switzerland (Schneebeli-Hermann et al., 2017). The revised correlation clearly shows that the sharp negative CIE at St. Audrie's Bay (UK; Hesselbo et al., 2002, Bonis et al., 2010b) and the sharp negative CIE near the last occurrence of the ammonoid *Choristoceras marshi* (Hillebrandt et al., 2013) occur on either side of the mass extinction interval (for further explanation of the differences between the traditional correlation and this revised correlation see Lindström et al., 2017b). Some authors still favour the old correlation (e.g. Fujisaki et al., 2018; Korte et al., 2019), while others who use the old correlation have remained open to the fact that the new Lindström et al. (2017b) correlation may be correct (Weedon et al., 2018). The main reason for these disagreements lies solely in the correlation between the GSSP section at Kuhjoch and the NW European sections.

Here, we review evidence for the possible geochemical imprints of CAMP magmatism on the sedimentary record and their importance for understanding the global environmental effects of this large igneous province. In order to investigate such a complex scenario, which involves correlation of sedimentary successions from various types of environments, a solid stratigraphic framework is indeed necessary. For this reason, we use the revised correlation of Lindström et al. (2017b) and also include biostratigraphic information gleaned from radiolarians and conodonts (Carter and Hori, 2005; Longridge et al., 2007; Rigo et al., 2018). The biostratigraphic information is used in combination with U-Pb ages of CAMP intrusives and extrusives (Blackburn et al., 2013; Davies et al., 2017; Heimdal et al., 2018; Marzoli et al., 2019), and ash beds from sedimentary sections (Schoene et al., 2010; Wotzlaw et al., 2014) in order to calibrate in time any published geochemical records that can be used to trace magmatic emissions from the CAMP.

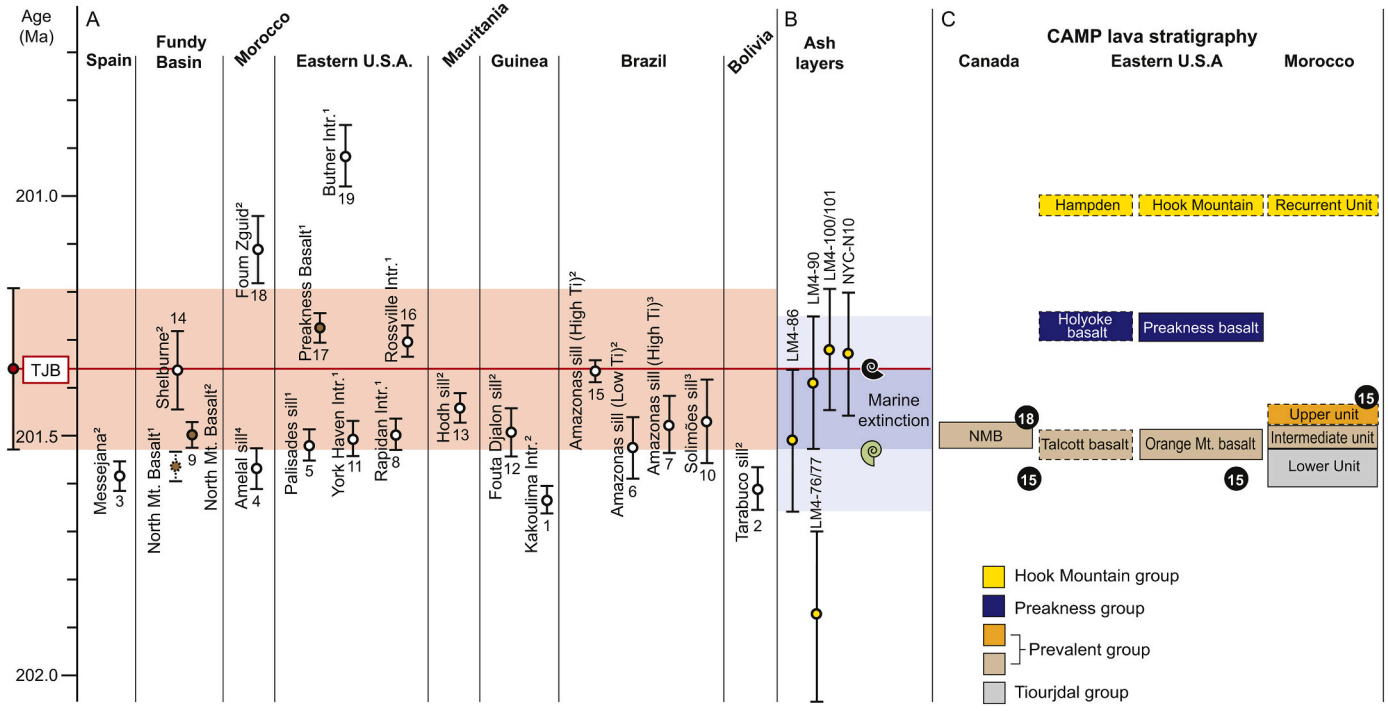

Fig. 2. A) Geochronology of CAMP intrusions (white circles) and lava flows (brown circles), after [1]Blackburn et al. (2013), [2]Davies et al. (2017), [3]Heimdal et al. (2018); [4]Marzoli et al. (2019). Ages of intrusions and lava flows, numbered 1–19, appear on Figs. 3–11. B) Geochronology of ash beds (yellow circles) from the sedimentary ammonoid bearing successions in Nevada (Schoene et al., 2010) and Pucara Basin, Peru (Schoene et al., 2010; Wotzlaw et al., 2014). Green ammonoid symbol represents the last occurrence (LO) of *Choristoceras crickmayi* and the black ammonoid symbol represents the first occurrence (FO) of *Psiloceras spelae* (Schoene et al., 2010; Wotzlaw et al., 2014). The latter defines the Triassic–Jurassic boundary (TJB), marked as a red line, estimated to 201.36±0.17 Ma by Wotzlaw et al. (2014); pink field represents the estimated error. Dark blue field marks the marine extinction interval, defined as the interval between the LO of *C. crickmayi* or *C. marshi* and the FO of *P. spelae* (Schoene et al., 2010; Hillebrandt et al., 2013). The light blue field shows the approximate maximum duration of the mass extinction interval, based on U-Pb ages of ash beds LM4-86 and LM4-90 (Schoene et al., 2010; Wotzlaw et al., 2014). C) Schematic stratigraphy of CAMP lavas, mainly after Marzoli et al. (2011). Hitherto undated units are marked by stippled boxes. Thickness (i.e. as a proxy for apparent duration) of volcanic units is only indicative. Black circles with numbers represent last occurrences of Triassic pollen taxa (shown on Fig. 3): 15) *Patinasporites densus,* and 18) *Lunatisporites rhaeticus,* after Cirilli et al. (2009) and Panfili et al. (2019). A complete list of all the biostratigraphic events used on Figs. 2–10 can be found on Fig. 7.

2. The Late Triassic world and the formation and age of the Central Atlantic Magmatic Province

During the Triassic the vast majority of the continental masses had merged to form Pangaea, a supercontinent that stretched almost from pole to pole (Fig. 1). The Panthalassic Ocean covered half of the globe to the west, with the Tethys Ocean intersecting equatorial Pangaea from the east (Fig. 1). In the wake of the end-Permian extinction large parts of continental Pangaea were subjected to harsh arid to semi-arid conditions, which persisted during much of the Early to Late Triassic (Preto et al., 2010), with only brief interruptions to more humid conditions, e.g. the Carnian Pluvial Event (Dal Corso et al., 2018). In NW Europe, an amelioration of the climate appears to have taken place during the Late Triassic, when step-wise sea level rise led to connections to the Tethys Ocean (Manspeizer, 1994; Ahlberg et al., 2002).

During this time, rift basins formed between northwestern Africa and eastern North America as these land masses started to drift apart during the Late Permian–Middle Triassic. Rifts in eastern Canada and Morocco propagated southward and northward, respectively, for >35 Myr (Medina, 1995; Leleu et al., 2016). Rifting and sedimentation continued until the end-Triassic and eruption of CAMP basaltic lava flows. This would suggest a syn-extensional volcanism and would be consistent with McHone (2000) who ruled out a simple mantle plume origin for the CAMP, based on geochemical and geological data. However, other authors have suggested that erosional truncation of the sedimentary basins in the southern Central Atlantic during the Carnian–Norian indicate crustal uplift related to mantle plume arrival focused underneath the southern tip of Florida (Ruiz-Martinez et al., 2012; Leleu et al., 2016).

The most voluminous CAMP sills occur in northern Brazil in the Trans-Amazonian basins (Davies et al., 2017; Heimdal et al., 2018) and in northwestern Africa e.g., Mali, and Guinea (Bertrand, 1991; Verati et al., 2005; Davies et al., 2017). The volume of the Brazilian shallow sills is estimated at >1 million km^3 (De Min et al., 2003; Svensen et al., 2017). Huge CAMP dykes can reach lengths of up to 500 km and widths of up to 300 m, while swarms of smaller but densely spaced dykes are known for example from Mali, Brazil, and the eastern USA. Preserved lava flows are relatively rare and are presently restricted to Triassic–Jurassic continental sedimentary basins, e.g., in Portugal, Canada, USA, Morocco, Algeria, Brazil and Bolivia (Nomade et al., 2007; Vérati et al., 2007; Martins et al., 2008; Bertrand et al., 2014; Callegaro et al., 2014a; Merle et al., 2011, 2014; Marzoli et al., 2019; Tegner et al., 2020a), where the volcanic piles do not exceed 500 m of cumulative thickness. CAMP lavas were mostly erupted sub-aerially or occasionally within shallow lakes or lagoons and are intercalated with sediments ranging in age from Rhaetian to Hettangian (Youbi et al., 2003; Marzoli et al., 2004, 2019; Cirilli et al., 2009; Panfili et al., 2019). Preserved pyroclastic (e.g., tuffs) CAMP rocks are extremely rare, which is quite anomalous compared to other large igneous provinces (Ross et al., 2005; White et al., 2009).

The origin of the CAMP is controversial. Several studies, (e.g. Merle et al., 2011, 2014; Callegaro et al., 2013, 2014a, 2017) have shown that the mantle source of the CAMP is dominated by shallow mantle components, which may mask the contribution from a mantle plume. High-precision U-Pb geochronological data indicate a near-synchronous onset of CAMP magmatism over a distance of several thousand km (e.g. from France to Bolivia) (Marzoli et al., 2019; Blackburn et al., 2013; Schoene et al., 2010; Davies et al., 2017; Heimdal et al., 2018). Moreover, modelling of mantle melting dynamics suggest that the potential temperature was moderately elevated (ca. 100°C above ambient mantle). Melting took place in the convecting mantle that was contaminated by sediments that were introduced into the mantle during subduction associated with the assembly of Pangaea (Herzberg and Gazel, 2009; Merle et al., 2011, 2014; Callegaro et al., 2013, 2014, 2017; Hole, 2015; Marzoli et al., 2019; Tegner et al., 2020a). The corollary of this is that most CAMP magmatism may be explained by the arrival of a mantle plume or by heat incubation underneath Pangaea (Coltice et al., 2007). This triggered melting over a large area. Convecting, contaminated mantle magma impinging the Pangaean lithosphere appears to have been the dominant source of molten material.

Radio-isotopic ages of CAMP rocks have been determined by $^{40}Ar/^{39}Ar$ analyses of plagioclase and, more recently, by U-Pb zircon and baddeleyite geochronology (e.g. Dunning and Hodych, 1990; Hodych and Dunning, 1992; Nomade et al., 2007; Vérati et al., 2007; Marzoli et al., 2011; Blackburn et al., 2013; Davies et al., 2017; Callegaro et al., 2017; Marzoli et al., 2019). In general, the U-Pb geochronological data for CAMP magmatism range between ca. 201.6 to 201.0 Ma, however Ar/Ar data suggest a longer range extending into the Sinemurian, ca. 195-192 Ma, although these younger ages may be inaccurate and should be interpreted with caution before they are confirmed by U-Pb techniques (Marzoli et al., 1999; Marzoli et al., 2011). The oldest measured age (U-Pb, 201.635 ± 0.029 Ma) has been recorded from an intrusive suite from northwestern Africa (Kakoulima intrusion in Guinea), which is older than the last occurrences of typical Triassic ammonoids that mark the onset of the marine mass extinction interval (Schoene et al., 2010; Wotzlaw et al., 2014; Davies et al., 2017; Lindström et al., 2017b) (Fig. 2). It should be noted that the samples dated by U-Pb techniques are mostly intrusive rocks where the presence of zircon is more frequent than in extrusive rocks. U-Pb ages for most CAMP rocks overlap with the estimated age of the onset of the marine mass extinction, which must have occurred prior to 201.51±0.15 Ma (Schoene et al., 2010; Wotzlaw et al., 2014), and was estimated to 201.564 Ma by Blackburn et al., 2013) (Fig. 2). Importantly, U-Pb ages for sills in the Trans-Amazonian basin also range in age from the Marshi CIE to the TJB (Davies et al., 2017; Heimdal et al., 2018) (Fig. 2). The Trans-Amazonian basin contains thick successions of organic-rich sediments and evaporite deposits and experienced a major hydrocarbon generation and migration event as a result of extensive contact metamorphism during sill emplacement (Heimdal et al., 2018, 2019). Therefore, since the sill emplacement into this basin is synchronous with the extinction interval, release of thermogenic gases generated by contact metamorphism could have contributed to climate change which led to the ETME (Davies et al., 2017; Heimdal et al., 2018, 2019).

3. Stratigraphy of CAMP rocks

Combined major and trace element data and Sr-Nd-Pb isotopic compositions suggest that CAMP basaltic lava flows, dykes and sills can be subdivided into six main groups (Marzoli et al., 2018). It should, however, be considered that it is not always easy to geochemically correlate lava flows and intrusive rocks, as the latter may have compositions controlled by mineral accumulation. The six groups of CAMP igneous rocks are the following:

1. The Tiourjdal group (after the locality in Morocco where the volcanic succession is thickest) includes the Lower Unit flows from Morocco and Algeria, a few lava flows from Canada (Fundy Basin), and some dykes and sills from northern Africa. The Tiourjdal group is formed by the oldest preserved lava flows from Africa and North America. According to Marzoli et al. (2019), one sample from this group yielded a U-Pb zircon age of 201.57 ± 0.04 Ma.
2. The Prevalent group includes the Moroccan Intermediate and Upper Unit flows, all flows from Portugal, the Orange Mountain Basalts from the Newark Basin (including its stratigraphically equivalent flows from Virginia to Connecticut; cf. Weems et al., 2016), most of the North Mountain Basalt flows (Nova Scotia, Fundy basin) and nearly all South American CAMP flows (Bolivia, Brazil). Most dykes from Africa and some from northeastern North America (New England to Canada) belong to this group. Lava flows and intrusions of this group have ages (201.61 ± 0.05 to 201.44 ± 0.04 Ma; Blackburn et al., 2013; Davies et al., 2017), which are indistinguishable from those of the Tiourjdal group, suggesting a near-synchronous eruption of the Tiourjdal and Prevalent group. However, in Morocco the

volcano-stratigraphy indicates that the Tiourjdal group was emplaced before the Prevalent group (Marzoli et al., 2019).

3. The Preakness group includes the Preakness flows and the stratigraphically equivalent flows from the nearby basins in the United States and their feeder dykes and sills. These rocks have yielded U-Pb ages of 201.31 ± 0.03 and 201.27 ± 0.03 Ma (Blackburn et al., 2013). An age difference of about 0.2 Myr between the Prevalent and the Preakness group is consistent with cyclostratigraphic studies for the Newark Basin (Olsen et al., 2003).
4. The Hook Mountain group is composed of the Moroccan Recurrent lava flows, and the Hook Mountain and Hampden basaltic flows from the northeastern U.S.A. (Newark and Hartford basins, respectively) and their feeder dykes. Field evidence and cyclostratigraphy indicates that this group follows the Prevalent and Preakness groups by about 0.4 Myr (Olsen et al., 2002; Panfili et al., 2019), however, U-Pb ages are missing for these rocks. Blackburn et al. (2013) claimed that the Butner sill (North Carolina; 200.92 ± 0.02 Ma) may be equivalent to the Hook Mt. flows, yet this is not consistent with geochemical data, in particular with isotopic compositions (Callegaro et al., 2013; Merle et al., 2014; Marzoli et al., 2018). The age of the Butner Sill is, however, consistent with the cyclostratigraphic constraints.
5. The Carolina group consists of dykes from the southeastern United States (Georgia to Virginia). No U-Pb age is available for these dykes and geochemical correlations with lava flows from the Newark basin are not straightforward.

The high-Ti group ($TiO_2 > 2.0$ wt.% in the basaltic rocks) includes lava flows from the Parnaiba basin (Brazil) and dykes and sills from Liberia, French Guiana, Suriname, and north-eastern Brazil. One high-Ti sill sample from the Trans-Amazonian basin was dated by Davies et al. (2017) and yielded an age of 201.36 ± 0.02 Ma.

4. Volatile release from the CAMP

In large enough quantities, the emission of volcanic volatiles, chiefly water vapor, carbon dioxide, sulfur dioxide, and halogens and their compounds, not only alters global atmospheric chemistry, but also influences radiative forcing (e.g. Von Glasow et al., 2009). Historical observations of climate effects caused by large eruptions, e.g. from Laki in 1783-84 to Pinatubo in 1991 (Robock, 2002; Thordarson and Self, 2003) forced by volcanogenic degassing, support the hypothesis that gas release from the CAMP was likely the driving force for the strong and global upheavals affecting the environment at the TJ-transition. However, few quantitative constraints exist for volcanogenic degassing from CAMP and other LIPs. This is due to the extreme challenges of quantifying volatiles from old, potentially altered and often variably degassed volcanic rocks. Three important aspects should be considered when addressing the problem of degassing both from the CAMP, and LIPs in general (Ernst and Youbi, 2017): 1) the proportion of the degassed species and their atmospheric effects, 2) the height at which gases are injected, and 3) the volume of released volatiles.

4.1. Degassed compounds and elements

4.1.1. Carbon

Volcanic activity releases large amounts of carbon to the atmosphere, both directly through volcanic emissions, and indirectly through thermogenic gas formation when magma intrudes sedimentary rocks (e.g. Heimdal et al., 2020 and references therein). The greenhouse gas CO_2 is one of the most common greenhouse gases emitted by volcanism, and it has a long residence time in the atmosphere, up to several thousands of years (e.g. Archer, 2005 and references therein). CO_2 emission from LIP volcanism was estimated at ca. 3000 Megatons per year for the Siberian Traps at the Permian-Triassic boundary (Black and Gibson, 2019). A recent study suggests that CAMP magmas may have emitted about 10^5 Gigatons CO_2 in total corresponding to maximum CO_2 emissions of about 7 Gt per year during the main volcanic pulses (Capriolo et al., 2020). For such degassing rates, CAMP volcanic pulses may have increased the global temperature by more than 4 °C (Landwehrs et al., 2020) suggesting that CAMP volcanism may have triggered the disruption of the global end-Triassic carbon cycle.

Methane (CH_4) is a potent greenhouse agent, but commonly constitutes a minor portion of direct emissions from volcanoes, and when released from volcanic vents it is readily oxidized to CO_2. In addition to direct volcanic release, contact metamorphism of organic-rich sediments in aureoles surrounding sill intrusions in organic-rich sedimentary basins are thought to release remarkable amounts of CO_2 and CH_4 (Svensen et al., 2004). This mechanism offers an alternative explanation to negative CIEs, including those at the TJB (Hesselbo et al., 2002; Ruhl and Kürschner, 2011; Ruhl et al., 2011), that does not involve the destabilization of gas hydrates buried in marine sediments as purveyors of light carbon (Dickens et al., 1995), a mechanism with limited possibilities of detection in the sedimentary record and so far undetected in the end-Triassic geologic record. Thermogenic gas can be generated from a metamorphic aureole up to 2.5 times thicker than the sill, depending on several factors, and can occur on time-scales of 10–1000 years (Aarnes et al., 2010), i.e. shortly after sill emplacement.

This process is particularly significant when volatile-rich sediments are intruded, such as shales, evaporites, limestones or coal, and particularly when mature hydrocarbons are already present in the series. Extensive CAMP sills are known to have intruded the $>10^6$ km^2 large Amazonas and Solimões basins in northern Brazil (De Min et al., 2003; Wanderley Filho et al., 2006; Heimdal et al., 2018), where the sedimentary succession consists predominantly of Paleozoic sediments, including black shales with high total organic carbon concentrations, sandstones, carbonates, and evaporites, as well as hydrocarbons, potentially already mature at the time of CAMP sill emplacement (Gonzaga et al., 2000). Numerical modelling quantifying carbon released from the Amazonas and Solimões basins has been presented by Heimdal et al. (2018, 2020) and may serve as a valuable constraint to paleoclimatic reconstructions and biogeochemical modeling. Notably, vent structures that are explained as the result of thermogenic gas migration have been observed around sills of other LIPs (e.g. the Karoo and Siberian Traps LIPs; Svensen et al., 2004, 2007, 2009; Ganino and Arndt, 2009), and are hypothesized for the CAMP (Svensen et al., 2009; Heimdal et al., 2018), but have yet to be observed, possibly due to forest and soil cover.

4.1.2. Sulfur

Basaltic volcanism is known to be capable of releasing significant amounts of sulfur dioxide both from direct and thermogenic degassing (Self et al., 2008; Callegaro et al., 2014b; Jones et al., 2016; Iacono-Marziano et al., 2017). However, the role of SO_2 as an agent of environmental change during mass extinctions has been discussed in connection with the Siberian Traps (Maruoka et al., 2003; Visscher et al., 2004), CAMP volcanism (Guex et al., 2004; van de Schootbrugge et al., 2009; Lindström et al., 2012; Callegaro et al., 2014b; Steinthorsdottir et al., 2018) and the Deccan Traps (Self et al., 2006). Since the magmatic fingerprint is not resolvable using sulfur isotopes in sedimentary records (Newton and Bottrell, 2007), the atmospheric injection of sulfur from the CAMP cannot easily be traced. Sulfur is readily oxidized by the atmosphere and has different impacts and residence times depending on the height at which it is emplaced, either tropospheric or stratospheric (Robock, 2000; Oppenheimer et al., 2011). Sulfur compounds do not reside long in the troposphere (only up to a few weeks), due to transformations to sulfuric acid (H_2SO_4), which is soluble in water and thus readily removed through precipitation. Such acid fallout (pH ~2–3 as calculated by Black et al. (2014) for the Siberian Traps) may be responsible for local poisoning of continental ecosystems and immediate damage to vegetation.

Sulfur residence times in the stratosphere is longer than in the troposphere, up to several years (Robock, 2000), thus stratospheric sulfur injection would likely have a global impact. This large scale

impact has been demonstrated for historical eruptions (Grattan and Pyatt, 1999; Grattan, 2005) where formation of a global sulfate aerosol cloud capable of reflecting the incoming solar radiation (higher albedo), leading to a net cooling of the troposphere and heating of the stratosphere (the so-called volcanic winter; Rampino et al., 1988), has been demonstrated. Therefore, some authors have hypothesized that reduced incoming solar radiation, cooling, and acid rain were major factors triggering a marine ecosystem collapse at the TJB (Guex et al., 2004; Schaltegger et al., 2008; van de Schootbrugge et al., 2009; Lindström et al., 2012). Such a scenario appears to be supported by high $\delta^{18}O$ values measured in oysters from UK sections following the sharp negative CIE (Korte et al., 2009; Clemence et al., 2010), considered to indicate a temperature drop at this time. However, this interpretation is complicated by the fact that the positive C-isotope interval precedes the sharp negative CIE in the UK records (Korte et al., 2009; Clemence et al., 2010), and although it is associated with a depauperate marine fauna, it postdates the extinction, and occurs during an interval where the terrestrial flora was already starting to recover (Mander et al., 2008; Lindström et al., 2012). In addition, others have suggested that the climatic impact of SO_2 release was rather limited, because of very little evidence for cooling associated with the ETME, and with mass extinction events in general (e.g. Wignall, 2001).

Schmidt et al. (2016) modelled the atmospheric response to volcanogenic injections of sulfur, demonstrating that sulfur loads compatible with those estimated for the Deccan Traps would only cause environmental stress if eruption rates were sustained and long-lived. For CAMP, studies of physical volcanology for extrusive sequences from geographically widespread locations such as the Fundy Basin in Canada, Algarve in Portugal, and the Argana Basin in Morocco have demonstrated that emplacement of CAMP lava fields occurred in multiple eruptive pulses (Kontak, 2008; Martins et al., 2008; El Hachimi et al., 2011). Each pulse was composed of several sustained eruptions, likely accompanied by fire-fountaining explosive activity, and apparently not interrupted by long volcanic hiatuses (Self et al., 2014; Brown and Lesher, 2014; Marzoli et al., 2019). SO_2 emissions from such short-lived, intense volcanic pulses may have induced short-lived temperature drops of up to 5-6 °C (Landwehrs et al., 2020). The sulfur degassed by the CAMP might not have been exclusively magmatic, but also thermogenic, i.e. derived from sediments in contact with CAMP basalts. Iacono-Marziano et al. (2017) demonstrated experimentally that contact metamorphism of evaporites can lead to sulfur transfer into picritic melts. Evaporitic sequences in Brazil intruded by CAMP sills might have served as significant additional sources of sulfur, although the occurrence and magnitude of this phenomenon is so far totally unaddressed for the CAMP.

4.1.3. Halogens

Despite their much lower concentration in volcanic systems compared to water, carbon or sulfur, halogens (chiefly Cl, F and Br; Aiuppa et al., 2009) can play a role in environmental disruption. Halogens participate in complex radical reactions within the troposphere and are responsible for ozone depletion in the stratosphere (cf. Von Glasow et al., 2009). Again, along with a primary magmatic origin, a secondary (perhaps predominant) source of halogens is contact metamorphism, particularly of evaporitic sediments (Svensen et al., 2009). Halocarbons such as methyl chloride (CH_3Cl), methyl bromide (CH_3Br), chloromethane and ethyl halides are generated during contact metamorphism, when natural evaporite samples are heated up to 275°C or higher. For the end-Permian crisis, halocarbon induced ozone layer depletion and increased UVB-radiation have been suggested as an explanation for mutations in plant spores and pollen (Visscher et al., 2004; Benca et al., 2018). By subjecting extant pine plants to increased levels of UVB radiation, Benca et al. (2018) reproduced the different forms of malformed pollen registered during the end-Permian crisis. The presence of evaporitic sediments intruded by CAMP sills in Brazilian basins suggests that the CAMP intrusions could have produced methyl halides by contact metamorphism (Heimdal et al., 2019). Recently, Lindström et al. (2019) reported high abundances of mutated fern spores from TJB sediments in the Danish and North German basins. In contrast to the mutations registered at the Permian-Triassic boundary (Benca et al., 2018), the TJB data showed no significant mutations to bisaccate gymnosperm pollen, therefore mercury toxicity was instead suggested as the cause for the spore malformations (Lindström et al., 2019). Further studies are needed to evaluate whether ozone layer depletion contributed to the extinction of end-Triassic flora and fauna.

4.2. Importance of injection height and atmospheric circulation patterns

The atmospheric response following volcanogenic gas release depends on whether the gasses were emitted to the troposphere or the stratosphere. This is particularly true for sulfur (e.g. Jones et al., 2016). The maximum impact is obtained when a volcanic plume reaches the stratosphere, which today lies at an altitude of ca.10 km, depending on latitude. Eruptive style plays an important role in the height of the eruptive column (Ernst and Youbi, 2017). Strongly explosive eruptions can penetrate the stratosphere and have an immediate and long-lasting effect on its chemistry and the climate. Quiescent degassing from volcanic vents or lava flows is instead merely tropospheric, where the more effective oxidation and the occurrence of precipitation can readily remove gas species like sulfur or chlorine.

The altitude of the tropopause above CAMP, which was emplaced across the equator (Knight et al., 2004), is estimated at around 14 km (Holton et al., 1995). Volcanological studies of CAMP lava piles (Martins et al., 2008; El Hachimi et al., 2011), the lack of thick tephra layers, ignimbrite deposits or acid volcanics suggest that the CAMP was not emplaced through highly explosive eruptions. Rather, basaltic fissure eruptions formed vast lava fields. Perhaps, as a basaltic fissure eruption epitome, Laki 1783-84 (Iceland) can be used as the closest modern analogue for the CAMP eruptions, although potentially on a smaller scale (Self et al., 2014; Marzoli et al., 2019).

Continental flood basalt eruptions emplace lava volumes of 10^3–10^4 km^3 at mean eruption rates of tens up to hundreds km^3/yr (calculated for the Columbia River Basalts, the Deccan Traps, and the CAMP; Self et al., 2006, 2008; Chenet et al., 2008; Marzoli et al., 2019), while the Laki eruption emplaced ca. 15 km^3 of basalt in 8 months (23 km^3/yr), with eruption columns reaching up to 9–13 km (Thordarson and Self, 2003). The amount of heat dispersed by large basaltic lava fields generates penetrative convection in the atmosphere, producing a thick hot mixed atmospheric layer in a few hours (Kaminski et al., 2011). The buoyancy of such a layer allows efficient transfer of volcanic gases to the stratosphere. Hence, despite not being explosive in style, CAMP eruptions may still have had the potential to burden the end-Triassic stratosphere with their discharged gases.

It is also important to consider the location of the eruptions with respect to atmospheric circulation patterns. The supraregional distribution of volcanic gases from the Laki fissure eruptions (1783–84), and recent air traffic disruptions due to volcanic eruptions on Iceland (Eyjafjallajökull volcano in 2010, Grimsvotn volcano in 2011), can be explained by an anticyclonic circulation pattern (Grattan, 2005). A low-pressure zone known as the Icelandic Depression is a dominant driving force of the tropospheric circulation over Greenland and Europe (Chenet et al., 2005). Volcanic gases that are injected in the heart of this low-pressure zone will be rapidly distributed to the upper troposphere/lower stratosphere (Chenet et al., 2005), and later drawn down in a high pressure cell and efficiently transported and distributed to the surface (Grattan, 2005), demonstrating the importance of the atmospheric circulation patterns. The paleogeographic position places the central parts of the CAMP straddling the equator (Fig. 1). Thus, volcanic emissions would have been injected into the equatorial low-pressure belt, reaching heights of 10-15 km and being distributed northwards and southwards in the Hadley cells to the mid latitudinal high pressure zones.

4.3. Volumes of gas output

Assessing the volume of gas output from the CAMP includes quantification of the original magmatic gas load and of degassing efficiency, as well as a study of the gases released from contact metamorphism. Quantifying the volatile budget in primitive CAMP melts is not an easy task, given the challenge to obtain high quality data for S, H, C, F and Cl from old, largely degassed, frequently slightly altered basaltic rocks and by the lack of primitive melt inclusions from CAMP samples.

The only comprehensive dataset published to date was compiled by Grossman et al. (1991) from the bulk-rock analyses of S, H_2O^+ CO_2, F and Cl from hundreds of samples of CAMP dykes and sills from Eastern North America. McHone (2003) interpreted these data as good estimations of the pristine content of volatiles in CAMP magmas. However, volatile element concentrations can be modified by secondary processes, and initial degassing may start within shallow crustal magma chambers such as those represented by the intrusive rocks analyzed by Grossman et al. (1991). These analyses set the basis for McHone (2003) to calculate the total budget of volatiles released by CAMP. Combined with the estimated volumes of CAMP lavas, McHone (2003) suggested that the total amount of CO_2 emitted from the volcanism was $5.19x10^{12}$ metric tons. He further estimated that the total sulfur emissions of the CAMP were $2.31x10^{12}$ metric tons, fluorine $1.11x10^{12}$ and chlorine $1.58x10^{12}$ metric tons (McHone, 2003). Since no lava flows were analyzed, McHone (2003) assumed a conservative degassing rate for the CAMP, compatible with those calculated for the Columbia River Basalts (Thordardson and Self, 1996) and the Laki fissure eruption (Thordardson et al., 2003), i.e. 70% of S, CO_2 and H_2O released and 50% F and Cl released. Notably, one glass shard from a Moroccan lava flow was found to contain ca. 1 ppm (virtually zero) S by Callegaro et al. (2014b), showing that in some cases sulfur degassing from CAMP might have reached a >90% efficiency. However, the available data are so far too limited to discuss these details conclusively.

For carbon, conservative estimates of magmatic degassing from the CAMP, i.e. not taking into account interaction with the sediments intruded by the volcanics or release of methane hydrates from shallow marine sediments, are around 8000 Gt of CO_2 (Beerling and Berner, 2002). The $\delta^{13}C$ signature of magmatic carbon (i.e. released from the mantle) is assumed to be close ca. -6 ± 2‰ VPDB (Gerlach and Taylor, 1990). It should be noted, however, that direct quantitative and isotopic carbon data are lacking for CAMP magmas, and for LIP magmas in general (Saunders et al., 2005), due to the tendency of carbon to readily exsolve from basaltic melt as a CO_2 gas phase early in the emplacement history of a magma (i.e. at depth; Edmonds and Wallace, 2017). A recent study by Capriolo et al. (2020) detected CO_2-bearing bubbles included in melt inclusions from CAMP clinopyroxenes crystallized in the intermediate crust. Such CO_2 is of deep magmatic origin, i.e. not related to heating and degassing of shallow sedimentary basins. As previously mentioned, a study by Capriolo et al. (2020) suggests that the average CO_2 concentration in CAMP basalts should be ca. 0.5 wt.%, leading to global CO_2 degassing at rates of about 7 Gigatons/year during peak activity of CAMP and a total of 10^5 Gigatons CO_2 during the entire CAMP activity.

Interpretation of the CIEs and stomatal index data suggests that the carbon degassed during the CAMP event was not solely magmatic (Beerling and Berner, 2002). Modelling indicates that a CAMP-related negative CIE up to ~ 6‰ could be achieved by the release in repeated pulses of volcanic CO_2 if its isotopic signature was significantly light ($\delta^{13}C$ –20‰; Paris et al., 2016), but as addressed above, CAMP basalts are (supposedly) isotopically too heavy to be solely responsible for the negative CIEs observed in end-Triassic sedimentary sequences. This calculation calls for an additional source of isotopically light carbon and can be seen as an indirect evidence in support of CAMP-driven isotopically light thermogenic methane release ($\delta^{13}C$ ca. –35‰ to –50‰; Svensen et al., 2004) from organic-rich sediments of e.g. the Amazon and Solimões basins in Brazil (Heimdal et al., 2018, 2019).

Quantitative data for volcanogenic sulfur emissions from several LIPs are based on in situ analyses of sulfur contained in melt inclusions (e.g. for Siberian Traps, Deccan Traps, Etendeka, Columbia River Basalt, Emeishan; cf. Thordarson and Self, 1996; Blake et al., 2010; Self et al., 2008; Black et al., 2012; Zhang et al., 2013; Marks et al., 2014; Sibik et al., 2015). Analysis of sulfur concentrations in CAMP clinopyroxenes (cpx) has been used by Callegaro et al. (2014b) to calculate the sulfur concentration in the melts from which they crystallized, by application of a cpx/melt sulfur partition coefficient. According to these calculations, CAMP melts were rich in sulfur, i.e. sulfide saturated. Near-anhydrous basaltic melts at low oxygen fugacity (around FMQ buffer) reach sulfide saturation at ca. 2000 ppm S. Such sulfur concentrations are reasonable for continental flood basalts, and similar to those found for Deccan Traps magmatism by melt inclusion analyses (Self et al., 2008). According to Callegaro et al. (2014b) CAMP flows were able to release up to 8 Mt per km^3 of volcanogenic SO_2 (assuming a ca. 90% degassing efficiency). Simply multiplying this by the total estimated volume ($2–4x10^6$ km^3, Svensen et al., 2017; Marzoli et al., 2018), results in a release of $16–32x10^{12}$ metric tons of SO_2 by the CAMP. The $4.62x10^{12}$ metric tons of SO_2 estimation by McHone (2003) is more conservative, which is not surprising since a) McHone (2003) calculations are based on analyses of whole rocks that may have suffered degassing and b) Callegaro et al. (2014b) calculate the S concentration in CAMP melts at the time of augite crystallization, i.e. early in their emplacement history, at 1000–1200°C and around 10–15 kbar. Furthermore, this simple calculation does not take into account that CAMP magmatic activity was not entirely composed by lava flows, thus degassing efficiency was most probably not uniform.

A third, significantly larger estimate of ~$210x10^{12}$ metric tons of SO_2 released by the CAMP is proposed by Guex et al. (2016) based on a model where melting of sulfide-rich metasomatized cratonic lithosphere occurs. Assuming that only 20% of this lithospheric sulfur is released to the atmosphere during a period of 100 kyr, a flux of 410 metric tons SO_2/yr is calculated for CAMP, which would be capable, if sustained, to trigger a biotic crisis (Schmidt et al., 2016).

All these estimates only consider magmatic degassing, while, similar to other large igneous provinces, volcanic degassing from the CAMP may have been exacerbated by metamorphic processes when the rising magma intruded volatile-rich bedrocks (Svensen et al., 2009, 2015; Aarnes et al., 2010; Heimdal et al., 2018, 2019).

5. Correlating CAMP to the sedimentary record

The lack of direct evidence of CAMP activity in the form of distal ash beds outside the CAMP area hampers detailed correlation between individual eruptive phases and the biotic record. Despite the improved geochronology of the CAMP, there are still controversies regarding the correlation between the volcanic/igneous activity and the mass extinction. The samples dated by U-Pb technique are mostly from intrusives and although, as previously discussed, intrusive activity may have played an important role in the ETME, such a connection remains speculative. Therefore, the age of CAMP volcanism relative to the end-Triassic extinction and CIE hinges on biostratigraphic, chemostratigraphic, and magnetostratigraphic studies, and improved calibration of the geological timescale that allows better use of CAMP U-Pb ages.

5.1. Biostratigraphic framework of the TJ-boundary interval

Establishing a biostratigraphic framework for the interval spanning the TJB is complicated and involves several fossil groups from various settings. As with all biostratigraphy, there is always some uncertainty whether the first or last occurrence of a specific taxon in a succession actually represent the first or last appearance datum of that taxon in time. This is especially true for successions where major facies changes coincide with faunal or floral turnovers, which is the case for several ETME successions. Here, we attempt to integrate marine and terrestrial

biostratigraphic events and zones, because this helps to overcome specific correlation issues, and draws attention to areas with major uncertainties.

Terrestrial TJB sections have primarily been dated by spores and pollen, macrofossil plant remains, and vertebrate or ichnofossils (e.g. Lund, 1977; Fowell and Olsen, 1993; Olsen et al., 2002; McElwain et al., 2007; and references therein). Various marine fossils are used depending on abundance, but the most common groups used at the TJB are ammonoids and radiolarians. In addition, conodonts are useful in Upper Triassic marine successions. Marine dinoflagellate cysts can also be useful, as several taxa become extinct during the ETME. The advantage of palynology is that in marine to marginal marine settings, dinoflagellate cysts occur together with terrestrial spores and pollen, and therefore palynology is the only discipline that can be used to correlate between marine and terrestrial zonations. Important biostratigraphic events within different fossil groups are briefly reviewed below and are marked on Fig. 3.

5.1.1. Ammonoids

The ammonoids are important markers for the TJB (e.g. Hillebrandt, 2000a–c; Guex et al., 2004, 2012; Schaltegger et al., 2008; Hillebrandt and Krystyn, 2009; Page et al., 2010; Schoene et al., 2010; Hillebrandt et al., 2013; Wotzlaw et al., 2014; Hillebrandt and Kment, 2015). The GSSP for the base of the Jurassic system is located at Kuhjoch in the Karwendel Mountains in the Northern Calcareous Alps, Austria (Hillebrandt et al., 2013). The base of the Hettangian Stage is defined by the first occurrence (FO) of the ammonoid *Psiloceras spelae tirolicum* Hillebrandt and Krystyn, 2009. Outside of the Northern Calcareous Alps, the ammonoid *Psiloceras spelae* has also been recorded in Nevada (Guex et al., 1998) and Peru (Hillebrandt, 2000a-c; Schaltegger et al., 2008) (Fig. 3). The FO of *P. spelae tirolicum* in Austria, is considered to be slightly older than the FO of *P. spelae spelae* in Nevada, where it occurs together with specimens of *P. tilmanni* (Hillebrandt and Kment, 2015). The FO of *P. spelae* is considered to mark the top of the end-Triassic mass extinction interval. The base of the extinction interval is marked by the last occurrence of the Triassic ammonoid *Choristoceras marshi* or the closely related *Choristoceras crickmayi* (Hillebrandt et al., 2013) (Figs. 2

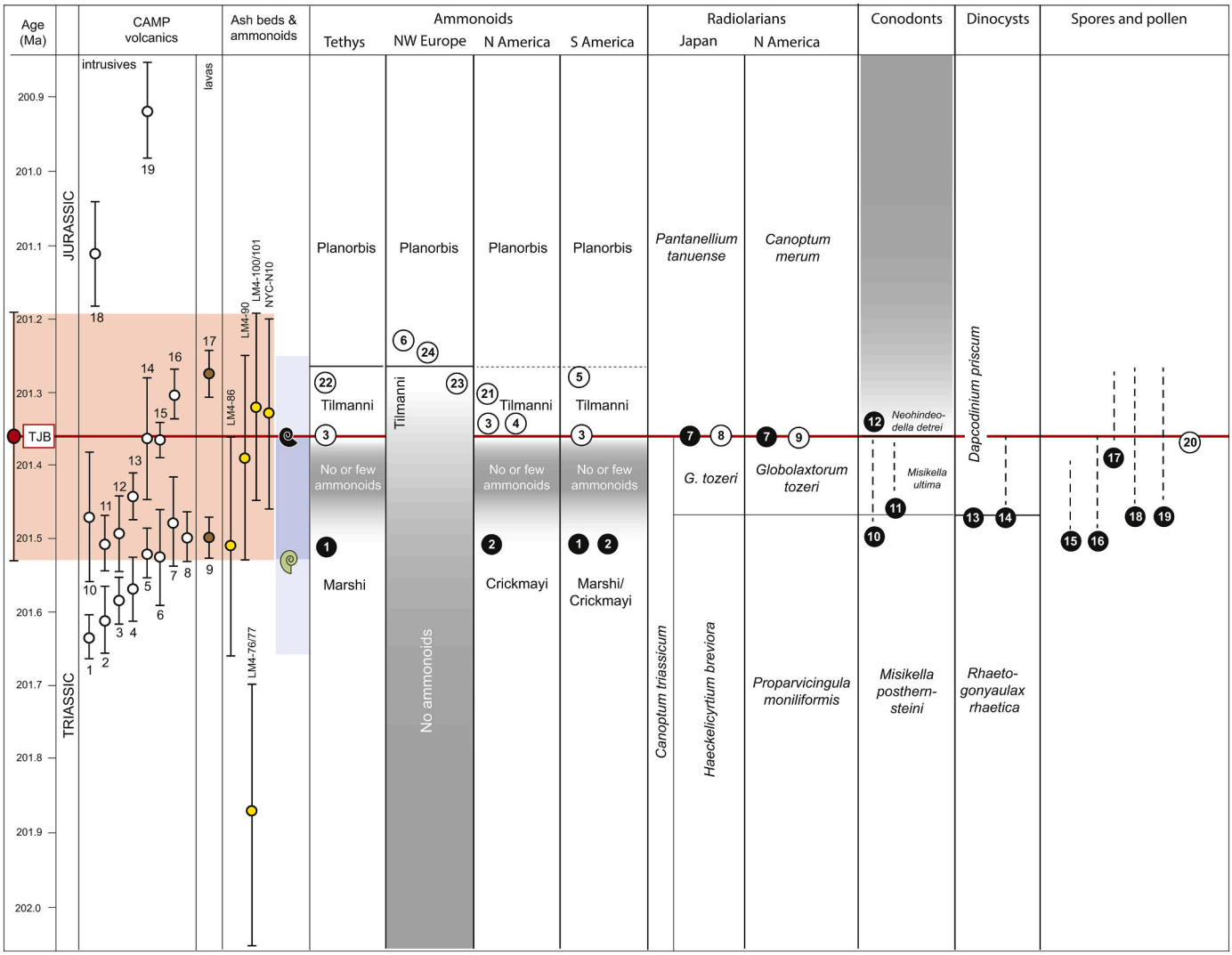

Fig. 3. A) CAMP and ash bed geochronology and numbering of ages from Fig. 2. B) Biostratigraphic zones for selected fossil groups across the TJB. Biostratigraphic events are marked with black circles for last occurrences and white circles for first occurrences: 1) *Choristoceras marshi*, 2) *Choristoceras crickmayi*, 3) *Psiloceras spelae*, 4) *Psiloceras tilmanni* group, 5) *Nevadaphyllites* sp., 6) *Psiloceras planorbis*, 7) *Globolaxtorum tozeri*, 8) *Pantanellium tanuense*, 9) *Canoptum merum*, 10) *Misikella posthernsteini*, 11) *Misikella ultima*, 12) *Neohindeodella detrei*, 13) *Suessia swabiana*, 14) *Rhaetogonyaulax rhaetica*, 15) *Patinasporites densus*, 16) *Rhaetipollis germanicus*, 17) *Ricciisporites tuberculatus*, 18) *Lunatisporites rhaeticus*, 19) *Ovalipollis ovalis*, 20) *Cerebropollenites thiergartii*, 21) *Psiloceras pacificum*, 22) *Psiloceras calliphyllum*, 23) *Psiloceras erugatum* and *P.* cf. *erugatum*, 24) *?Neophyllites* sp. References can be found in the main text. A complete list of all the biostratigraphic events on Figs. 2–10 can be found on Fig. 7.

and 3). Hence, even though the Marshi ammonoid Zone extends up to the TJB, ammonoid occurrences between the LOs of *C. marshi* and *C. crickmayi* and the FO of *P. spelae* are exceedingly rare (Fig. 3).

5.1.2. Radiolarians

The identification of the TJB in Panthalassan sections relies to a great extent on radiolarian biostratigraphy. There are two well established zonations; one from Haida Gwaii (Queen Charlotte Islands) on the Pacific coast of Canada (Carter, 1993; Longridge et al., 2007), and one from Japan (Carter and Hori, 2005; Hori et al., 2007), and these two are thought to correlate well (Fig. 3).

In Japan, the *Haeckelicyrtium breviora* Zone encompasses the lower and middle Rhaetian, while the upper Rhaetian belongs to the *Globolaxtorum tozeri* Zone (Hori et al., 2007; Kuroda et al., 2010; Fujisaki et al., 2018; Rigo et al., 2018). The TJB is defined by a marked turnover at the top of the *G. tozeri* Zone, which coincides with the last occurrence of conodonts (see below). The FO of the radiolarian *Pantanellium tanuense* is used as a marker for the base of the Jurassic and the Hettangian *Pantanellium tanuense* Zone (Hori et al., 2007; Kuroda et al., 2010; Fujisaki et al., 2018). In Haida Gwaii, most of the Rhaetian is assigned to the *Proparvicingula moniliformis* Zone, but also here the *Globolaxtorum tozeri* Zone encompasses the upper Rhaetian (Carter, 1993; Longridge et al., 2007). Similar to the Japanese zonation, there is a turnover at the top of the *G. tozeri* Zone, but in Haida Gwaii Hettangian radiolarian faunas are instead assigned to the *Canoptum merum* Zone (Carter, 1993; Longridge et al., 2007) (Fig. 3).

In the Tethys realm, radiolaria have only been recorded in the Csővár succession in Hungary (Pálfy et al., 2007). In this section radiolarians of the *G. tozeri* Zone were recorded in the basal *Misikella ultima* conodont Zone (see below 5.1.3), i.e. within the Marshi ammonoid Zone (Pálfy et al., 2007) (Fig. 3). Ammonoids assigned to *Choristoceras* were recorded above this level. Radiolarians indicative of the *C. merum* Zone were recorded above the LO of *Misikella ultima*, and below the first psiloceratid ammonoid, but also below the level with the last conodont *"Neohineodella" detrei* (see 5.1.3 below and Fig. 3). This indicates that the *C. merum* Zone pre-dates the last occurrence of conodonts, and that the last occurrence of radiolarians of the *G. tozeri* Zone occurs within the *Misikella ultima* conodont Zone, as shown on Fig. 3.

5.1.3. Conodonts

Conodonts are generally considered as one of the major groups that went extinct at the TJB, although rare occurrences of conodont elements referred to *Neohindeodella detrei* have been reported in the earliest Hettangian of Hungary (Pálfy et al., 2007). Apart from this, the *Misikella posthernsteini* Zone covers the middle to upper Rhaetian (Fig. 3). In Hungary, Turkey, and some Austrian localities (but not Kuhjoch) a zone with *Misikella ultima* is present in the uppermost Rhaetian (Fig. 3). At Kuhjoch, *M. posthernsteini* has its LO at the top of the Kössen Fm (Hillebrandt et al., 2013).

In a newly published conodont biozonation for the Tethyan realm, Rigo et al., 2018 correlated the *Misikella ultima* with the *Globolaxtorum tozeri* radiolarian Zone, and this is followed herein. In the UK, *M. posthernsteini* has been recovered from the pre-Planorbis beds by Swift, 1989, but is considered reworked (Swift, 1999; Wignall and Bond, 2008). Therefore, the last conodonts in the UK have been recovered from the Langport Member, and these were considered aberrant specimens, according to Swift, 1999. The assertion of Swift, 1999 is particularly intriguing considering the high abundances of aberrant fern spores registered at the same stratigraphic level in the Danish and North German basins (Lindström et al., 2019). In Japan, the LO of the *M. posthernsteini* coincides with the top of the radiolarian *Globolaxtorum tozeri* Zone, but *M. ultima* was recovered lower in the Katsuyama section (Hori et al., 2007; Kuroda et al., 2010; Fujisaki et al., 2018; Du et al., 2020). A recent paper by Du et al. (2020) suggested that the extinction of conodonts was asynchronous, making correlations of TJB sections based on conodonts alone difficult.

5.1.4. Dinoflagellate cysts

The global distribution of two of the most common dinoflagellate cyst taxa, *Rhaetogonyaulax rhaetica* and *Dapcodinium priscum*, allows them to be used for correlation over wide distances. There are a number of zonal schemes that include a *R. rhaetica* Zone and a *D. priscum* Zone (e.g. Woollam and Riding, 1983; Poulsen and Riding, 2003; Nicoll and Foster, 1994; Backhouse et al., 2002), but the definitions of these zones differ slightly. Here, we follow the definition of Woollam and Riding (1983) for NW Europe, with the top of the *R. rhaetica* Zone marked by the last common or consistent occurrence of *R. rhaetica,* which occurs in the lower part of the mass extinction interval (Poulsen and Riding, 2003). The LO of *R. rhaetica* usually occurs within the lower part of the succeeding *D. priscum* Zone, which encompasses the uppermost Rhaetian, Hettangian and lowermost Sinemurian (Poulsen and Riding, 2003; Fig. 3). Another group of dinoflagellate cysts that lost a large number of taxa during the ETME are the suessioid dinoflagellates, including *Suessia swabiana* (Poulsen and Riding, 2003; Mangerud et al., 2019).

5.1.5. Spores and pollen

In Morocco, the first CAMP lava flows were emplaced on sediments that have yielded palynological assemblages typical for the Rhaetian (Marzoli et al., 2004; Deenen et al., 2010; Panfili et al., 2019). Of particular importance is the pollen taxon *Patinasporites densus*, which in NW Europe and northern Tethys margins declines in abundance close to the Norian–Rhaetian boundary, and has its last occurrence at the onset of the mass extinction event at the top of the Contorta Bed and its equivalents in NW Europe (e.g. Kürschner and Herngreen, 2010; Fig. 3). Similar assemblages have also been recovered below the oldest flows in Eastern North America, i.e. below the North Mountain Basalt and the Orange Mountain Basalt of the Prevalent group of the Newark Basin (Fowell et al., 1993; Cirilli et al., 2009). In Morocco, Upper flows of the Prevalent group are capped by sediments containing a palynological assemblage indicating a Rhaetian age, as it includes specimens of *Patinasporites densus* (Panfili et al., 2019). On the North American continent, a palynological turnover (Fowell et al., 1993) was described within the Passaic Formation, a few meters below the first lava flows from the Newark basin. According to some authors (e.g., Blackburn et al., 2013), this palynological turnover marks the end-Triassic extinction event in the Newark Basin. However, a latest Triassic palynological assemblage was recorded in sediments outcropping on top of the CAMP lava pile in Nova Scotia suggesting that the Canadian CAMP volcanism also occurred mostly within the topmost Triassic (Cirilli et al., 2009).

Typical Late Triassic pollen taxa that are important constituents of Rhaetian assemblages include *Rhaetipollis germanicus, Ovalipollis* spp., *Lunatisporites rhaeticus* and *Ricciisporites tuberculatus.* The former three decline markedly in abundance during the onset of the mass extinction interval, only to linger on and disappear either during the mass extinction interval or shortly thereafter in the early Hettangian (see e.g. Hillebrandt et al., 2013; Lindström, 2016; Lindström et al., 2017a, 2017b). *Ricciisporites tuberculatus* is generally abundant before and during the mass extinction interval and disappears either during the mass extinction interval or shortly thereafter (Lindström, 2016; Lindström et al., 2017b; Gravendyck et al., 2020; van de Schootbrugge et al., 2020). In some areas, low quantities of *R. tuberculatus* have been encountered in younger strata, but these occurrences are most likely due to reworking. As noted by Lindström (2016), *R. tuberculatus* is only known to thrive at Kuhjoch during the Hettangian (Bonis et al., 2009; Hillebrandt et al., 2013). As discussed by Lindström et al. (2017b) it is not clear whether this is because the Northern Calcareous Alps acted as a refugium for the parent plant, or whether the common presence of *R. tuberculatus* in the Hettangian at Kuhjoch is also due to reworking.

5.2. Age constraints on the mass extinction interval and the TJB

In the GSSP section at Kuhjoch, the base of the Jurassic is defined by the first occurrence (FO) of the ammonoid *Psiloceras spelae tirolicum*

(Hillebrandt et al., 2013). The most recent estimate for the age of the Triassic–Jurassic boundary (TJB) is 201.36 ± 0.17 Ma Schoene (Schoene et al., 2010; Wotzlaw et al., 2014) (Fig. 2). This age was calculated based on U-Pb ages on zircons from ash beds close to the FO of *Psiloceras spelae* in TJB sections in Nevada (New York Canyon) and Peru (Pucara Basin), originally dated by Schoene et al. (2010) and later recalculated by Wotzlaw et al. (2014) using an updated isotopic tracer composition. It is important to note that *Psiloceras spelae* in the New York Canyon succession belongs to the subspecies *P. spelae spelae,* which, due to its co-occurrence with *Psiloceras* ex gr. *P. tilmanni*, is considered to be younger that *P. spelae tirolicum* (Hillebrandt and Krystyn, 2009). In Nevada an ash bed occurring above the FO of *Psiloceras spelae* and *P. tilmanni* yielded an age of 201.33±0.13 Ma (Schoene et al., 2010) (Fig. 2). In Peru, two ash beds bracket the FO of *P. spelae*; the oldest yielding an age of 201.39±0.14 Ma and the younger dated at 201.32±0.13 Ma according to Wotzlaw et al. (2014). The extinction interval can be defined as the interval between the LO of *C. marshi* or *C. crickmayi* and the FO of *P. spelae*, because within this interval many taxa of various marine fossil groups go extinct (e.g., Hillebrandt et al., 2013). U-Pb dating of one ash bed in Peru, located before the FO of *P. spelae* but after and closer to the last occurrence (LO) of the Triassic ammonoid *Choristoceras crickmayi*, was dated at 201.51±0.15 Ma (Wotzlaw et al., 2014). The duration of the extinction interval in the continental realm has been estimated to ~20 to 40 kyr, based on cyclostratigraphy and magnetostratigraphy (Deenen et al., 2010), while Blackburn et al. (2013) suggested a duration of ~100±40 kyr.

Magnetostratigraphic studies detected a short-lived reversed magnetozone (E23r) just below the base of the CAMP volcanic pile in the Newark basin (see Kent et al., 2017 and references therein). While detection of magnetic reversals within the African CAMP is controversial (Knight et al., 2004, vs. Font et al., 2011), detailed magnetostratigraphic data for the Moroccan volcanic piles suggest that these may have been emplaced within 4 volcanic pulses, with each pulse lasting probably less than 500 years (Knight et al., 2004).

6. Traces of CAMP activity in a stratigraphic context

Ash beds produced by the CAMP volcanism were either very rare or have not been preserved. A basaltic ash layer, the Pompton Tuff, is known from the Eastern North American basins (Whiteside et al., 2010. Outside of the CAMP area, Pálfy and Zajzon, 2012 reported goethite pseudomorphs of altered, euhedral pyroxene and amphibole crystals

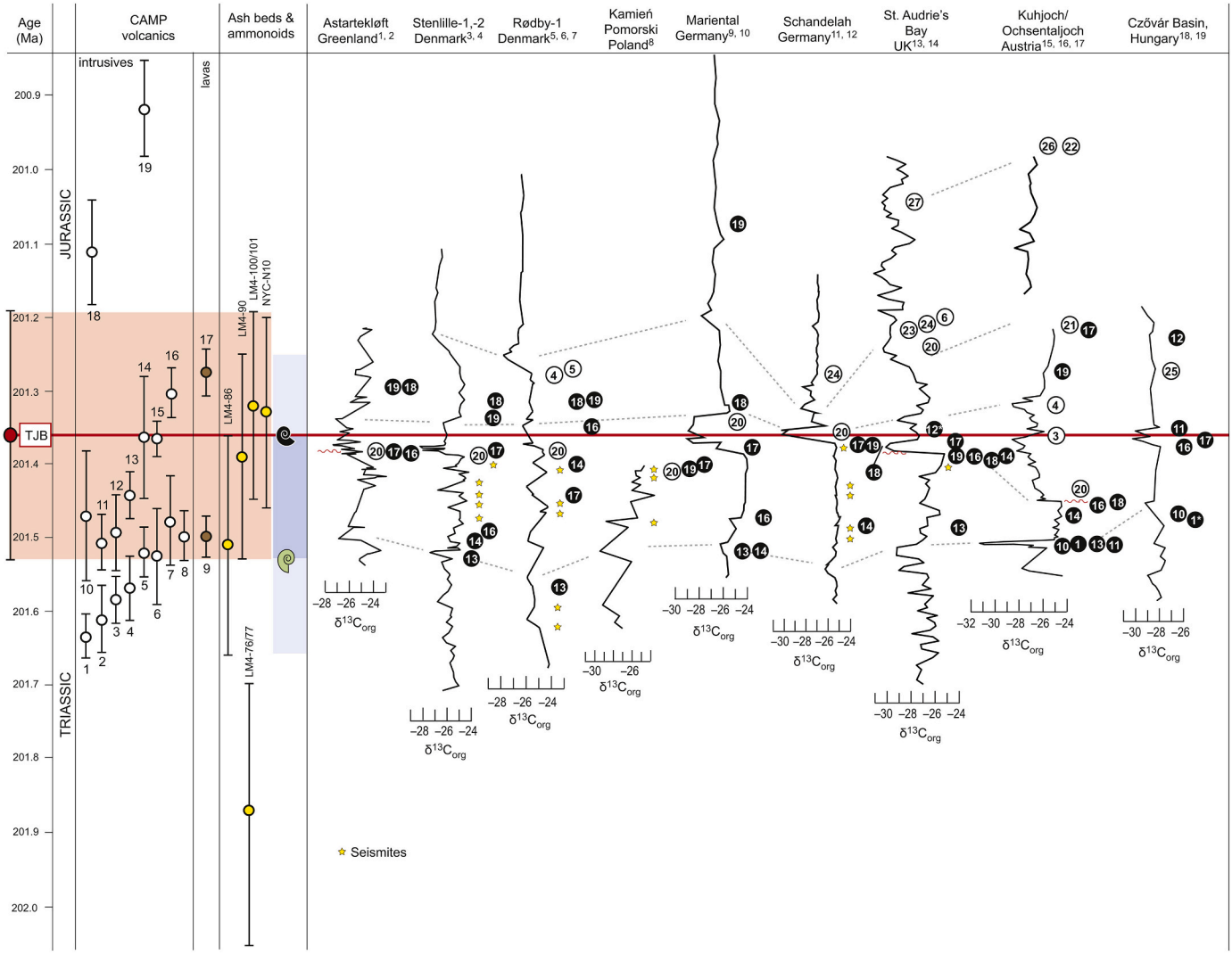

Fig. 4. Correlation of organic δ^{13}C-records from the NW European epicontinental sea and northern Tethys margin, primarily after Lindström et al. (2017b). [1]Hesselbo et al. (2002), [2]Mander et al. (2013); [3]Lindström et al., 2017b, 2019), [4]Lindström et al. (2017b); [5]Lindström et al. (2017b), [6]Lund (1977), [7]Hansen (2013); [8]Pienkowski et al. (2011); [9]Heunisch et al. (2010); [10]van de Schootbrugge et al., 2013; [11]Lindström et al. (2017b), [12]van de Schootbrugge et al. (2018); [13]Hesselbo et al. (2002), [14]Bonis et al. (2010b); [15]Bonis et al., 2009; [16]Hillebrandt (2000a, 2000b, 2000c) [17]Du et al. (2020); [18]Götz et al. (2009); [19]Pálfy et al. (2001). Yellow stars mark seismites previously reported by Simms (2003, 2007) and Lindström et al. (2015). A list of all the biostratigraphic events can be found on Fig. 7.

and green clay-spherules interpreted as altered glass spherules in the topmost part of the Kössen Formation in the Kendelbachgraben section in Austria, just below the Marshi CIE and the onset of the mass extinction (Hillebrandt et al., 2013; Lindström et al., 2017b). Pálfy and Zajzon, 2012 interpreted the goethite pseudomorhs and green clay-spherules to be of volcanic origin and linked to CAMP volcanism. In addition, there are various geochemical signals recorded in TJB strata that can potentially be interpreted as indications of volcanic activity, including records of $\delta^{13}C$, biomarkers, iridium, REE, and mercury, which are all discussed below.

Although the correlation charts discussed below are constructed using the above described stratigraphic framework, it needs to be emphasized that the individual records are not normalized to deposition rate. The only points that are fixed relative to the timescale on the right are the dated ash beds, However, these are associated with substantial errors. In principal, the ammonoid occurrences and the dated ash beds constrain each other. Because the LO of *C. marshi* or *C. crickmayi* and the FO of *P. spelae* always occur separated by strata, we know that they cannot be of the same age. The occurrence of these ammonoid events can be used to constrain the interval between them in time, i.e. the extinction interval, albeit with errors, and all other biostratigraphic events hinges on these. This means that the positions of stratigraphically important levels in the individual records on Figs. 4–10 can sometimes appear slightly offset compared to the stratigraphic framework (Figs. 4–10). This becomes especially apparent when deposition rates varied within sections.

6.1. Organic $\delta^{13}C$ records

Numerous records of fluctuating $\delta^{13}C$ values from organic material across the end-Triassic event and the TJB, indicate that the carbon cycle was highly unstable at this time (Hesselbo et al., 2002; Williford et al., 2007; van de Schootbrugge et al., 2008; Korte et al., 2009; Ruhl and Kürschner, 2011; Ruhl et al., 2011; Lindström et al., 2012; Schobben et al., 2019). Major negative excursions in these C-isotope records are generally attributed to large scale input of light carbon to the atmosphere, either from volcanic CO_2 or methane (Hesselbo et al., 2002; Ruhl et al., 2011). However, the records vary extensively depending on the

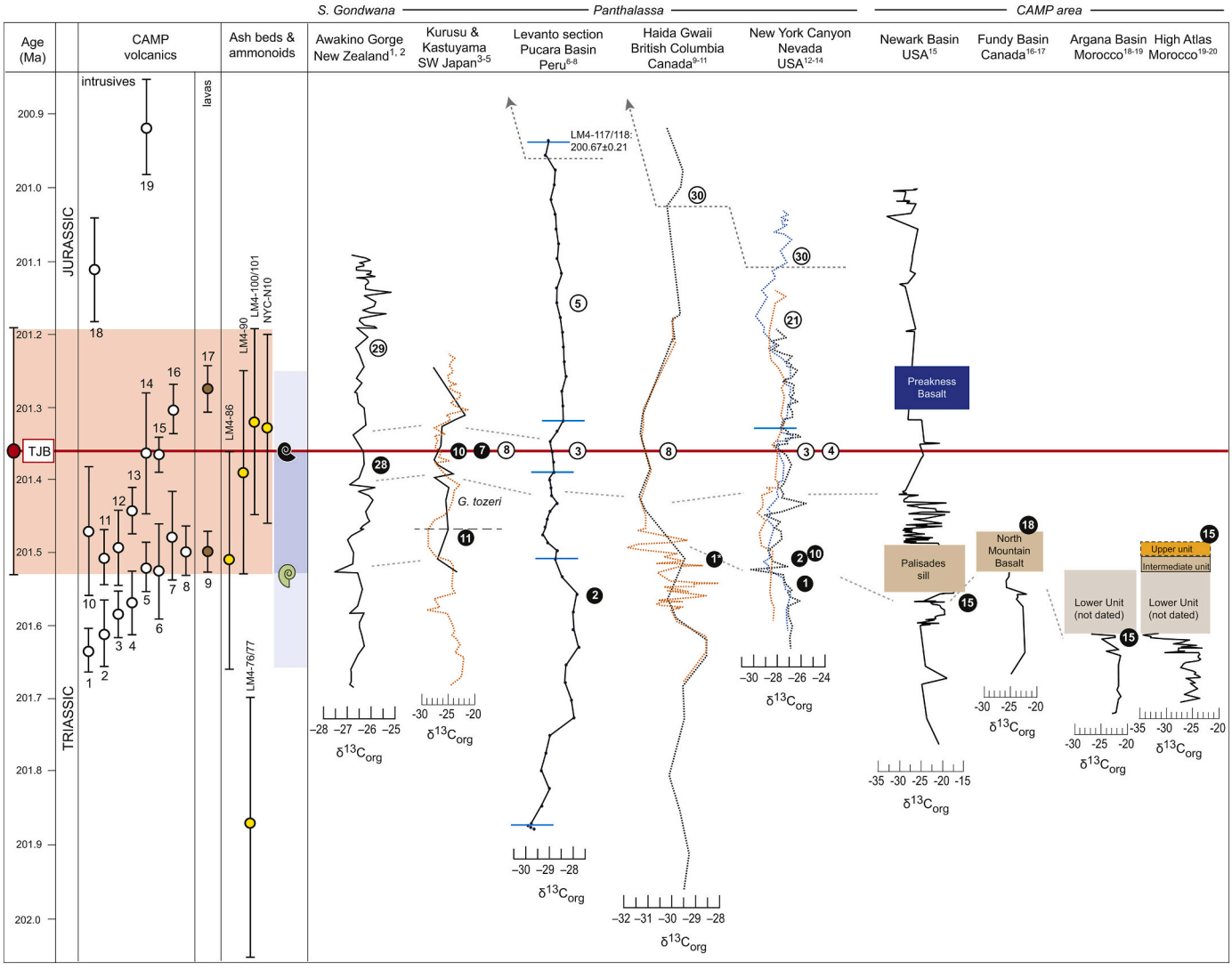

Fig. 5. Correlation of organic $\delta^{13}C$-records from the Panthalassa and the CAMP area, after [1]Akikuni et al. 2010, [2]De Jersey and McKellar 2013; [3]Hori et al. 2007, [4]Kuroda et al. 2011; black line, [5]Fujisaki et al. 2018; orange dotted line; [6]Schoene et al. 2010, [7]Wotzlaw et al. 2014, [8]Yager et al., 2017; [9]Ward et al. 2004; orange dotted line, [10]Longridge et al. 2007, [11]Williford et al. 2007; black line; [12]Guex et al. 2004; orange stipled line, [13]Guex et al. 2008; blue stipled line, [14]Thibodeau et al. 2016; orange dotted line; [15]Whiteside et al., 2010; [16]Cirilli et al. 2009, [17]Deenen et al. 2011; [18]Deenen et al. 2010, [19]Panfili et al. 2019; [20]Dal Corso et al. 2014. Horizontal blue lines marks position of U/Pb dated ash beds on the C-isotope curves of Nevada and Peru. A list of all the biostratigraphic events can be found on Fig. 7.

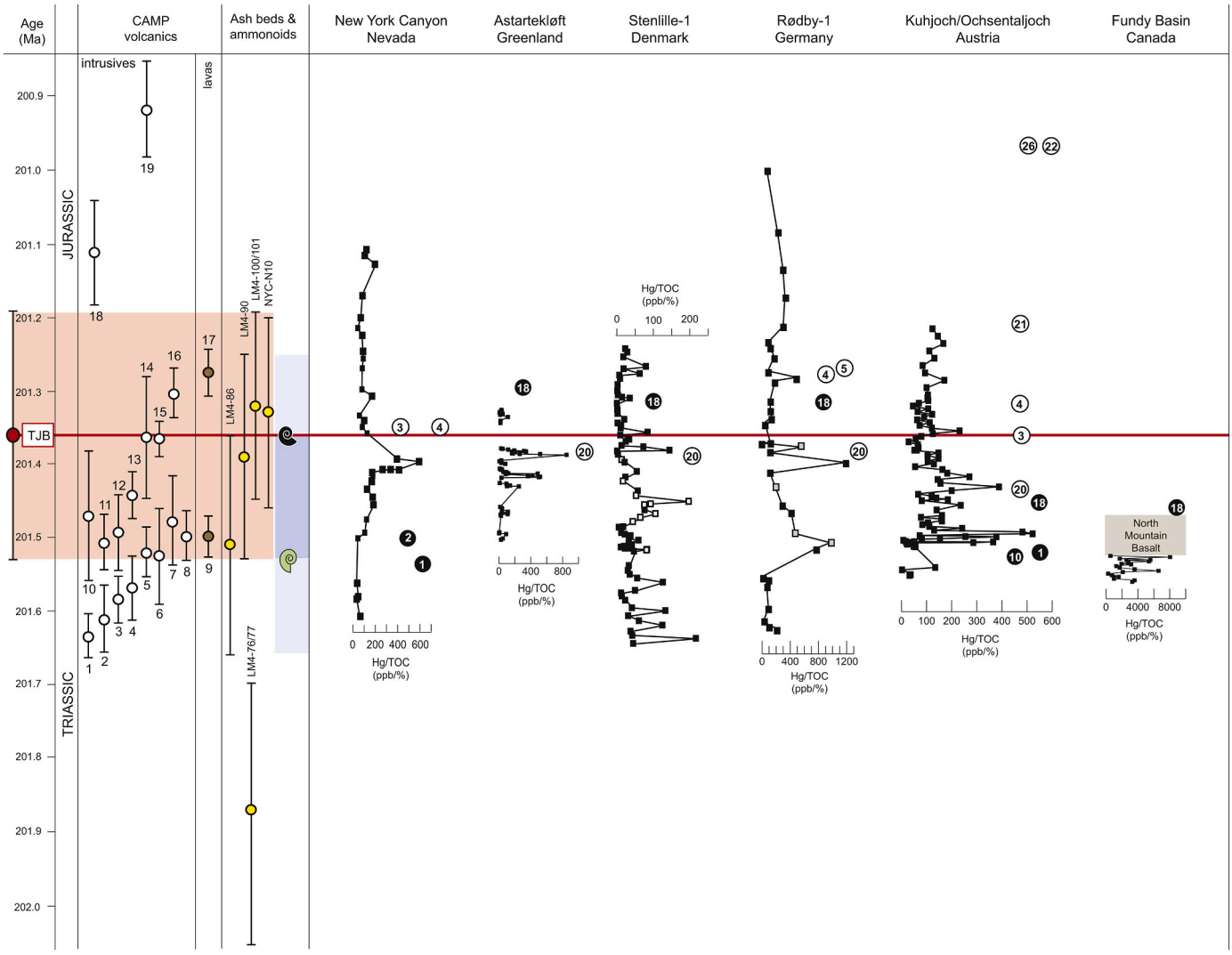

Fig. 6. Correlation of Hg/TOC records from Nevada (Thibodeau et al., 2016), Greenland (Percival et al., 2017), Danish Basin and North German Basin (Lindström et al., 2019), Austria and Fundy Basin (Percival et al., 2017), with selected events shown. A list of all the biostratigraphic events can be found on Fig. 7.

analyzed material, and also seem to vary depending on the palaeogeographical position of the analyzed site, as demonstrated by van de Schootbrugge et al., 2008 and Schobben et al., 2019. Here we focus on organic C-isotopes, as this reflects the carbon fractionation of primary producers, i.e. land plants and freshwater algae, and marine organic-walled phytoplankton and green algae. Because of differences in fractionation between various plants and algae, the average $\delta^{13}C$ value of terrestrial organic matter today is c. –23‰, while marine organic matter is more depleted, c. –29‰ (Foster et al., 1997). These are important considerations when interpreting C-isotope records from bulk organic matter. However, because photosynthetic organisms prefer ^{12}C over ^{13}C (O'Leary, 1988), an increase in light carbon in the atmosphere, e.g. from a volcanic source or methane, will lead to more negative $\delta^{13}C$ values regardless of the specific plant/phytoplankton fractionation. However, marked changes in the type of organic matter can mask this effect (Foster et al., 1997).

6.1.1. Europe: the NW European epicontinental sea and northern Tethys margin – terrestrial and marine records

Marine records of organic $\delta^{13}C$ across the TJB in the Tethys and central parts of northern Pangea, i.e. the NW European epicontinental sea and adjacent land areas, exhibit several negative shifts, which are evident in both marine and terrestrial successions (Hesselbo et al., 2002) (Fig. 4). The most widely used record for correlation is that of Hesselbo et al. (2002) from St. Audrie's Bay in the UK. This record clearly shows two negative CIEs as well as one shift to more consistently negative values in the Hettangian (Hesselbo et al., 2002). The lower negative shift, which occurs within the Westbury Formation, was not discussed by Hesselbo et al. (2002) who instead dubbed the sharp negative CIE in the Lilstock Formation "the initial negative excursion" and concluded that it coincided with both the onset of volcanic activity in the CAMP area, and floral and faunal turnovers on land and in the oceans.

However, several authors have pointed out that the "initial negative excursion" is above the main extinction level (Wignall and Bond, 2008; Mander et al., 2008; Lindström et al., 2012, 2017b). It is also above a stratigraphically restricted interval characterized by soft-sediment deformation, which can be traced across large parts of NW Europe (Simms, 2003, 2007; Lindström et al., 2015). As shown by Lindström et al., 2015, the seismite interval encompasses several episodes of soft-sediment deformation, separated by non-disturbed sediments, and calculations of distance to epicenter for each site indicates that the seismites were formed by repeated local/regional earthquakes. The seismite interval generally occurs within the *Polypodiisporites polymicroforatus* abundance interval of Lindström et al., 2017b, i.e. within the extinction interval as defined by ammonoids. During the *Polypodiisporites polymicroforatus* abundance interval, pollen from gymnospermous trees

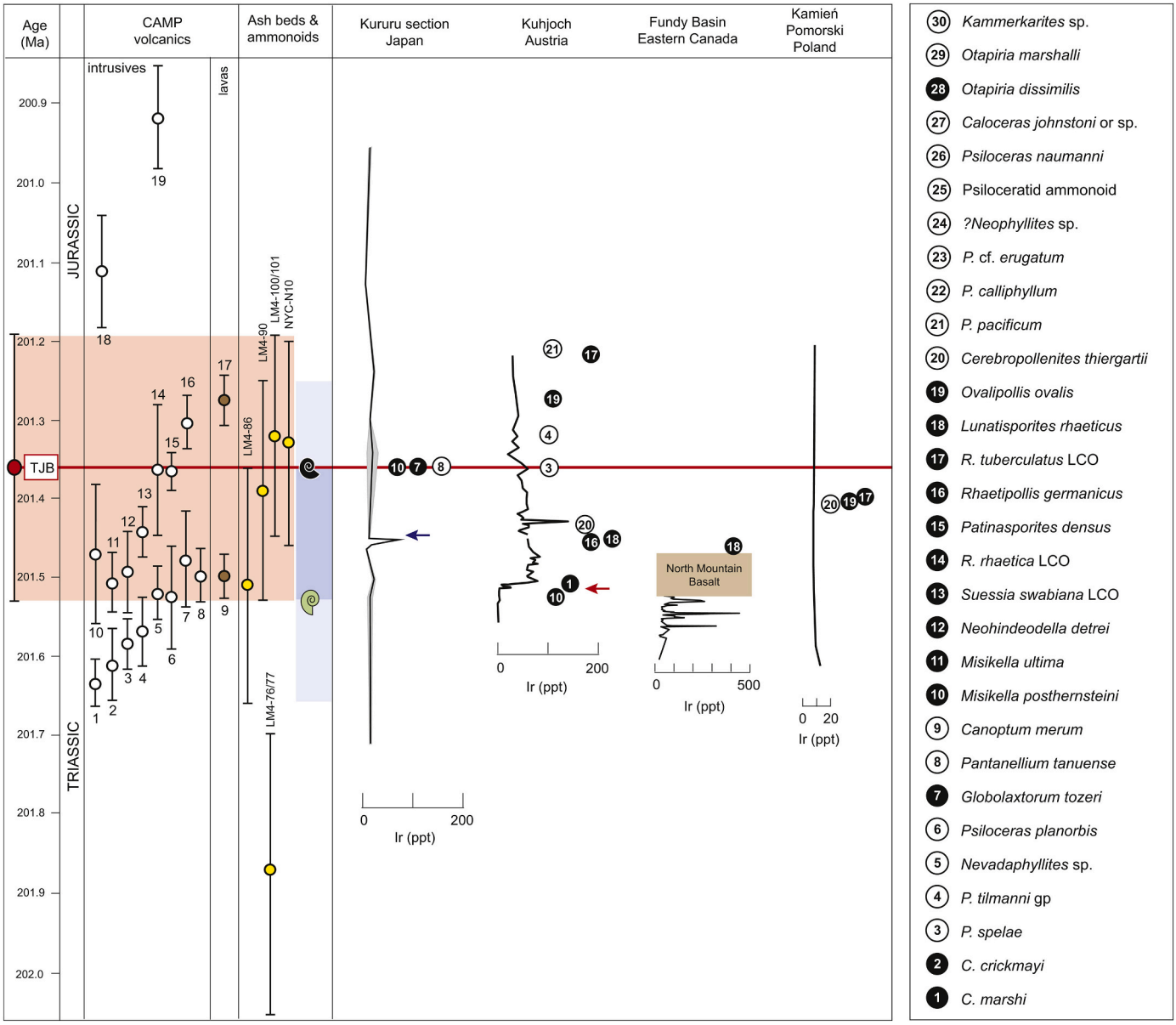

Fig. 7. Correlation of iridium records from the Kurusu section in Japan (Hori et al., 2007), Kuhjoch in Austria (Tanner et al., 2016), Fundy Basin in Eastern Canada (Tanner et al., 2008), and Kamień Pomorski in Poland (Pieńkowski et al., 2014). The red arrow marks the corresponding level with clay spherules and pseudomorphs of altered euhedral pyroxen and amphibol crystals reported by Pálfy and Zajzon (2012) from the Kendelbachgraben section, Eiberg Basin. Blue arrow marks position of a level in the Kurusu section with basaltic rock fragments mentioned in Hori et al. (2007). Expanded from Tegner et al. (2020b). Also showing on the right is a list of all the biostratigraphic events used in Figs. 2–10.

show a marked decline in abundance, and Dipteridaceae/Cyathaceae (*Deltoidospora/Concavisporites* spp., respectively) proliferate. As suggested by van de Schootbrugge et al., 2009 this indicates supra-regional deforestation during the extinction interval, which is evident from records in NW Europe and the Tethys realm (Lindström et al., 2017b). At St. Audrie's Bay, this interval coincides with the seismite interval and the main extinction level and precedes the "initial negative CIE" (Simms, 2003, 2007; Wignall and Bond, 2008; Mander et al., 2008; Lindström et al., 2012; Lindström et al., 2017b). However, most of the *P. polymicroforatus* abundance interval is probably missing at St. Audrie's Bay, due to a hiatus prior to the "initial negative CIE" (Lindström et al., 2017b). This hiatus is a sequence boundary associated with a transgression (Hesselbo et al., 2004; Hallam and Wignall, 1999). At Kuhjoch, the *P. polymicroforatus* abundance interval also occurs within the extinction interval, i.e. it is constrained between the LO of *Choristoceras marshi* and the FO of *Psiloceras spelae* (Hillebrandt et al., 2013; Lindström et al., 2017b). Hence, the sharp negative CIE at Kuhjoch, i.e. the Marshi CIE (Lindström et al., 2017b), cannot correlate with the "initial CIE" at St. Audrie's Bay, but instead equates with the negative CIE in the Westbury Formation at St. Audrie's Bay (Lindström et al., 2017b).

The organic C-isotope records from Europe and Tethys appear to indicate multiple episodes of light carbon emissions to the atmosphere across the TJB, commencing in conjunction with the Marshi event. At least three negative CIEs are commonly recognized: the Marshi, the Spelae and the top-Tilmanni CIEs (Lindström et al., 2017b), and these are separated by two intervals with more positive organic C-isotope values (Fig. 4).

Most of the records from the NW European epicontinental sea and northern Tethys margin are marine records that contain a mixture of terrestrial and marine organic matter. The best known terrestrial record is that from the Kap Stewart Group at Astartekløft in Greenland

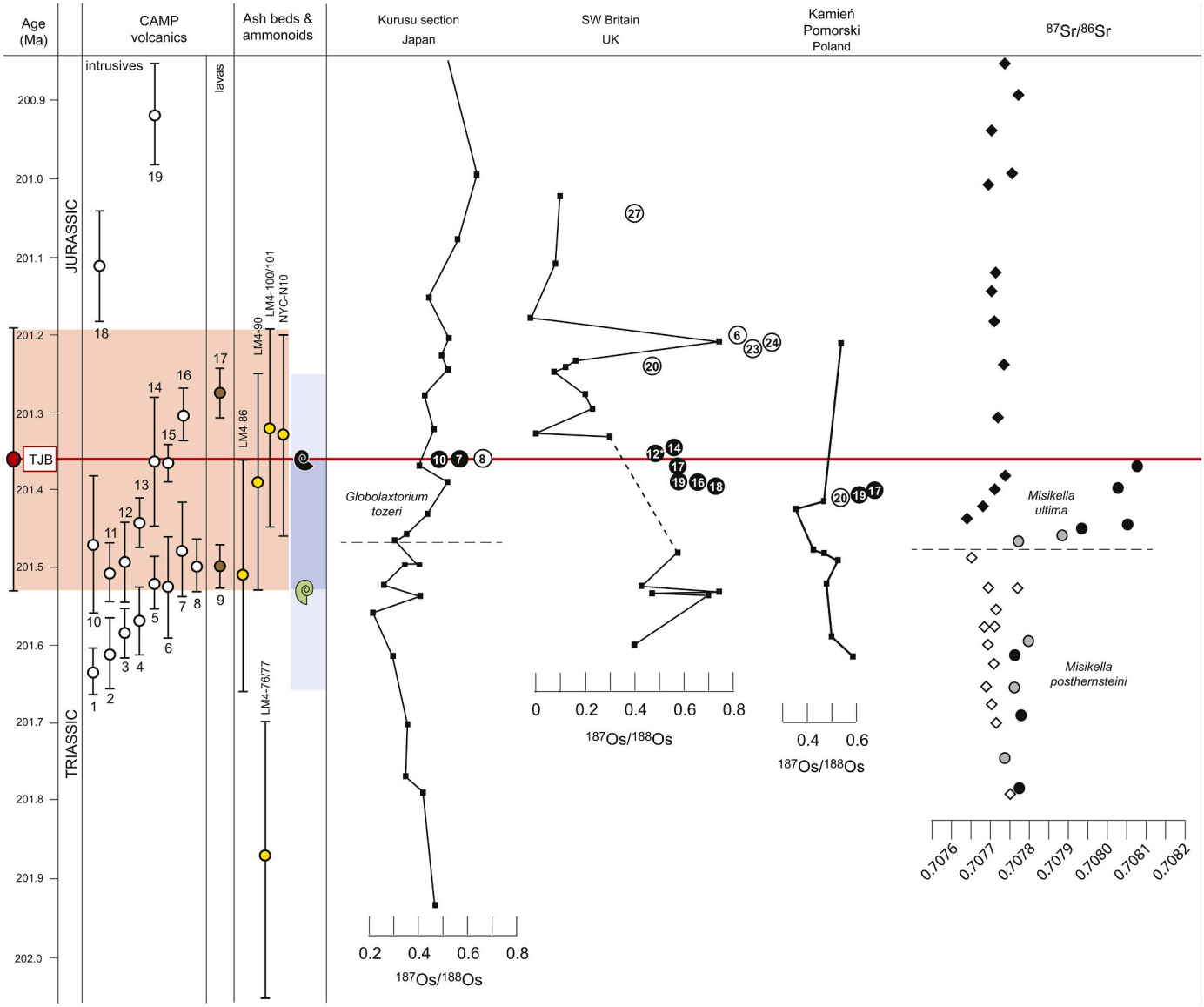

Fig. 8. Correlation of Os-isotope records reported from the Kurusu section in Japan (Kuroda et al., 2010), SW Britain in the UK (Cohen and Coe, 2002), Kamień Pomorski in Poland (Pieńkowski et al., 2011, 2014), and Sr-isotopes from Callegaro et al. (2012), Korte et al. (2003) and Jones et al. (2003). Black circles = conodonts with Conodont Alteration Index (CAI) ≤ 2 (Callegaro et al., 2012). Grey circles = conodonts (Korte et al., 2012). Black diamonds = brachiopods (Korte et al., 2003), White diamonds = oysters (Jones et al., 2003). A list of all the biostratigraphic events can be found on Fig. 7.

(Hesselbo et al., 2002), a succession famous for its' distinct terrestrial plant beds (Harris, 1937; McElwain et al., 2007 and references therein). This record, based only on wood fragments, shows two negative CIEs; a lower one with the amplitude ~ –3‰ and an upper with an amplitude of ~ –4‰ (Hesselbo et al., 2002; Fig. 4). There is a sampling gap of c. 5 m just below the start of the upper CIE (Hesselbo et al., 2002). This gap also separates plant bed 4 from plant bed 5, the latter which contains the onset of the upper CIE (Hesselbo et al., 2002; McElwain et al., 2007). The TJB is commonly placed within plant bed 5, as this bed contains the FO of *Cerebropollenites thiergartii* in its upper part, and also the LO of *Ricciisporites tuberculatus* (Mander et al., 2013). The upper CIE at Astartekløft has been suggested to encompass both the so called "initial CIE" and the "Main CIE" of Hesselbo et al. (2002) (See e.g. Hesselbo et al., 2002; McElwain et al., 2007; Mander et al., 2013). Hesselbo et al. (2002) indicate a hiatus above plant bed 5, i.e. within the upper CIE (Fig. 4). However, from a palynological point of view, it is more likely that the upper CIE corresponds to the Spelae CIE, and perhaps, the sharp negative C-isotope peak registered in other areas at this level, could be missing. The co-occurrence of *C. thiergartii* and *R. tuberculatus* in plant bed 5 suggests that it was deposited close to the TJB (Lindström, 2016; Lindström et al., 2017b). In addition, plant bed 5 is placed in the transition zone between the *Lepidopteris* and *Thaumatopteris* macrofossil plant zones (Harris, 1937; McElwain et al., 2007), further suggesting it was deposited close to the TJB. It is also possible that the top-Tilmanni CIE (equivalent to the "Main CIE" of Hesselbo et al., 2002) is not recorded in the C-isotope record at Astartekløft. The Kap Stewart Group is regarded to have been deposited in or around a large lake during Rhaetian–Sinemurian times, but erosion and non-deposition along the southeastern margin of the lake (where Astartekløft was located) resulted in a major hiatus that encompasses all of the Sinemurian (Surlyk, 2003). Hence, In this paper we correlate the upper CIE at Astartekløft with the Spelae CIE, and the lower CIE with the Marshi CIE (Fig. 4). Because land plants are in direct contact with the atmosphere, this record suggests that there was indeed an increase in light carbon in the atmosphere during both the onset of, and towards the end of the extinction interval. A terrestrial organic C-isotope record from Poland

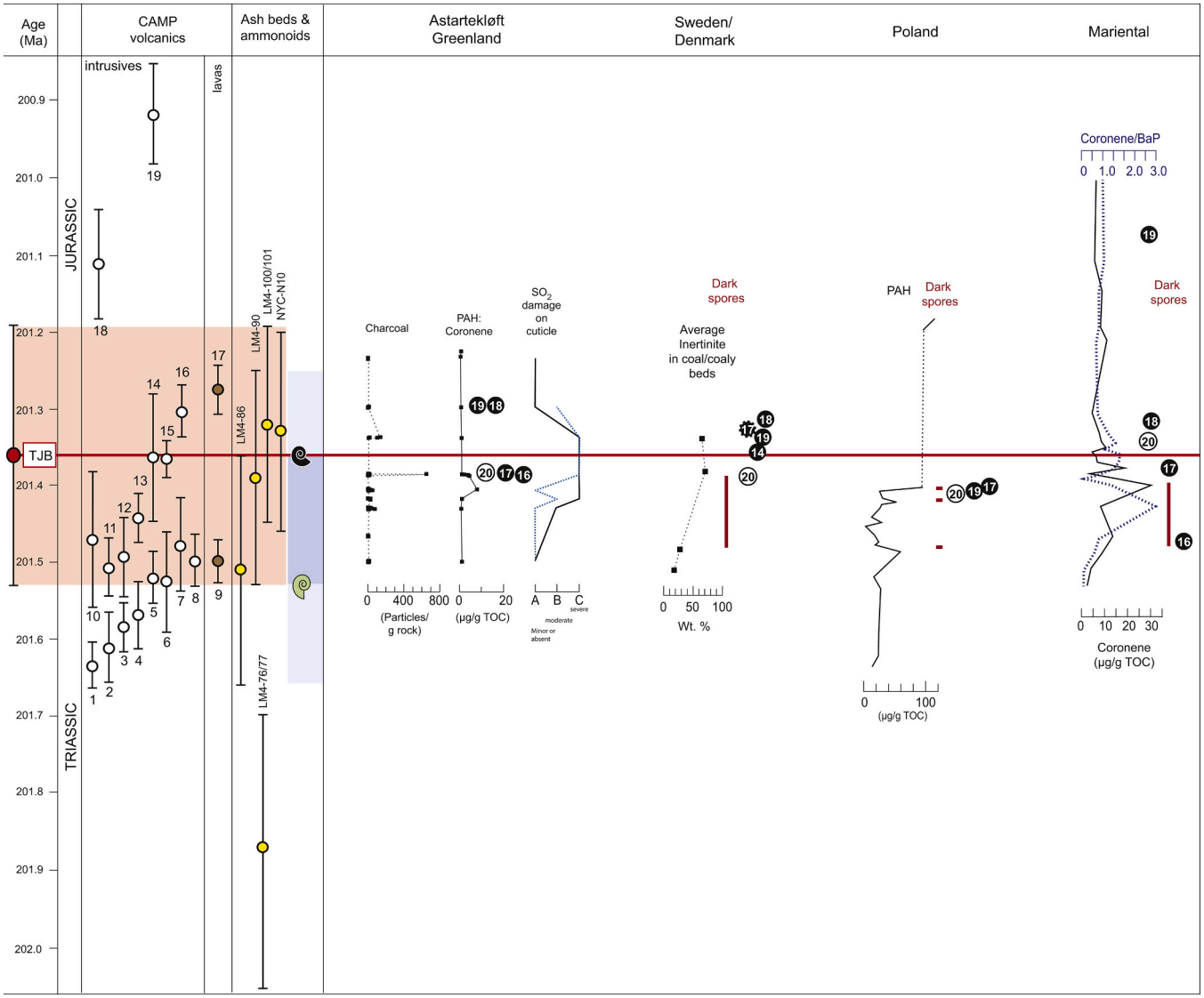

Fig. 9. Charcoal- (Belcher et al., 2010), PAH-records (Williford et al., 2014) and SO_2 damages on cuticles (Steinthorsdottir et al., 2018) from Jameson Land, Greenland. SO_2 damages on Ginkgoales marked with black line, and on Bennettitales with a stippled blue line. Charcoal record from coal beds and coaly beds in the Danish Basin (Petersen and Lindström, 2012). PAH-record from Poland (Marynowski and Simoneit, 2009), and PAHs from Mariental in the North German Basin reported by van de Schootbrugge et al., 2009. Vertical red lines represent levels with darkened palynomorphs, first noted by Lund, 1977 and discussed by him in Lund, (2003), and by van de Schootbrugge et al., 2009 and Pienkowski et al., 2011. A list of all the biostratigraphic events can be found on Fig. 7.

also shows a shift from more negative values during the mid-Rhaetian to more positive ones in the upper Rhaetian (Pienkowski et al., 2014) (Fig. 4).

The Marshi CIE is thus expressed with very variable amplitude in different areas (Fig. 4). In many of the records from the NW European epicontinental sea, the shift from pre-Marshi to the Marshi CIE is less dramatic than the shift from the Marshi CIE to more positive values above (Fig. 4). From the records that extend further below the Marshi CIE (Stenlille-1, Rødby-1 and St. Audrie's Bay), the pre-extinction interval appears to be characterized by fluctuating C-isotopes values exhibiting a slight negative trend upsection (Fig. 4). The positive C-isotope interval succeeding the Marshi CIE basically coincides with the mass extinction interval. As described by Hallam and Wignall (1999) the post-Marshi positive C-isotope interval is also linked to a major regression. This regression affected successions within the NW European epicontinental sea and the northern Tethys margin, and may have had a profound influence on the organic C-isotope records. The Stenlille-1 and Rødby-1 records exhibit highly variable C-isotope values within this positive interval, while e.g. Mariental, Schandelah, and Kuhjoch exhibit more consistently positive values (Fig. 4). The reason for this is not clear, but it may be related to enhanced input of reworked organic material in some of the records (e.g. Lindström et al., 2012; van de Schootbrugge et al., 2020).

6.1.2. *Panthalassa and western Pangaea*

Compared to those from the Europe and Tethys, organic C-isotope records from the Panthalassa and western Pangaea appear to show fewer and less prominent shifts (Fig. 5). The Japanese Kurusu section represents a Panthalassan deep sea record, and is therefore highly condensed (Hori et al., 2007; Kuroda et al., 2010). Kuroda et al. (2010) presented an organic C-isotope record for the upper Rhaetian–lower Hettangian interval of the Kurusu section of ~1 m in thickness with fourteen C-isotope values, containing negative values reaching down to –28 ‰ (Fig. 5). Although the section is biostratigraphically constrained by conodonts and radiolarians it is, as pointed out by Kuroda et al. (2010, upplementary text therein), difficult to pinpoint the TJB in this section. Kuroda et al. (2010) tentatively placed the TJB somewhere between the level with the LO of the conodont *Misikella posthernsteini* and the FO of

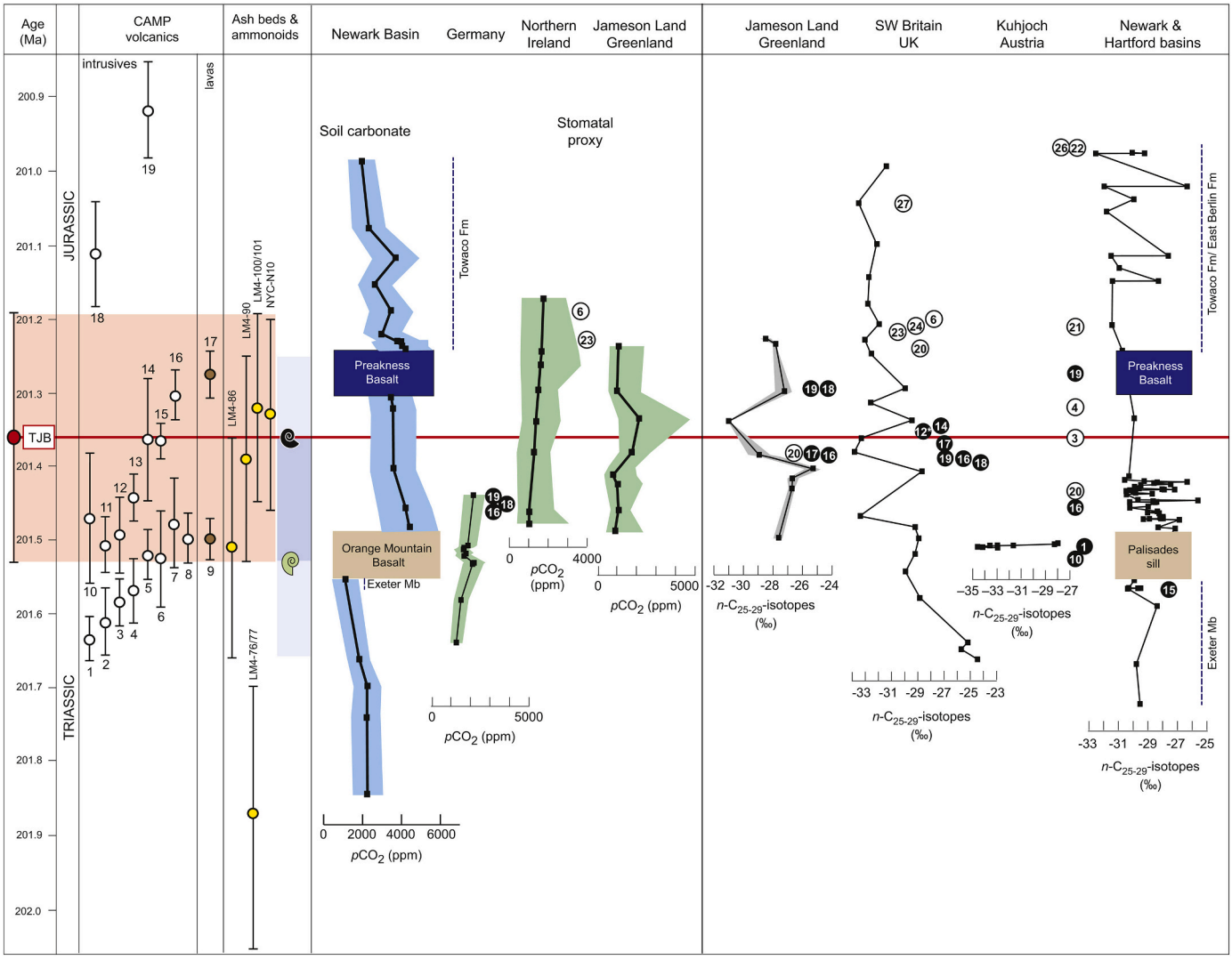

Fig. 10. Correlation and comparison of pCO_2-records from pedogenic carbonate in the Newark Basin (Schaller et al., 2011; Schaller et al., 2016) and from plant fossil cuticles (stomatal index) from Germany (Bonis et al., 2010a), Northern Ireland and Jameson Land, Greenland (Steinthorsdottir et al., 2011), with C-isotopes from $C_{25–29}$ n-alkanes from Greenland (Williford et al., 2014), SW Britain in UK (Whiteside et al., 2010), Kuhjoch in Austria (Ruhl et al., 2011) and the Newark and Hartford basins in eastern USA (Whiteside et al., 2010). Please note that there is a difference in scale of the Exeter Member, between the soil carbonate record (Schaller et al., 2011, 2016) and the n-alkane record (Whiteside et al., 2010). A list of all the biostratigraphic events can be found on Fig. 7.

the radiolarian *Pantanellium tanuense*, and the level where several species of the radiolarian genus *Bipedis* occur. However, as *P. tanuense* is considered a lower Hettangian index taxon indicative of the *Canoptum merum* Zone (Hori et al., 2007; Kuroda et al., 2010), the TJB boundary must be placed at or below its FO in the Kurusu section. Fujisaki et al. (2018) published an organic C-isotope record from the Katsuyama section in the Inuyama area, Japan (Fig. 5). The Katsuyama record is more expanded across the TJB compared to the Kurusu section, and displays three major negative shifts in $\delta^{13}C$ (Fig. 5). The lowermost negative CIE occurs in the upper part of the *Haeckelicyrtium breviora* radiolarian Subzone and the second negative CIE straddles the boundary between this zone and the succeeding *Globolaxtorum tozeri* Subzone (Fujisaki et al., 2018) (Figs. 3, 5). The latter subzone is considered to be Rhaetian in age and has been correlated in part to the *C. marshi* ammonoid Zone (Fujisaki et al., 2018). The third negative CIE straddles the boundary between the *G. tozeri* Subzone and the lower Jurassic (Hettangian–Sinemurian) *Pantanellium tanuense* radiolarian Zone (Fujisaki et al., 2018). The authors correlated this CIE with the top-Tilmanni CIE (Fujisaki et al., 2018). Here, we instead follow the arguments given above regarding the age of the *G. tozeri* Subzone and the FO of *P. tanuense*, thus correlating the third CIE of Fujisaki et al. (2018) with the Spelae CIE (Figs. 3 and 5).

The Haida Gwaii (western Canada) and the Peru records both encompass data from the Norian to the Sinemurian (Williford et al., 2007; Yager et al., 2017), and also have relatively few data points across the end-Triassic event and the TJB (Fig. 5). The Peru record of Yager et al. (2017) is constrained by U-Pb ages of zircons from volcanic ash beds that were dated by Guex et al. (2012) and Schoene et al., 2010 and then re-calibrated by Wotzlaw et al. (2014). The Peru record is calibrated to the stratigraphic framework suggested here using these U-Pb ages and ammonoid events (Fig. 5). This results in a very protracted negative CIE encompassing the entire extinction interval, as defined by the LO of Triassic ammonoids and the FO of *P. spelae* (Fig. 5).

Correlation of the Haida Gwaii record is challenging. Organic C-isotope records for this succession were published by Ward et al., 2004 and Williford et al., 2007, respectively. The two records are form the same locality, but the Williford et al., 2007 record extends the Ward et al. (2004) record upwards and downwards. In addition, the fluctuations in the Ward et al., 2004 record, were disregarded in the Williford et al., 2007 paper. According to Williford et al., 2007, the two records

can be correlated and are assumed to be equally complete. The organic C-isotope curve presented by Ward et al., 2004 is of much higher resolution across the extinction interval and exhibits strongly fluctuating C-isotope values with an upward increasing negative trend. The last typical Triassic radiolarians mark the upper boundary of the upper Rhaetian *Globolaxtorum tozeri* Zone, which coincides with a positive organic C-isotope excursion with values around –28.5 ‰ in the Williford et al., 2007 record. This occurs before the LO of *Choristoceras* ammonoids by c. 3 m (Williford et al., 2007). The TJB is placed at the first occurrence of radiolarians typical of the *Canoptum merum* Zone (Longridge et al., 2007), which occurs within an interval with C-isotope values around –31 ‰ (Ward et al., 2004; Williford et al., 2007; Schoepfer et al., 2016). The first psiloceratid ammonite occurs 8 m higher in the succession where C-isotope values are around or just above –30 ‰ (Ward et al., 2004; Williford et al., 2007). Ward et al. (2004) doccumented the last occurrence of ammonoids assigned to *Choristoceras* 4 m below the FO of *C. merum*, and merely one meter above the last occurrence of Triassic radiolarian (Fig. 4). Also, three published organic C-isotope records exist for the New York Canyon section in Nevada (Guex et al., 2004; Ward et al., 2007; Guex et al., 2008; Thibodeau et al., 2016), and these are shown on Fig. 5.

An organic $\delta^{13}C$ record from the Awakino Gorge in New Zealand (Akikuni et al., 2010) displays remarkably similar trends to that of Guex et al. (2004) from the New York Canyon in Nevada (Fig. 5). In the New Zealand record, the TJB is placed close to but above the last occurrence of *Otapiria dissimilis* (Akikuni et al., 2010; De Jersey and McKellar, 2013; Lindström, 2016).

6.1.3. CAMP-area

The most extensive published organic C-isotope record from the CAMP area is the composite record from the terrestrial Newark and Hartford Basins by Whiteside et al., 2010, which was calibrated to the astronomical cycles (Fig. 5). Here, we only show the data from the Newark Basin and we have used the published ages of the Palisades Sill (geochemically equivalent to the Orange Mountain basalt) and Preakness basalt (Blackburn et al., 2013) to calibrate the record to our stratigraphic framework (Fig. 5). This continental record shows highly fluctuating, but more positive values during the extinction interval, similar to records from Europe, with a pronounced negative CIE prior to the Palisades Sill and Orange Mt. flows (Fig. 5). Two organic C-isotope records from the sedimentary successions below the oldest basalts in the Fundy Basin (Deenen et al., 2011) and Morocco (Dal Corso et al., 2014) indicate increasingly negative values prior to the onset of magmatic activity in these areas (Fig. 5).

The pre-basalt continental records from the Tiourjdal section in the High Atlas, Morocco (Dal Corso et al., 2014; Panfili et al., 2019), and also from the Newark Basin (Whiteside et al., 2010), show marked fluctuations to positive C-isotope values (between 3–6 ‰) prior to the negative CIE (Fig. 5). In the Newark Basin, the duration of this positive interval is thought to be c. 40 kyr based on cyclostratigraphy (Whiteside et al., 2010).

6.2. Mercury

In pre-industrial times, volcanic activity was one of the primary release mechanisms of mercury (Hg) to the atmosphere. In the marine realm, atmospheric Hg^0 is quickly oxidized to Hg^{2+}, which is scavenged by phytoplankton (Sanei et al., 2012). In the terrestrial realm, atmospheric Hg^0 is taken up directly through plant stomata, while some Hg may be incorporated in soils and then taken up by plant roots (Outridge et al., 2018). Chemostratigraphic mercury anomalies were first observed by Sanei et al., 2012 in a black shale succession deposited during the latest Permian extinction. The anomalies were explained as excess Hg deposition overwhelming the normal scavenging capacity of organic matter. Mercury anomalies are expressed as the anomalous increase in Hg/TOC over the typically constant background values. Sanei et al., 2012 attributed the anomalous temporal Hg/TOC pulses to a rise in global Hg in the biosphere during the period leading to and through the end-Permian extinction event caused by the eruption of the Siberian Traps (Sanei et al., 2012). Over the last two years, the use of Hg/TOC anomalies as a proxy for large scale volcanism alone, especially in marine sedimentary successions, has been met with some criticism as summarized in Grasby et al., 2019, and references therein. The fact that Hg/TOC-anomalies have been registered contemporaneously in a wide variety of depositional settings from marine (fully marine to marginal marine; carbonate-mixed to fully siliciclastic) to terrestrial environments during the ETME interval, argues strongly for the Hg to be derived from CAMP-volcanism (Lindström et al., 2019).

To date, three papers have published Hg records for the TJB interval. Thibodeau et al. (2016) analyzed Hg from the New York Canyon section in Nevada and found enhanced levels of Hg/TOC across the extinction interval, with values almost reaching 600 ppb/% TOC at some levels (Fig. 6). They also showed that Hg returned to background levels during most of the Hettangian and Sinemurian (Thibodeau et al., 2016). An extensive Hg study was carried out by Percival et al., 2017, who analyzed Hg from multiple sections; marine successions in the UK, Austria, and Argentina, as well as terrestrial successions from Greenland, Canada and Morocco, and concluded that Hg- and Hg/TOC-enrichment was contemporaneous with CAMP volcanism. Lindström et al., 2019 presented Hg- and Hg/TOC-records from the Danish and North German Basins, further demonstrating pulsed Hg-loading in a variety of depositional environments, including a terrestrial succession. The Hg/TOC records of New York Canyon (Thibodeau et al., 2016), Astartekløft, Kuhjoch and Fundy Basin (Percival et al., 2017), Stenlille-1 and Rødby-1 (Lindström et al., 2019), are presented in Fig. 6.

In the Fundy Basin, three levels with elevated Hg concentrations (up to 337 ppb) were found below the North Mountain Basalt (Percival et al., 2017) (Fig. 6). The Hg/TOC record shows exceptionally high values due to very low TOC values in this section, and therefore may be unreliable (Percival et al., 2017). It is, however, interesting to note that the high Hg/TOC levels also correlate with iridium and platinum anomalies in the same section (Tanner and Kyte, 2005; Tanner et al., 2008), and may thus be a primary signal of volcanic fallout despite the low TOC values (Tegner et al., 2020b). Based on the C-isotope record of the same section (Deenen et al., 2011; Percival et al., 2017), and in accordance with the stratigraphic framework herein, these levels correspond to intervals just prior to or during the onset of the extinction, i.e. Marshi CIE (Fig. 6). The Iguonane succession from below the lowest basalt in Morocco was only analyzed for Hg and not TOC and is therefore not discussed here (Percival et al., 2017). The Argentinian Hg/TOC record of Percival et al., 2017 is not shown on Fig. 6 as the position of the TJB is very uncertain in this section (Percival et al., 2017 supplementary text therein). However, Percival et al., 2017 show two levels of Hg/TOC enrichment prior to the FO of the ammonoid *Psiloceras rectocostatum,* which is correlated with the upper Planorbis Zone of Hillebrandt and Kment, 2015. The lower peak is associated with the beginning of a negative CIE (Percival et al., 2017).

In the Danish Basin, there also appears to be Hg enrichment and increased Hg/TOC values (220 ppb/% TOC) in the pre-extinction interval (Lindström et al., 2019). In the Kuhjoch section, high Hg/TOC values, reaching almost 400 ppb/% TOC, are found directly above the Marshi CIE (Percival et al., 2017), whereas, in the New York Canyon record Hg/TOC levels increase upsection from this level. In the Stenlille-1 record, only a moderate rise in Hg/TOC above background levels is registered right above the Marshi CIE, but in the Stenlille-4 record a marked peak of ~110 ppb/% TOC is registered (Lindström et al., 2019). These differences in the two records may be due to the more pristine condition of the Stenlille-4 core, i.e. the latter has previously only been sampled to a minor extent, while Stenlille-1 has been sampled for various purposes. The Hg- and Hg/TOC-records from the Danish Basin demonstrate that Hg-enrichment took place contemporaneously in both the marine and the terrestrial environments within the basin (Lindström

et al., 2019). A similar pattern was noted by Percival et al. (2017). From all these records it appears that Hg-loading is often restricted to very narrow time intervals, i.e. distal Hg-peaks may be easily missed when sampling.

6.3. Iridium, other platinum group elements (PGE), Os and Sr isotopes

Iridium anomalies have been recorded in sediments less than one meter below the North Mountain Basalt in the Fundy Basin (Tanner and Kyte, 2005; Tanner et al., 2008), and ~9–12 m below the Orange Mountain Basalt in the Newark Basin (Olsen et al., 2002; not on Fig. 7). In the Newark Basin, the data comes from four different sections. According to Olsen et al., 2002, the Ir anomalies are registered ~1 m above the LO of *Patinasporites densus* and other typical Triassic spores and pollen in the Exeter Member. Iridium anomalies have also been recorded within the upper Rhaetian of the Kurusu section in Japan (Hori et al., 2007), and within the uppermost Kössen Formation and the Tiefengraben Member, including the Schattwald beds, at Kuhjoch in Austria (Tanner et al., 2016), although the Kuhjoch section shows a protracted Ir enrichment during the extinction interval (Fig. 7). Iridium analyses from the terrestrial Kámien Pomorski TJB-succession in Poland did, however, not record any anomalies (Pieńkowski et al., 2011). Interestingly, the Ir anomalies in the Fundy Basin appear to occur approximately at the same levels as the Hg enrichments registered by Percival et al., 2017 (Figs. 6 and 7). Similarly, the onset of the Ir enrichment at Kuhjoch coincides with a marked increase in Hg/TOC, and a sharp Ir anomaly also occurs at the same level as the second increase in Hg/TOC (Figs. 6 and 7). In addition, the iridium anomalies in the Fundy Basin and the Kurusu section (Japan) are accompanied by peaks in other PGEs (e.g. Pt, Pd, Rh) (Tanner and Kyte, 2005; Hori et al., 2007). It has been debated whether the PGE anomalies relate to an extraterrestrial impactor (Olsen et al., 2002; Hori et al., 2007) or to CAMP volcanism (Tanner and Kyte, 2005; Tanner et al., 2008, 2016). Recently, it was shown that the fractionated nature of the PGEs (e.g. high Pt/Ir, Pd/Ir and Pt/Rh) of the ETME sediments matches those of the CAMP basalts and are inconsistent with chondritic or iron impactors (Tegner et al., 2020b).

Published osmium and strontium isotope records are difficult to interpret. This is due to complexities of these isotope systems and analytical and geological aspects, including: Os contents close to detection limit (e.g., Kuroda et al., 2010); possible diagenesis and alteration of the carbonates and fossil samples analyzed for Sr isotopes (e.g., Callegaro et al., 2012; Kovàcs et al., 2020); possible discrepancies between epicontinental, shallow or deep marine records, and a terrestrial record (e.g., Cohen and Coe, 2002, 2007; Pienkowski et al., 2011; Pienkowski et al., 2014; Kuroda et al., 2010).

In general, the Os and Sr isotopic records show some common aspects (Fig. 8). A decrease of the radiogenic component starts from the late Norian or early Rhaetian. This early shift is unlikely to be due to early CAMP magmatism, which is not known to have started before the late Rhaetian (e.g., Davies et al., 2017), but probably relates to global environmental or plate-organization changes. The lowest Os and Sr isotopic values are reached during the late Rhaetian in strata that are deposited during emplacement of the CAMP (Fig. 8). A subsequent shift towards higher $^{187}Os/^{188}Os$ and $^{87}Sr/^{86}Sr$ is observed close to the end of the Rhaetian or into the early Jurassic (e.g., Cohen and Coe, 2002, 2007; Callegaro et al., 2012; Kuroda et al., 2010; Kovács et al., 2020) in a time interval, which also corresponds to emplacement of the CAMP. These isotopic shifts may be due to fluctuations of CAMP activity, or, more likely, to increased weathering and erosion of continental rocks due to climate change induced by CAMP activity. Thus, the Sr and Os isotopic shifts seem to reflect general geological and environmental changes rather than being controlled exclusively by weathering and erosion of newly erupted basalts (Kovács et al., 2020). This is also consistent with the dominantly intrusive character of the CAMP.

Hori et al., 2007 suggested that the PGE and thus Os isotopic anomalies were the result of an extraterrestrial impact. However, the temporal-scale of the Os and Sr isotope trends, and the negative correlation between Os isotope ratios and elemental concentrations seem to be incompatible with an impactor as the source material (Tegner et al., 2020b).

6.4. Polycyclic aromatic hydrocarbons

Polycyclic aromatic hydrocarbons (PAHs) are highly toxic to living organisms. Increased levels of PAH's have been reported in TJB successions in Germany, Poland and Greenland (van de Schootbrugge et al., 2009; Marynowski and Simoneit, 2009; Williford et al., 2014) (Fig. 9), however the origin of these PAHs at the TJB is still debated. Pre-industrial, high levels of PAHs can be derived either from forest fires or from incomplete combustion of coal/organic matter through contact metamorphism. Nabbefeld et al., 2010 showed that pyrolytic PAHs, as a complement to charcoal data, can be used as a robust proxy for wildfires in pre-Anthropocene strata. Charcoal data have been used to doccument wildfires at the TJB in Poland, East Greenland and the Danish Basin (Marynowski and Simoneit, 2009; Belcher et al., 2010; Petersen and Lindström, 2012) (Fig. 9). Lindström et al., 2019 correlated and compared the charcoal records and Hg records of the Danish Basin and Greenland, but did not find a conclusive link between these two proxies. A high ratio of the combustion-ascribed coronene relative to benzo(a) pyrene has been used as evidence for a volcanic source (van de Schootbrugge et al., 2009; Williford et al., 2014). In Germany, the highest ratios of coronene/benzo(a)pyrene are registered in the uppermost Triletes beds, i.e. during the extinction interval, and around the Spelae CIE (Fig. 9). van de Schootbrugge et al. (2009) suggested that the high coronene/benzo(a)pyrene ratio was the result of incomplete combustion of organic-rich rocks intruded by CAMP basalts. However, the PAH data across the TJB in Poland were primarily interpreted as reflecting wildfires, based mainly on a correlation between charcoal abundance and PAH (Marynowski and Simoneit, 2009). Song et al., 2020 reported pyrolytic PAHs from the Sichuan Basin in Southwest China. In this succession, two levels with increased amounts of PAH were found, the lowest in the Rhaetian succession and the second interval occurred in the lower part of an interval assigned a Hettangian–Sinemurian age, both anomalies were interpreted as representing increased wildfires (Song et al., 2020).

In East Greenland, charcoal was found to be particularly abundant in plant bed 5B (Belcher et al., 2010) which, due to the presence of *Cerebropollenites thiergartii,* is close to the TJB (Fig. 9). Combustion-ascribed PAHs, specifically retene and coronene, were recorded in the Astartekløft succession by Williford et al., 2014. Retene in this section correlates strongly with charcoal abundances in the lower part of the succession (plant beds 1 to 5B), but not in the upper part (see Fig. 4 of Williford et al., 2014). Coronene increased in plant beds 4 and 5A, but a decreased in plant bed 5B (Williford et al., 2014). Despite these discrepancies, Williford et al., 2014 linked the PAHs to wildfire activity as the coronene to benzo(a)pyrene ratio was very low, ~0.33 on average, for the Astartekløft section. Thus, the currently available data seem to indicate that pyrolytic PAHs found during the extinction interval and in the earliest Jurassic may have been derived from both wildfires and incomplete combustion of organic-rich rocks intruded by CAMP basalts (Fig. 9).

6.5. SO_2 and acid rain

Several authors have suggested that the end-Triassic climate was affected by SO_2 emissions and associated acid rain from the CAMP, and that this could have caused a rapid cooling trend (Guex et al., 2004), soil acidification (van de Schootbrugge et al., 2009), induced stomatal closure and increased $\delta^{13}C$ values in trees and leaves (Lindström et al., 2012). However, because of the short residence time of sulfur in the atmosphere (see above under 4.3) direct evidence for these SO_2 emissions have not been presented (Guex et al., 2004; van de Schootbrugge

et al., 2009; Lindström et al., 2012). A first indication of the possibility of ecosystem perturbation produced by potentially CAMP-related high tropospheric levels of SO_2 at the TJ boundary was indicated by damage structures on fossil leaves from Greenland (Bacon et al., 2013; Elliot-Kingston et al., 2014) or soil acidification (van de Schootbrugge et al., 2009). A subsequent semi-quantitative assessment of SO_2 damages on Ginkgoalean and Bennettitalean fossil leaf cuticles from Astartekløft, show that acid rain was likely affecting the terrestrial ecosystem during the ETME and also immediately after the TJB (Steinthorsdottir et al., 2018) (Fig. 9). Steinthorsdottir et al. (2018) found that plant cuticles began to exhibit SO_2-damages already from plant bed 2, and increased in severity in plant beds 3 to 6 in the Astartekløft section, i.e. across the TJB (Fig. 9).

6.6. pCO_2 estimates from cuticles and pedogenic carbonate

Because land plants are in direct contact with the atmosphere, and exchange gases through their stomata, they respond directly to changes in atmospheric CO_2 concentration. The abundance or frequency of stomata per unit area of plant leaves are known to decrease with rising atmospheric CO_2-levels (Woodward, 1987), and this physiological response in plants to can therefore be used to calculate changes in pCO_2 in fossil plants. Stomatal proxy data from Greenland, Sweden, and Northern Ireland suggest global warming across the TJB (McElwain et al., 1999; Steinthorsdottir et al., 2011) (Fig. 10). McElwain et al. (1999) and a four-fold increase in atmospheric CO_2 at the TJB (from ca. 600 ppm to 2400 ppm; McElwain et al., 1999). These novel calculations were based on studies of stomatal density in fossil leaves (McElwain et al., 1999) and of oolitic goethites and pedogenic calcite from end-Triassic sections (Yapp and Poths, 1996). However, the stomatal density calculations were performed on plant fossils from Greenland and southern Sweden from museum collections, and represent a variety of taxa (McElwain et al., 1999). It should be noted that the stratigraphic order of the localities from southern Sweden was tentative. Based on published palynological records at the time, McElwain et al., 1999 also cautiously suggested that the *Ricciisporites – Polypodiisporites* Zone was missing in southern Sweden, something which was later proven incorrect (Lindström and Erlström, 2006).

Based on cuticles of *Lepidopteris ottonis,* Bonis et al. (2010a, 2010b) estimated a >1000 ppm increase in atmospheric CO_2 between the presumed Postera beds and the Contorta beds in the Wüstenwelsberg section (Fig. 10). In addition, this section also contains a minor drop in calculated CO_2 around some coal measures in the middle of the Contorta beds (Fig. 10). However, because *Lepidopteris* has no nearest living relative today, more pCO_2 calibrations between this and other fossil taxa are needed. To address the limitations of these previous studies, Steinthorsdottir et al. (2011) focused on plant cuticles from four phylogenetically distinct plant groups (*Ginkgo*, bennettites and two gymnosperms) that straddle the TJB in Greenland and Northern Ireland. Their study corroborated the occurrence of an increase in pCO_2, but their data suggested a doubling rather than a quadrupling across the TJB at both localities (Steinthorsdottir et al., 2011) (Fig. 10).

It has also been argued that atmospheric concentration of CO_2 at the time were so high that individual eruptions would have had a negligible climatic effect (Robock, 2000). Calculated changes in pCO_2 from stomatal proxy data, suggest a slow increase in atmospheric CO_2 during the middle Rhaetian with at least a doubling (Steinthorsdottir et al., 2011) in the latest Rhaetian and earliest Hettangian (Fig. 10). The CAMP magmatism and related mechanisms were initially suggested as a plausible source for this carbon input by McElwain et al., 1999.

Analyzing pedogenic carbonates in the Newark and Hartford basins, Schaller et al., 2011, Schaller et al., 2012, Schaller et al., 2016 reported a major increase in atmospheric CO_2 immediately after several of the magmatic episodes of the CAMP, but also a steady decrease in pCO_2 after each spike. C-isotope ratios of soil carbonate and organic matter from the eastern North American basins, indicate that Rhaetian pCO_2 values were declining steadily from a maximum around the Norian–Rhaetian to just before the eruption of the CAMP basalts (Schaller et al., 2012; Schaller et al., 2016). The atmospheric pCO_2 is estimated to have been below ~2000 ppm just before the onset of CAMP volcanism in the ENA basins, i.e. the Newark Basin containing the Orange Mountain Basalt and Hartford Basin containing the Talcott Basalt (Schaller et al., 2012, Schaller et al., 2016) (Fig. 10). Following each eruptive pulse of the CAMP the pCO_2 is estimated to have increased two- or threefold, declining relatively rapidly between each volcanic pulse but not returning to pre-CAMP values until around 200 Ma (Schaller et al., 2012) (Fig. 10). Schaller et al., 2012 interpreted the rapid decline in pCO_2 after each initial increase to be the result of increased weathering of freshly formed basalts.

6.7. n-alkane C-isotopes

Because land plants are in direct contact with the atmosphere, changes in compound specific C-isotopes from leaf wax derived lipids from land plants may reflect changes in the isotopic composition of $\delta^{13}C$ and pCO_2. However, changes in these n-alkane C-isotopes may also reflect changes in vegetation composition. To date, there are only a few published records of n-alkane C-isotopes across the TJB, and data is only available from odd n-alkanes. Because the odd n-alkane record from Astartekløft, Greenland, is limited to C25, C27 and C29 (Williford et al., 2014), we herein only show the compound specific C-isotopes from these n-alkanes from all records. The n-alkane record from Astartekløft (Williford et al., 2014) is consistent with the C_{wood}-isotope record of Hesselbo et al., 2002. It also mirrors the pCO_2 estimates derived from stomatal proxy record (Steinthorsdottir et al., 2011), and suggests increased input of light carbon to the atmosphere across the TJB (Fig. 10). The n-alkane record from St. Audrie's Bay (Whiteside et al., 2010), exhibits consistently decreasing C-isotope values from the middle to the upper Rhaetian. From the mass extinction interval below the Spelae CIE (i.e. the initial CIE of Hesselbo et al., 2002) and into the lowermost Hettangian, the n-alkane record fluctuates widely, but shows an overall similar trend to the Greenland record (Fig. 10). Overall, the n-alkane C-isotope record from the Newark Basin is also similar, although less clear, it contains a slight decrease from the middle Rhaetian to the Hettangian (Whiteside et al., 2010). The compound specific n-alkane record of Kuhjoch, Austria (Ruhl et al., 2011) only covers the upper part of the Marshi CIE and shows a subsequent ~7‰ negative shift at the onset of the mass extinction interval (Fig. 10). This negative CIE, the Marshi CIE, does not seem to correspond to the other n-alkane records, and may therefore have been driven entirely by changes in organic matter that would lead to artefacts in the n-alkane record (Fig. 10).

7. Discussion

7.1. Traces of the onset of CAMP

Figs. 4–10 review various types of data showing variations that have been ascribed to the volcanic activity of the CAMP. These data are presented using the same stratigraphical framework and so they can be used to distinguish trends that may allow more accurate interpretations of the effects of the CAMP. These effects are summarized in Fig. 11.

The organic C-isotope curves show significant differences between the continental Pangean records, the NW European epicontinental sea and the northern Tethys margin, and the deep sea Panthalassan records (Figs. 4 and 5). Increased input of ^{12}C to the atmosphere through volcanic degassing of CO_2 and methane from the CAMP and also thermogenically generated gasses from the intruded sediments should ultimately lead to negative shifts in the organic C-isotope curves, as plants and phytoplankton fractionate carbon in favor of ^{12}C. An ash layer in the Levanto section in Peru is dated by U-Pb geochronology to 201.87±0.17 Ma (Wotzlaw et al., 2014), which constrains the lower part of the Peruvian organic C-isotope curve published in Yager et al., 2017

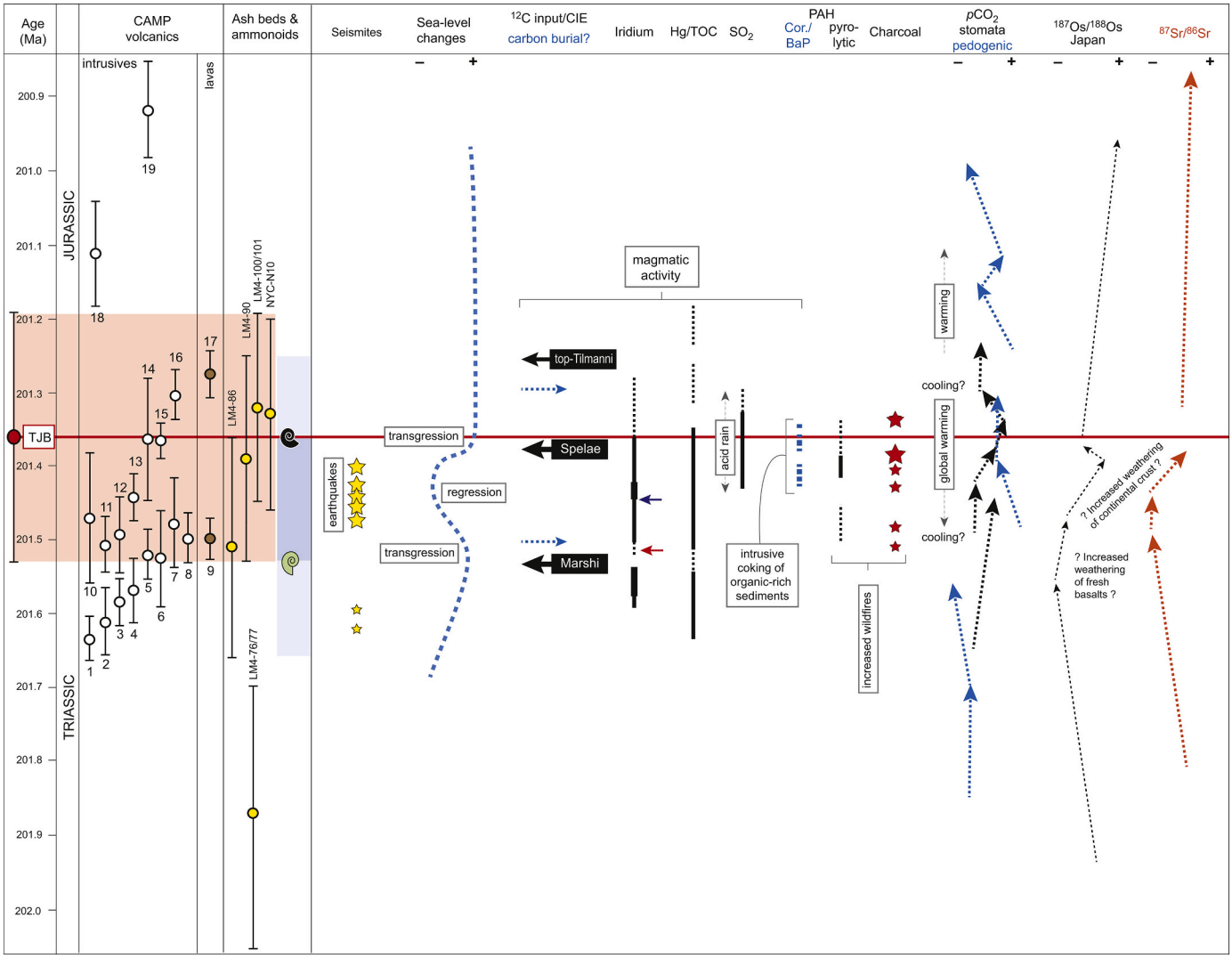

Fig. 11. A synthesis of Figs. 4–10. Yellow stars denote seismites. Red stars mark relative charcoal abundance. Small red arrow represents clay spherules and pseudomorphs interpreted to be of volcanic origin by Pálfy and Zajzon 2010. Small blue, non-stipled arrow marks level of basaltic fragments in the Kurusu section by Hori et al., 2007.

(Fig. 5). Close to the ash bed, organic C-isotopes display negative values just above –30 ‰, but subsequently increase to around–28 ‰ up to the level of the last occurrence of *Choristoceras crickmayi* (Yager et al., 2017) (Fig. 5). A similar, but more pronounced drop of 3‰ is also evident in the record from Kennecott Point between the LO of *C. crickmayi* and the last occurrence of ammonoids assigned to *Choristoceras* (Fig. 5). In the Japanese deep sea Panthalassic record from Katsuyama, two intervals with very positive C-isotope values are separate by a negative CIE in the upper part of the *Haeckelicyrtium breviora* Zone, which can be correlated to the upper part of the *Marshi* Zone (Fujisaki et al., 2018) (Figs. 3 and 5). A similar trend is also present in the New York Canyon record from Nevada, although this record does not extend far into the middle Rhaetian (Guex et al., 2004; Ward et al., 2007; Guex et al., 2008; Thibodeau et al., 2016). Although there are some differences between these records, there appears to be a slight negative trend upsection from positive middle Rhaetian C-isotopes in Panthalassa (Fig. 5). Even the organic C-isotope records from the immediate CAMP area suggest more positive values during the middle Rhaetian (Whiteside et al., 2010; Deenen et al., 2011; Dal Corso et al., 2014). In the NW European epicontinental sea and northern Tethys margin, records that extend into the middle Rhaetian show a similar although perhaps less pronounced, slight decreasing trend upsection (Fig. 4). The noted differences between the middle Rhaetian sections in various areas could be a result of differences in sample density. However, it should to be noted that the only record that has independent age constraints is the Peru record (Wotzlaw et al., 2014; Yager et al., 2017). So, it is possible that the negative trend upsection during the middle Rhaetian is an expression of increased output of light carbon from CAMP. The currently oldest dated CAMP intrusive is the Kakoulima intrusion in Guinea (201.635±0.029 Ma; Davies et al., 2017) (Fig. 2). The organic C-isotope records below the oldest basalts in Morocco, Fundy Basin and other the eastern North American basins exhibit highly fluctuating values, which may be related to outgassing from hitherto undated (and unknown) CAMP extrusives or from intrusive activity with venting from contact metamorphic reactions between magma and organic-rich sediments. The iridium record from the Fundy Basin (Tanner and Kyte, 2005; Tanner et al., 2008) seem to indicate ongoing volcanic activity even before the preserved lava flows of that basin, but Tanner et al. (2008) also discussed remobilization of Ir from the overlying basalt as a possibility. An early onset of magmatism is suggested by the Hg/TOC record from Stenlille (Figs. 6 and 11).

7.2. Traces at the Marshi CIE and the onset of the mass extinction

The C_{org}-isotope values reached a minimum during the Marshi CIE

(Lindström et al., 2017b) in most areas, except in western Canada and Peru (Figs. 4 and 5). The negative peak itself appears to be of short duration and may therefore be easily missed unless high-resolution sampling has been carried out. The amplitude of this negative CIE is clearly related to the composition of the organic material at each site, and may thus not just reflect the amount of light carbon emitted to the atmosphere. However, it is interesting that despite a marked shift in organic matter within the Marshi CIE at Kuhjoch, from terrestrial dominated in the lower half of the CIE to a dominance of marine prasinophyte algae in its upper half, the $\delta^{13}C$ values remained low (Ruhl et al., 2010). In contrast to the NW European and Tethyan records, $\delta^{13}C$ records from Peru and western Canada appear to decrease from this point (Fig. 5). There is also an uncertainty that should be considered in the correlation between the Peru record and the general fossil record at this level. The ash layer LM4-86 dated to 201.51±0.15 Ma (Schoene et al., 2010; Wotzlaw et al., 2014), post-dates the LO of *Choristoceras crickmayi* in the Peru section, but including the uncertainties, could be as old as 201.66 Ma, older than any CAMP extrusive (Fig. 2). In that case, the most negative point on the Peru record could correlate with the Marshi CIE in other areas. However, it could also correlate to the Spelae CIE, following the same line of reasoning.

In areas where the onset of the extinction in marine invertebrates is well described, the Marshi CIE appears to immediately precede or coincide with the onset of the extinction. This is particularly clear at Kuhjoch (Hillebrandt et al., 2013) and in Nevada (Guex et al., 2004). At Kuhjoch, an increase in iridium from virtually 0 to around 30 ppt is registered during the onset of the Marshi CIE and just after the CIE minimum, iridium reaches ~80 ppt (Tanner et al., 2016) (Fig. 6). In the Panthalassic deep sea record of Japan a marked but brief 70 ppt iridium peak is registered at the same level (Hori et al., 2007) (Fig. 6). The Marshi CIE also marks the onset of Hg-loading in many areas, expressed both in Hg- and Hg/TOC records globally, even though there are indications of Hg-loading prior to the Marshi CIE in some areas (Thibodeau et al., 2016; Percival et al., 2017; Lindström et al., 2019) (Fig. 5 and 11). Thus, both the iridium and the Hg-record indicate increased extrusive activity from this point (Fig. 11), which is in agreement with previous studies (Thibodeau et al., 2016; Percival et al., 2017; Lindström et al., 2019; Tegner et al., 2020b). These anomalies appear to coincide with decreasing Os and Sr isotope values, up to around the Marshi CIE (Fig. 11). Minima in the Os-isotope record from Japan (Kuroda et al., 2010) as well as the Sr isotopes around and just above the Marshi CIE, may reflect weathering of fresh basalts from the CAMP and thus input of unradiogenic Os and Sr to the ocean, as suggested by Callegaro et al. (2012). At this level pedogenic carbonate indicate global warming following the oldest dated extrusives in the Eastern North America (Schaller et al., 2012; Fig. 11).

7.3. Tracers during the mass extinction interval, prior to the Spelae CIE

This onset of global warming appears to have coincided with increased wildfire activity and formation of pyrolytic PAHs in Greenland, Poland and the Danish Basin (Fig. 11). At the same time during the mass extinction interval, the NW European epicontinental sea area, and possibly also the northern Tethys margin experienced repeated earthquake activity, likely caused by crustal tension due to CAMP activity (Lindström et al., 2015). A marked regression is evident during this interval in many sedimentary records from the NW European epicontinental sea area, as well as in Nevada (Hallam, 1997; Hallam and Wignall, 1999, 2000; Lindström et al., 2017b) (Fig. 11). This regression coincided with increased weathering and erosion based on a signal of increased reworking in the Danish and North German basins (Lindström et al., 2012; van de Schootbrugge et al., 2020). The regression, as well as the seismites, possibly reflects tectonic/epirogenic activity due to CAMP emplacement (Hallam and Wignall, 1999) (Fig. 11).

A pCO_2-record from pedogenic carbonate above the Palisades sill/Orange Mountain Basalt indicates a period of rapid warming, followed quickly by cooling, which is thought to reflect CO_2 drawdown through amplified continental silicate weathering of the basalts (Schaller et al., 2012) (Fig. 11). The $\delta^{13}C_{org}$-records from the NW European epicontinental sea and the northern Tethys margin seem to corroborate on-going CO_2-drawdown, as they exhibit more positive values, but often fluctuating, during the extinction interval (Fig. 11). However, this is not evident in the sections from Haida Gwaii and Peru, but seems to be consistent with the data from New Zealand, Japanese, Nevada and New York Canyon (Fig. 5).

The n-alkane isotope records also seem to indicate carbon burial at the onset of the mass extinction interval, followed by strongly fluctuating values indicating a highly unstable C-cycle (Fig. 10 and 11). In the stomatal proxy records a decrease in atmospheric pCO_2 in the record from Germany (Bonis et al., 2010a), may correspond to a drop in the n-alkane C-isotope records after the Marshi CIE (Fig. 10 and 11). The drop in pCO_2 at this level appears short-lived on Fig. 10, but its association with coal mire deposition means it probably equates to a longer time interval. This could be in line with modelled climate effects of SO_2 and CO_2, suggesting that a first Marshi-event volcanic pulse could have caused a ~10^2–10^3 yr phase of global cooling and high climate variability, followed by a subsequent global warming (Landwehrs et al., 2020). SO_2-damage on cuticles has, however, so far only been detected during the latter part of the mass extinction interval, but before when cuticles of land plants in Greenland begin to show evidence of increased pCO_2 (McElwain et al., 1999; Steinthorsdottir et al., 2011; Steinthorsdottir et al., 2018) (Fig. 11).

Wildfires; as indicated by the presence of pyrolitic PAH and charcoal from the Danish Basin, Poland, Greenland and also China, appear to have increased in abundance during the late Rhaetian (Marynowski and Simoneit, 2009; Belcher et al., 2010; Petersen and Lindström, 2012; Song et al., 2020), further corroborating a global warming scenario. Both the Sr and Os isotope records appear to increase slightly up to the Spelae CIE (Fig. 11), and this may indicate increased weathering and erosion of continental crust. Around this time, high ratios of coronene/benzo(a)pyrene likely indicate intrusive coking of organic-rich sediments by CAMP (van de Schootbrugge et al., 2009) (Fig. 11). Modelling by Heimdal et al., 2019, Heimdal et al., 2020) show that thermogenic release of ^{12}C from sill emplacement in evaporitic, organic-rich and oil prone sediments in the Trans-Amazonian basin is a credible source for the three negative CIEs, but also for SO_2 emissions. So far only four sills from the Trans-Amazonian basin have been dated, namely the sills numbered 6, 7, 10 and 15 on Fig.s 2, 4–11 (Davies et al., 2017; Heimdal et al., 2018), and these overlap in time with the Marshi and Spelae CIEs.

7.4. Traces at the Spelae CIE and across the TJB

In the NW European epicontinental sea area a transgression occurred just prior to the Spelae CIE, and in some areas this resulted in condensed strata or a hiatus (Lindström et al., 2017). The transgression in the NW European epicontinental sea definitely affected the composition of organic matter in the sediments, and this may have had an influence on the amplitude of the Spelae CIE. Continued input of Ir and Hg to the depositional systems indicate on-going volcanic activity at this time (Fig. 11). Likewise, the continued presence of pyrolytic PAH and elevated coronene/benzo(a)pyrene across the TJB point to continued wildfires as well as intrusive activity at this stage (Fig. 10). On-going volcanic degassing is further suggested by continued SO_2-damage to plants in Greenland and further increased pCO_2 during the Spelae CIE (Fig. 11). Most of the seismic activity in NW Europe ceased after this time.

After the Spelae CIE C-isotope records from the NW European epicontinental sea and the northern Tethys margin exhibit more positive values (Fig. 4). Contemporaneously, relatively heavy $\delta^{18}O$ values in oysters in the Langport Member in southwestern UK have been interpreted to reflect a brief cooling episode triggered by volcanism (Korte et al., 2009), followed by a subsequent slow warming during the

lowermost part of the succeeding Blue Lias Formation. The cooling episode in the Langport Member appears to correspond with the stomatal proxy record from Greenland, but not with the one from Northern Ireland (Steinthorsdottir et al., 2011). Soil carbonate data from the Newark Basin show a decrease in pCO_2 possibly at a higher level (Schaller et al., 2012; Schaller et al., 2016)(Fig. 10 and 11). In addition, the n-alkane C-isotope record from the UK and Greenland show heavier values at this stage (Whiteside et al., 2010; Williford et al., 2014) (Fig. 10).

At the top-Tilmanni CIE $\delta^{13}C_{org}$ values again become more depleted in records from NW Europe, the Tethys and Nevada (Figs. 4–5). The top-Tilmanni CIE appears to be the onset of a longer interval, perhaps a new steady state, with values generally more negative than prior to the Marshi CIE (Figs. 4–5). At the top-Tilmanni CIE psiloceratid ammonoids were beginning to diversify (Hillebrandt and Krystyn, 2009), and the terrestrial floras had stabilized both on the northern and southern hemispere (Lindström, 2016).

The records from Newark Basin, Haida Gwaii, Peru and New Zealand, on the other hand, do not appear to display a similar trend (Fig. 5), but the reason for this is unclear. The n-alkane C-isotope record from the UK, also indicates continuously depleted values at this time, but the Newark/Hartford basins n-alkane record displays depleted values above the Preakness Basalt but higher up the record show wildly fluctuating values (Whiteside et al., 2010) (Fig. 10). Similarly, after initially high pCO_2 values from pedogenic carbonate above the Preakness Basalt, pCO_2 slowly decrease upsection with ~2000 ppm (Schaller et al., 2012).

By the onset of the top-Tilmanni CIE (Lindström et al., 2017), input of iridium to the sedimentary system appears to have ceased, but it should be noted that younger Hettangian strata have not been tested for Ir. Minor mercury-anomalies occur sporadically around this level and appear to testify to on-going but weakened CAMP volcanic activity in the early Hettangian (Fig. 11). In the Nevada record Hg-loading drops markedly in the upper Planorbis Ammonite Zone, only displaying background values in to the Sinemurian (Thibodeau et al., 2016). This is in line with the youngest dated CAMP rock, the Butner Intrusive, which has yielded a U-Pb age of 200.916±0.064 Ma (Blackburn et al., 2013), i.e. ~mid-Hettangian. It should be noted that combined geochronologic and biostratigraphic data (e.g., Blackburn et al., 2013; Davies et al., 2017; Panfili et al., 2019; Marzoli et al., 2019) suggest that the Tiourjdal and in particular the Prevalent group (Marzoli et al., 2018) where emitted early in the history of CAMP, probably close to the Marshi CIE. This early activity was probably the most voluminous and had probably the largest impact on the environment and biosphere as also supported by high CO_2 contents found in these basalt groups (Capriolo et al., 2020). Subsequent magmatic activity, between the Marshi and Spelae CIES are represented by the volcanic products of Holyoke group and possibly by intrusive activity in Brazil and northwestern Africa (Blackburn et al., 2013; Davies et al., 2017).

8. Conclusions

During the last decade improved geochronological dating of both CAMP basalts and lavas, and ash beds in sedimentary successions containing biostratigraphically useful fossils has led to refined calibration of the timescale. This has improved our understanding of the timing, duration and impact of this large igneous province. However, for most sedimentary successions it is not possible to geochronologically tie changes in sediment proxy records to the CAMP, which is why correlations must rely solely on biostratigraphy and geochemical traces of volcanism. Changes in sedimentation rate, possible sedimentary gaps and the incompleteness of the fossil record are to be taken into account when correlating. These points are crucial to come to a full understanding the impact of the CAMP on the biosphere and climate. When bringing together geochronology of the CAMP, fossil events and geochemical indicators of volcanic activity across the end-Triassic mass extinction interval and into the earliest Hettangian, it is possible to construct a coherent succession of events for this major crisis. Mercury and iridium indicate CAMP volcanic activity was occurring prior to the oldest known (preserved) basalt (the Lower unit of the Tiourjdal group in Morocco), and before the Marshi CIE and the last occurrence of Triassic ammonoids (*Choristoceras*) that mark the onset of the mass extinction interval in the marine realm. Decreasing Sr and Os isotope values up to the Marshi CIE, may reflect weathering of fresh basalts, but may also be related to more long-term geological or environmental factors. The Marshi CIE signals input of light carbon to the atmosphere and may coincide in time with extrusives of the Tiourjdal and Prevalent groups of CAMP. Pedogenic carbonate nodules below and above the Orange Mountain Basalt of the Prevalent Group indicate a more than twofold pCO_2 increase in the atmosphere at this time. At the same time stomatal proxy data from Germany and n-alkane C-isotope records from the Newark Basin, Austria and the UK suggest an at least temporary cooling, which may be consistent with climate models incorporating both volcanic emissions of CO_2 and SO_2. Hg and Ir data continue to indicate on-going volcanism during the mass extinction interval, and after the possible short-term cooling several proxies point to rising global temperatures: such as records of pyrolytic PAH and increased abundances of charcoal indicating increased wildfire activity; increased Os and Sr isotopes indicating increased weathering of continental crust; and increased pCO_2 levels in both pedogenic carbonate and stomatal proxy data indicating global warming, which culminated across the Spelae CIE. High coronene/benzo(a)pyrene that may have formed through incomplete combustion of organic-rich sediments by intruding lavas, as well as plant cuticle damage from sulfuric acid rain, are recorded in the later stages of the mass extinction interval and across the Spelae CIE. These proxies suggest that thermogenic release of light carbon and sulfur from sill intrusions in the Trans-Amazonian basin, where both evaporites and organic-rich sediments are known to have been intruded, may have played a part at this time. Global warming during the Spelae CIE seems to be succeeded by another short-term cooling event, indicated by stomatal proxy data from Greenland and n-alkane C-isotope data from the UK. This cooling event has previously been suggested by oxygen isotope data from carbonate fossils in the UK. Hg and Ir signals appear to weaken at this point, although sporadic minor loading peaks in Hg through the lower Hettangian may indicate later phases of CAMP volcanism. A gradual decrease in $\delta^{13}C$ culminates at the top-Tilmanni CIE, which seems to be the beginning of a long-term steady state with more negative C-isotope values than prior to the ETME. At this time, psiloceratid ammonoids are diversifying and terrestrial ecosystems appear to have stabilized.

It seems clear that the organic C-isotope record contains several pulses of input of light carbon to the atmosphere across the ETME and the TJB. These signals may be hampered or amplified by the composition of the organic matter analyzed in individual successions. However, when combined with traces of volcanic activity in the sedimentary record a more detailed chain of events can be deduced. It should be noted that many of these records are from one or a few localities only, and more and consistent data is needed from successions that cover not only the ETME, but also the middle Rhaetian to Upper Hettangian, in order to fully constrain the impacts of CAMP activity on the sedimentary record.

Declaration of Competing Interest

The authors declare that they have no known competing financial interests or personal relationships that could have appeared to influence the work reported in this paper.

Acknowledgements

This paper was supported by Geocenter Denmark grant 6-2013 to SL. SL publishes with the permission of the Director of the Geological Survey of Denmark and Greenland. N.Y. is supported by Megagrant 14. Y26.31.0012, Russian Federation from the government of the Russian

Federation. A.M. acknowledges financial support from MIUR, PRIN grant 20178LPCP, Italy. J.D acknowledges financial support from the NSERC, Canada, discovery grant RGPIN-2019-07078. S.C. is funded by the Research Council of Norway, young researcher "MAPLES" (project number 301096). The authors would like to sincerely thank the detailed and helpful comments we received from two reviewers, and also the patience, perseverance and helpful comments given by the guest editors Thomas Algeo.

References

Aarnes, I., Svensen, H., Connolly, J.A.D., Podladchikov, Y.Y., 2010. How contact metamorphism can trigger global climate changes: modeling gas generation around igneous sills in sedimentary basins. Geochim. Cosmochim. Acta 74, 7179–7195.

Ahlberg, A., Arndorff, L., Guy-Ohlson, D., 2002. Onshore climate change during the late triassic marine inundation of the Central European Basin. Terra Nova 14, 241–248.

Aiuppa, A., Baker, D.R., Webster, J.D., 2009. Halogens in volcanic systems. Chem. Geol. 263, 1–18.

Akikuni, K., Hori, R.S., Vajda, V., Grant-Mackie, J.A., Ikehara, M., 2010. Stratigraphy of Triassic–Jurassic boundary sequences from the Kawhia coast and Awakino gorge, Murihiku Terrane, New Zealand. Stratigraphy 7, 7–24.

Archer, D., 2005. Fate of fossil fuel CO_2 in geologic time. J. Geophys. Res. Oceans 110 (C9).

Bachan, A., Payne, J.L., 2016. Modelling the impact of pulsed CAMP volcanism on pCO_2 and $\delta^{13}C$ across the Triassic–Jurassic transition. Geol. Mag. 153, 252–270.

Backhouse, J., Balme, B.E., Helby, R., Marshall, N.G., Morgan, R., 2002. 2002. Palynological zonation and correlation of latest Triassic, Northern Carnarvon Basin. In: Keep, M., Moss, S.J. (Eds.), The Sedimentary Basins of Western Australia 3, Proceedings of the Petroleum Exploration Society of Australia, Symposium, Perth WA, pp. 13–24.

Bacon, K.L., Belcher, C.M., Haworth, M., McElwain, J.C., 2013. Increased atmospheric SO_2 detected from changes in leaf physiognomy across the Triassic–Jurassic boundary interval of East Greenland. PLoS One 8, e60614.

Barry, P.H., Hilton, D.R., Füri, E., Halldórsson, S.A., Grönvold, K., 2014. Carbon isotope and abundance systematics of Icelandic geothermal gases, fluids and subglacial basalts with implications for mantle plume-related CO_2 fluxes. Geochim. Cosmochim. Acta 134, 74–99.

Beerling, D.J., Berner, R.A., 2002. Biogeochemical constraints on the Triassic-Jurassic boundary carbon cycle event. Global Biogeochem. Cycles 16.

Belcher, C.M., Mander, L., Rein, G., Jervis, F.X., Haworth, M., Hesselbo, S.P., Glasspool, I. J., McElwain, J.C., 2010. Increased fire activity at the Triassic/Jurassic boundary in Greenland due to climate-driven floral change. Nat. Geosci. 3, 426–429.

Benca, J.P., Duijnstee, I.A.P., Looy, C.V., 2018. UV-B–induced forest sterility: Implications of ozone shield failure in Earth's largest extinction. Science Advances 4, e1700618.

Berner, R.A., Beerling, D.J., 2007. Volcanic degassing necessary to produce a $CaCO_3$ undersaturated ocean at the Triassic-Jurassic boundary. Palaeogeogr. Palaeoclimatol. Palaeoecol. 244, 368–373.

Bertrand, H., 1991. 5. The Mesozoic Tholeiitic Province of Northwest Africa: A Volcano-Tectonic Record of the Early Opening of Central Atlantic. In: Kampunzu, A.B., Lubala, R.T. (Eds.), Magmatism in Extensional Structural Setting. Springer, New York, pp. 147–191.

Bertrand, H., Fornari, M., Marzoli, A., Garcia-Duarte, R., Sempere, T., 2014. The Central Atlantic Magmatic Province extends into Bolivia. Lithos 188, 33–43.

Black, B.A., Gibson, S.A., 2019. Deep carbon and the life cycle of Large Igneous Provinces. Elements 15, 319–324.

Black, B.A., Elkins-Tanton, L.T., Rowe, M.C., Ukstins Peate, I., 2012. Magnitude and consequences of volatile release from the Siberian Traps. Earth Planet. Sci. Lett. 317–318, 363–373.

Black, B.A., Hauri, E.H., Elkins-Tanton, L.T., Brown, S.M., 2014. Sulfur isotopic evidence for sources of volatiles in Siberian Traps magmas. Earth Planet. Sci. Lett. 394, 58–69.

Blackburn, T.J., Olsen, P.E., Bowring, S.A., McLean, N.M., Kent, D.V., Puffer, J., McHone, G., Rasbury, E.T., Et-Touhami, M., 2013. Zircon U-Pb Geochronology Links the End-Triassic Extinction with the Central Atlantic Magmatic Province. Science 340, 941–945.

Blake, S., Self, S., Sharma, K., Sephton, S., 2010. Sulfur release from the Columbia River Basalts and other flood lava eruptions constrained by a model of sulfide saturation. Earth Planet. Sci. Lett. 299, 328–338.

Blakey, R., 2014. http://cpgeosystems.com/paleomaps.html.

Bond, D.P.G., Wignall, P.B., 2014. Large igneous provinces and mass extinctions: an update. In: Keller, G., Kerr, A.C. (Eds.), Volcanism, Impacts, and Mass Extinctions : Causes and Effects, 505. The Geological Society of America, pp. 29–55. Spe. Paper.

Bonis, N.R., Kürschner, W.M., Krystyn, L., 2009. A detailed palynological study of the Triassic–Jurassic transition in key sections of the Eiberg Basin (Northern Calcareous Alps, Austria). Rev. Palaeobot. Palynol. 156, 376–400.

Bonis, N.R., van Konijnenburg, C.J.H.A., Kürschner, W.M., 2010a. Changing CO2 conditions during the end-Triassic inferred from stomatal frequency analysis on *Lepidopteris ottonis* (Goeppert) Schimper and *Ginkgoites taeniatus* (Braun) Harris. Palaeogeogr. Palaeoclimatol. Palaeoecol. 295, 146–161.

Bonis, N.R., Ruhl, M., Kürschner, W.M., 2010b. Milankovitch-scale palynological turnover across the Triassic–Jurassic transition at St. Audrie's Bay, SW UK. J. Geol. Soc. London 167, 877–888.

Brown, E.L., Lesher, C.E., 2014. North Atlantic magmatism controlled by temperature, mantle composition and buoyancy. Nat. Geosci. 7, 820–824.

Callegaro, S., Rigo, M., Chiaradia, M., Marzoli, A., 2012. Latest Triassic marine Sr isotopic variations, possible causes and implications. Terra Nova 24, 130–135.

Callegaro, S., Marzoli, A., Bertrand, H., Chiaradia, M., Reisberg, L., Meyzen, C., Bellieni, G., Weems, R.E., Merle, R., 2013. Upper and lower crust recycling in the source of CAMP basaltic dykes from southeastern North America. Earth Planet. Sci. Lett. 376, 186–199.

Callegaro, S., Rapaille, C., Marzoli, A., Bertrand, H., Chiaradia, M., Reisberg, L., Bellieni, G., Martins, L., Madeira, J., Mata, J., Youbi, N., De Min, A., Azevedo, M.R., Bensalah, M.K., 2014a. Enriched mantle source for the Central Atlantic magmatic province: new supporting evidence from Southwestern Europe. Lithos 188, 15–32.

Callegaro, S., Baker, D.R., De Min, A., Marzoli, A., Geraki, K., Bertrand, H., Viti, C., Nestola, F., 2014b. Microanalyses link sulfur from large igneous provinces and Mesozoic mass extinctions. Geology 42, 895–898.

Callegaro, S., Marzoli, A., Bertrand, H., Blichert-Toft, J., Reisberg, L., Cavazzini, G., Jourdan, F., Davies, J., Parisio, L., Bouchet, R., Paul, A., Schaltegger, U., Chiaradia, M., 2017. Geochemical constraints provided by the Freetown Layered Complex (Sierra Leone) on the origin of high-Ti tholeiitic CAMP magmas. J. Petrol. 58, 1811–1840.

Capriolo, M., Marzoli, A., Aradi, L.E., Callegaro, S., Dal Corso, J., Newton, R.J., Mills, B.J. W., Wignall, P.B., Bartoli, O., Baker, D.R., Youbi, N., Remusat, L., Spiess, R., Szabó, C., 2020. Deep CO_2 in the end-Triassic Central Atlantic Magmatic Province. Nat. Commun. 11, 1670.

Carter, E.S., 1993. Biochronology and paleontology of uppermost Triassic (Rhaetian) radiolarians, Queen Charlotte Islands, British Columbia, Canada. Mémoires de Géologie, Lausanne, 11, 175 pp., 21 pls.

Carter, E.S., Hori, R.S., 2005. Global correlation of the radiolarian faunal change across the Triassic–Jurassic boundary. Can. J. Earth Sci. 42, 777–790.

Chenet, A.-L., Fluteau, F., Courtillout, V., 2005. Modelling massive sulphate aerosol pollution following the lagre 1783 Laki basaltic eruption. Earth Planet. Sci. Lett. 236, 721–731.

Chenet, A.-L., Fluteau, F., Courtillot, V., Gerard, M., Subbarao, K.V., 2008. Determination of rapid Deccan eruptions across the KTB using paleomagnetic secular variation II: Results from a 1200-m-thick section in the Mahabaleshwar escarpment. J. Geophys. Res. 113, B04101, 27 pp.

Cirilli, S., Marzoli, A., Tanner, L., Bertrand, H., Buratti, N., Jourdan, F., Bellieni, G., Kontak, D., Renne, P.R., 2009. Latest Triassic onset of the Central Atlantic Magmatic Province (CAMP) volcanism in the Fundy Basin (Nova Scotia): New stratigraphic constraints. Earth Planet. Sci. Lett. 286, 514–525.

Clemence, M.-E., Bartolini, A., Gardin, S., Paris, G., Beaumont, V., Page, K.N., 2010. Early Hettangian benthic-planktonic coupling at Doniford (SW England): Palaeoenvironmental implications for the aftermath of the end-Triassic crisis. Palaeogeogr. Palaeoclimatol. Palaeoecol. 295, 102–115.

Cohen, A.S., Coe, A.L., 2002. New geochemical evidence for the onset of volcanism in the Central Atlantic Magmatic Province and environmental change at the Triassic–Jurassic boundary. Geology 30, 267–270.

Cohen, A.S., Coe, A.L., 2007. The impact of the Central Atlantic Magmatic Province on climate and on the Sr- and Os-isotope evolution of seawater. Palaeogeogr. Palaeoclimatol. Palaeecol. 244, 374–390.

Coltice, N., Phillips, B.R., Bertrand, H., Ricard, Y., Rey, P., 2007. Global warming of the mantle at the origin of flood basalts over supercontinents. Geology 35, 391–394.

Courtillot, V., 1999. Evolutionary Catastrophes: The Science of Mass Extictions. Cambridge University Press, Cambridge, UK, 173 p.

Dal Corso, J., Marzoli, A., Tateo, F., Jenkyns, H.C., Bertrand, H., Youbi, N., Mahmoudi, A., Font, E., Buratti, N., Cirilli, S., 2014. The dawn of CAMP volcanism and its bearing on the end-Triassic carbon cycle disruption. J. Geol. Soc. London 171, 153–164.

Davies, J., Marzoli, A., Bertrand, H., Youbi, N., Ernesto, M., Schaltegger, U., 2017. End-Triassic mass extinction started by intrusive CAMP activity. Nat. Commun. 8, 15596.

Dal Corso, Jacopo, Bernardi, Massimo, Sun, Yadong, Song, Haijun, Seyfullah, Leyla J., Preto, Nereo, Gianolla, Piero, Ruffell, Alastair, Kustatscher, Evelyn, Roghi, Guido, Merico, Agostino, Hohn, Sönke, Schmidt, Alexander R., Marzoli, Andrea, Newton, Robert J., Wignall, Paul B., Benton, Michael J., 2018. Extinction and dawn of the modern world in the Carnian (Late Triassic). . Science Advances 8, EABA0099. https://doi.org/10.1016/j.earscirev.2018.07.004.

De Jersey, N.J., McKellar, J.L., 2013. The palynology of the Triassic–Jurassic transition in southeastern Queensland, Australia, and correlation with New Zealand. Palynology 37, 77–114.

De Min, A., Piccirillo, E.M., Marzoli, A., Bellieni, G., Renne, P.R., Ernesto, M., Marques, L. S., 2003. The Central Atlantic Magmatic Province (CAMP) in Brazil: Petrology, geochemistry, 40Ar/39Ar ages, paleomagnetism and geodynamic implications. In: Hames W, McHone G, Renne, P.R., Ruppel, C. (Eds.), The Central Atlantic magmatic province: Insights from fragments of Pangaea. Am. Geophys. Un. Geophys. Monogr. 136, 91–128.

Deenen, M.H.L., Ruhl, M., Bonis, N.R., Krijgsman, W., Kuerschner, W.M., Reitsma, M., van Bergen, M.J., 2010. A new chronology for the end-Triassic mass extinction. Earth Planet. Sci. Lett. 291, 113–125.

Deenen, M.H.L., Krijgsman, W., Ruhl, M., 2011. The quest for chron E23r at Partridge Island, Bay of Fundy, Canada: CAMP emplacement postdates the end-Triassic extinction event at the North American craton. Can. J. Earth Sci. 48, 1282–1291.

Dickens, G.R., Oneil, J.R., Rea, D.K., Owen, R.M., 1995. Dissociation of oceanic methane hydrate as a cause of the carbon-isotope excursion at the end of the Paleocene. Paleoceanography 10, 965–971.

Du, Y., Chiari, M., Karádi, V., Nicora, A., Onoue, T., Pálfy, J., Roghi, G., Tomimatsu, Y., Rigo, M., 2020. The asynchronous disappearance of conodonts: New constraints

from Triassic–Jurassic boundary sections in the Tethys and Panthalassa. Earth Sci. Rev. 203, 103176.
Dunning, G.R., Hodych, J., 1990. U/Pb zircon and baddeleyite ages for the Palisades and Gettysburg sills of the northeastern United States: Implications for the age of the Triassic/Jurassic boundary. Geology 18 (8), 795–798. https://doi.org/10.1130/0091-7613(1990)018<0795:UPZABA>2.3.CO;2.
Edmonds, M., Wallace, P., 2017. Volatiles and exsolved vapor in volcanic systems. Elements 13, 29–34.
El Hachimi, H., Youbi, N., Madeira, J., Bensalah, M.K., Martins, L., Mata, J., Bertrand, H., Marzoli, A., Medina, F., Munhá, J., Bellieni, J., Mahmoudi, A., Ben Abbou, M., Assafar, H., 2011. Morphology, internal architecture, and emplacement mechanisms of lava flows from the Central Atlantic Magmatic Province (CAMP) of Argana basin (Morocco). In: Van Hinsbergen, D.J.J., Buiter, S., Torsvik, T.H., Gaina, C., Webb, S. (Eds.), Out of Africa–A synopsis of 3.8 Ga of Earth History. Geol. Soc. London, Spec. Publ, 357, pp. 167–193.
Elliot-Kingston, C., Haworth, M., McElwain, J.C., 2014. Damage structures in leaf epidermis and cuticle as an indicator of elevated atmospheric Sulphur dioxide in early Mesozoic floras. Rev. Palaeobot. Palynol. 208, 25–42.
Ernst, R.E., 2014. Large Igneous Provinces. Cambridge University Press, 653 p.
Ernst, R.E., Youbi, N., 2017. How Large Igneous Provinces affect global climate, sometimes cause mass extinctions, and represent natural markers in the geological record. Palaeogeogr. Palaeoclimatol. Palaeoecol. 478, 30–52. https://doi.org/10.1016/j.palaeo.2017.03.014.
Font, E., Youbi, N., Fernandes, S., El Hachimi, H., Kratinova, Z., Hamim, Y., 2011. Revisiting the magnetostratigraphy of the Central Atlantic Magmatic Province from Morocco. Earth Planet. Sci. Lett. 309, 302–317.
Foster, C.B., Logan, G.A., Summons, R.E., Gorter, J.D., Edwards, D.S., 1997. Carbon isotopes, kerogen types and the Permian–Triassic boundary in Australia: implications for exploration. APPEA J. 472–489.
Fowell, S.J., Olsen, P.E., 1993. Time calibration of Triassic/Jurassic microfloral turnover, eastern North America. Tectonophysics 222, 361–369.
Fujisaki, W., Matsui, Y., Asanuma, H., Sawaki, Y., Suzuki, K., Maruyama, S., 2018. Global perturbatioms of carbon cycle during the Triassic–Jurassic transition recorded in the mid-Panthalassa. Earth Planet. Sci. Lett. 500, 105–116.
Ganino, C., Arndt, N.T., 2009. Climate changes caused by degassing of sediments during the emplacement of large igneous provinces. Geology 37, 323–326.
Gerlach, T.M., Taylor, B.E., 1990. Carbon isotope constraints on degassing of carbon dioxide from Kilauea Volcano. Geochim. Cosmochim. Acta 54, 2051–2058.
Gonzaga, F.G., Gonçalves, F.T.T., Coutinho, L.F.C., 2000. Petroleum geology of the Amazonas Basin, Brazil: modeling of hydrocarbon generation and migration. In: Mello, M.R., Katz, B.J. (Eds.), Petroleum Systems of South Atlantic Margins, 73, pp. 159–178. AAPG Memoir.
Götz, A.E., Ruckwied, K., Pálfy, J., Haas, J., 2009. Palynological evidence of synchronous changes within the terrestrial and marine realm at the Triassic/Jurassic boundary (Csovár section, Hungary). Rev. Palaeobot. Palynol. 156, 401–409.
Grasby, S.E., Them II, T.R., Chen, Z., Yin, R., Ardakani, O.H., 2019. Mercury as a proxy for volcanic emissions in the geologic record. Earth Sci. Rev. 196, 102880.
Grattan, J., 2005. Pollution and paradigms: lessons from Icelandic volcanism for continental flood basalt studies. Lithos 79, 343–353.
Grattan, J.P., Pyatt, F.B., 1999. Volcanic eruptions dry fogs and the European palaeoenvironmental record: localised phenomena or hemispheric impacts? Global Planet. Change 21, 173–179.
Gravendyck, J., Schobben, M., Bachelier, J.B., Kürschner, W.M., 2020. Macroecological patterns of the terrestrial vegetation history during the end-Triassic biotic crisis in the central European Basin: A palynological study of the Bonenburg section (NW Germany) and its supra-regional implications. Global Planet. Change 103286.
Greene, S.E., Martindale, R.C., Ritterbush, K.A., Bottjer, D.J., Corsetti, F.A., Berelson, W. M., 2012. Recognising ocean acidification in deep time: an evaluation of the evidence for acidification across the Triassic-Jurassic boundary. Earth Sci. Rev. 113, 72–93.
Grossman, J.N., Gottfried, D., Froelich, A.J., 1991. Geochemical data for Jurassic diabase associated with Early Mesozoic basins in the eastern United States. In: U.S. Geological Survey, Open-file report 91-322-K.
Guex, J., Taylor, D., Rakus, M., Bucher, H., 1998. Two new genera and four new species of Lower Liassic ammonites (Cephalopoda). Bull. Soc. Vaud. Sc. Nat. 86, 73–85.
Guex, J., Bartolini, A., Atudorei, V., Taylor, D., 2004. High-resolution ammonite and carbon isotope stratigraphy across the Triassic-Jurassic boundary at New York Canyon (Nevada). Earth Planet. Sci. Lett. 225, 29–41.
Guex, J., Bartolini, A., Taylor, D., Atudorei, V., Thelin, P., Bruchez, S., Tanner, L., Lucas, S., 2008. Comment on: "The organic carbon isotopic and paleontological record across the Triassic-Jurassic boundary at the candidate GSSP section at Ferguson Hill, Muller Canyon, Nevada, USA" by Ward et al. (2007). Palaeogeogr. Palaeoclimatol. Palaeoecol. 273, 200–204.
Guex, J., Schoene, B., Bartolini, A., Spangenberg, J., Schaltegger, U., O'Dogherty, L., Taylor, D., Bucher, H., Atudorei, V., 2012. Geochronological constraints on post-extinction recovery of the ammonoids and carbon cycle perturbations during the Early Jurassic. Palaeogeogr. Palaeoclimatol. Palaeoecol. 346, 1–11.
Guex, J., Pilet, S., Müntener, O., Bartolini, A., Spangenberg, J., Schoene, B., Sell, B., Schaltegger, U., 2016. Thermal erosion of cratonic lithosphere as a potential trigger for mass-extinction. Sci. Rep. 6, 23168. https://doi.org/10.1038/srep23168.
Hallam, A., 1997. Estimates of the amount and rate of sea-level change across the Rhaetian–Hettangian and Pliensbachian–Toarcian boundaries latest Triassic to early Jurassic. J. Geol. Soc. London 154, 773–779.
Hallam, A., Wignall, P.B., 1999. Mass extinction and sea-level change. Earth Sci. Rev. 48, 217–258.
Hallam, A., Wignall, P.B., 2000. Facies change across the Triassic–Jurassic boundary in Nevada USA. J. Geol. Soc. London 157, 49–54.
Hansen, K.H., 2013. Vegetational Changes at the Triassic–Jurassic boundary – A Palynological Analysis of the Rødby-1 Well, Southern Denmark. (Master's Thesis). Department of Geosciences and Natural Resource Management, Faculty of Science, University of Copenhagen, pp. 1–72.
Harris, T.M., 1937. The fossil flora of Scoresby Sound East Greenland, Part 5. In: Stratigraphic relations of the plant beds, 112, pp. 1–112. Meddelelser om Grønland.
Hautmann, M., 2004. Effect of end-Triassic CO_2 maximum on carbonate sedimentation and marine mass extinction. Facies 50, 257–261.
Heimdal, T.H., Svensen, H.H., Ramezani, J., Iyer, K., Pereira, E., Rodrigues, R., Jones, M. T., Callegaro, S., 2018. Large-scale sill emplacement in Brazil as a trigger for the end-Triassic crisis. Sci. Rep. 8, 141.
Heimdal, T.H., Callegaro, S., Svensen, H.H., Jones, M.T., Pereira, E., Planke, S., 2019. Evidence for magma - evaporite interactions during the emplacement of the Central Atlantic Magmatic Province (CAMP) in Brazil. Earth Planet. Sci. Lett. 506, 476–492.
Heimdal, T.H., Jones, M.T., Svensen, H.H., 2020. Thermogenic carbon release from the Central Atlantic magmatic province caused major end-Triassic carbon cycle perturbations. PNAS 117, 11968–11974.
Herzberg, C., Gazel, E., 2009. Petrological evidence for secular cooling in mantle plumes. Nature 458, 619–622.
Hesselbo, S.P., Robinson, S.A., Surlyk, F., Piasecki, S., 2002. Terrestrial and marine extinction at the Triassic-Jurassic boundary synchronized with major carbon-cycle perturbation: a link to initiation of massive volcanism? Geology 30, 251–254.
Hesselbo, S.P., Robinson, S.A., Surlyk, F., 2004. Sea-level changes and facies development across potential Triassic–Jurassic boundary horizons, SW Britain. J. Geol. Soc. London 161, 365–379.
Heunisch, C., Luppold, F.W., Reinhardt, L., Röhling, H.-G., 2010. Palynofazies, bio- und lithostratigraphie im Grenzbereich Trias/Jura in der Bohrung Mariental 1 (Lappwaldmulde, Ostniedersachsen). Z. Dt. Ges. Geowiss. 161, 51–98.
Hillebrandt, A.v., 2000a. Die ammoniten-Fauna des südamerikanischen Hettangium (basaler Jura), Teil I. Palaeontographica A 257, 85–189.
Hillebrandt, A.v., 2000b. Die ammoniten-Fauna des südamerikanischen Hettangium (basaler Jura), Teil II. Palaeontographica A 258, 1–64.
Hillebrandt, A.v., 2000c. Die ammoniten-Fauna des südamerikanischen Hettangium (basaler Jura), Teil I. Palaeontographica A 258, 65–116.
Hillebrandt, A.V., Kment, K., 2015. Psiloceratid ammonites from the Lower Hettangian of the Karwendel Mountains (Northern Calcareous Alps, Austria) and their biostratigraphic significance. N. Jb. Geol. Paläont. (Abh.) 275–306, 277/3.
Hillebrandt, A.v., Krystyn, L., 2009. On the oldest Jurassic ammonites of Europe (Northern Calcareous Alps, Austria) and their global significance. N. Jahrb. Geol. Paläontol.-Abh. 253, 163–195.
Hillebrandt, A.v., Krystyn, L., Kurschner, W.M., Bonis, N.R., Ruhl, M., Richoz, S., Schobben, M.A.N., Urlichs, M., Bown, P.R., Kment, K., McRoberts, C.A., Simms, M., Tomasovych, A., 2013. The Global Stratotype Sections and Point (GSSP) for the base of the Jurassic System at Kuhjoch (Karwendel Mountains, Northern Calcareous Alps, Tyrol, Austria). Episodes 36, 162–198.
Hodych, J., Dunning, G.R., 1992. Did the Manicouagan impact trigger end-of-Triassic mass extinction? Geology 20, 51–54.
Hole, M.J., 2015. The generation of continental flood basalts by decompression melting of internally heated mantle. Geology 43, 311–314.
Holton, J.R., Haynes, P.H., McIntyre, M.E., Douglass, A.R., Rood, R.B., Pfister, L., 1995. Stratosphere-troposphere exchange. Rev. Geophys. 33, 403–439.
Hori, R.S., Fujiki, T., Inoue, E., Kimura, J.-I., 2007. Platinum group element anomalies and bioevents in the Triassic–Jurassic deep-sea sediments of Panthalassa. Palaeogeogr. Palaeoclimatol. Palaeoecol. 244, 391–406.
Iacono-Marziano, G., Ferraina, C., Gaillard, F., Carlo, I.D., Arndt, N.T., 2017. Assimilation of sulfate and carbonaceous rocks: Experimental study, thermodynamic modeling and application to the Noril'sk-Talnakh region Russia. Ore Geol. Rev. 90, 399–413. https://doi.org/10.1016/j.oregeorev.2017.04.027.
Jones, M.T., Jerram, D.A., Svensen, H.H., Grove, C., 2016. The effects of large igneous provinces on the global carbon and sulphur cycles. Palaeogeogr. Palaeoclimatol. Palaeoecol. 441, 4–21.
Kaminski, E., Chenet, A.-L., Jaupart, C., Courtillot, V., 2011. Rise of volcanic plumes to the stratosphere aided by penetrative convection above large lava flows. Earth Planet. Sci. Lett. 301, 171–178.
Kent, D.V., Olsen, P.E., Muttoni, G., 2017. Astrochronostratigraphic polarity time scale (APTS) for the Late Triassic and Early Jurassic from continental sediments and correlation with standard marine stages. Earth Sci. Rev. 166, 153–180.
Knight, K., Nomade, B., Renne, S., Marzoli, P.R., Bertrand, A., Youbi, N., 2004. The Central Atlantic Magmatic Province at the Triassic–Jurassic boundary: paleomagnetic and $^{40}Ar/^{39}Ar$ evidence from Morocco for brief, episodic volcanism. Earth Planet. Sci. Lett. 228, 143–160.
Kontak, D.J., 2008. On the edge of CAMP: Geology and volcanology of the Jurassic North Mountain Basalt, Nova Scotia. Lithos 101, 74–101.
Korte, C., Kozur, H.W., Bruckschen, P., Veizer, J., 2003. Strontium isotope evolution of Late Permian and Triassic seawater. Geochim. Cosmochim. Acta 67, 47–62.
Korte, C., Hesselbo, S.P., Jenkyns, H.C., Rickaby, R.E.M., Spotl, C., 2009. Palaeoenvironmental significance of carbon- and oxygen-isotope stratigraphy of marine Triassic-Jurassic boundary sections in SW Britain. J. Geol. Soc. London 166, 431–445.
Korte, C., Ruhl, M., Pálfy, J., Ullmann, C.V., Hesselbo, S.P., 2019. Chemostratigraphy across the Triassic–Jurassic boundary. In: Sial, A.N., Gaucher, C., Ramkumar, M., Ferreira, V.P. (Eds.), Chemostratigraphy across major chronological boundaries, 240, pp. 185–210. AGU Geophys. Monogr. Book Ser.

Kovács, Z., Demangel, I., Richoz, S., Hippler, D., Baldermann, A., Krystyn, L., 2020. New constraints on the evolution of $^{87}Sr/^{86}Sr$ of seawater during the upper Triassic. Global Planet. Change 192, 103255.
Kuroda, J., Hori, R.S., Suzuki, K., Grocke, D., Ohkouchi, N., 2010. Marine osmium isotope record across the Triassic-Jurassic boundary from a Pacific pelagic site. Geology 38, 1095–1098.
Kürschner, W.M., Herngreen, G.F.W., 2010. Triassic palynology of central and northwestern Europe: a review of palynofloral diversity patterns and biostratigraphic subdivisions. In: Lucas, S.G. (Ed.), Triassic Timescale, pp. 263–283. Geol. Soc. Spec. Publ.
Landwehrs, J.P., Feulner, G., Hofmann, M., Petri, S., 2020. Climatic fluctuations modeled for carbon and sulfur emissions from end-Triassic volcanism. Earth Planet. Sci. Lett. 537, 116174.
Leleu, S., Hartley, A.J., van Oosterhout, C., Kennan, L., Ruckwied, K., Gerdes, K., 2016. Structural, stratigraphic and sedimentological characterisation of a wide rift system: The Triassic rift system of the Central Atlantic Domain. Earth Sci. Rev. 158, 89–124.
Lindström, S., 2016. Palynofloral patterns of terrestrial ecosystem change during the end-Triassic event - a review. Geol. Mag. 153, 223–251.
Lindström, S., Erlström, M., 2006. The Late Rhaetian transgression in southern Sweden: regional (and global) recognition and relation to the Triassic-Jurassic boundary. Palaeogeogr. Palaeoclimatol. Palaeoecol. 241, 339–372.
Lindström, S., van de Schootbrugge, B., Dybkjaer, K., Pedersen, G.K., Fiebig, J., Nielsen, L.H., Richoz, S., 2012. No causal link between terrestrial ecosystem change and methane release during the end-Triassic mass extinction. Geology 40, 531–534.
Lindström, S., Pedersen, G.K., van de Schootbrugge, B., Hansen, K.H., Kuhlmann, N., Thein, J., Johansson, L., Petersen, H.I., Alwmark, C., Dybkjaer, K., Weibel, R., Erlstrom, M., Nielsen, L.H., Oschmann, W., Tegner, C., 2015. Intense and widespread seismicity during the end-Triassic mass extinction due to emplacement of a large igneous province. Geology 43, 387–390.
Lindström, S., Erlström, M., Piasecki, S., Nielsen, L.H., Mathiesen, A., 2017a. Palynology and terrestrial ecosystem change of the Middle Triassic to lowermost Jurassic succession of the eastern Danish Basin. Rev. Palaeobot. Palynol. 244, 65–95.
Lindström, S., van de Schootbrugge, B., Hansen, K.H., Pedersen, G.K., Alsen, P., Thibault, N., Dybkjær, K., Bjerrum, C.J., Nielsen, L.H., 2017b. A new correlation of Triassic-Jurassic boundary successions in NW Europe, Nevada and Peru, and the Central Atlantic Magmatic Province: A time-line for the end-Triassic mass extinction. Palaeogeogr. Palaeoclimatol. Palaeoecol. 478, 80–102.
Lindström, S., Sanei, H., van de Schootbrugge, B., Pedersen, G.K., Lesher, C.E., Tegner, C., Heunisch, C., Dybkjær, K., Outridge, P.M., 2019. Volcanic mercury and mutagenesis in land plants during the end-Triassic mass extinction. Sci. Adv. 5 eaaw4018.
Longridge, L.M., Carter, E.S., Smith, P.L., Tipper, H.W., 2007. Early Hettangian ammonites and radiolarians from the Queen Charlotte Islands, British Columbia and their bearing on the definition of the Triassic–Jurassic boundary. Palaeogeogr. Palaeoclimatol. Palaeoecol. 244, 142–169.
Lund, J.J., 1977. Rhaetic to Lower Liassic palynology of the onshore south-eastern North Sea Basin. Danm. Geol. Undersøg. II Række 109, 1–128.
Lund, J.J., 2003. Rhaetian to Pliensbachian palynostratigraphy of the central part of the NW German Basin exemplified by the Eitzendorf 8 well. Cour. Forschungsinst. Senck. 241, 69–83.
Mander, L., Twitchett, R.J., Benton, M.J., 2008. Palaeoecology of the Late Triassic extinction event in the SW UK. J. Geol. Soc. London 165, 319–332.
Mander, L., Kurschner, W.M., McElwain, J.C., 2013. Palynostratigraphy and vegetation history of the Triassic-Jurassic transition in East Greenland. J. Geol. Soc. London 170, 37–46.
Mangerud, G., Paterson, N.W., Riding, J.B., 2019. The temporal and spatial distribution of Triassic dinoflagellate cysts. Rev. Palaeobot. Palynol. 261, 53–66.
Manspeizer, W., 1994. The break-up of Pangea and its impact on climate: Consequences of Varsican-Alleghanide orogenic collapse. In: Klein, G.D. (Ed.), Pangea: Paleoclimate, Tectonics and Sedimentation during accretion, zenith and breakup of a supercontinent, 288, pp. 169–185. Geol. Soc. Am. Spec. Pap.
Marks, L., Keiding, J., Wenzel, T., Trumbull, R.B., Veksler, I., Wiedenbeck, M., Markl, G., 2014. F, Cl, and S concentrations in olivine-hosted melt inclusions from mafic dikes in NW Namibia and implications for the environmental impact of the Parana-Etendeka Large Igneous Province. Earth Planet. Sci. Lett. 392, 39–49.
Martins, L.T., Madeira, J., Youbi, N., Munhá, J., Mata, J., Kerrich, R., 2008. Rift-related magmatism of the Central Atlantic magmatic province in Algarve, Southern Portugal. Lithos 101, 102–124.
Maruoka, T., Koeberl, C., Hancox, P.J., Reimold, W.U., 2003. Sulfur geochemistry across a terrestrial Permian-Triassic boundary section in the Karoo Basin. South Africa. Earth Planet. Sci. Lett. 206, 101–117.
Marynowski, L., Simoneit, B.R.T., 2009. Widespread Upper Triassic to Lower Jurassic wildfire records from Poland: evidence from charcoal and pyrolytic polycyclic aromatic hydrocarbons. Palaios 24, 785–798.
Marzoli, A., Renne, P.R., Piccirillo, E.M., Ernesto, M., Bellieni, G., De Min, A., 1999. Extensive 200-million-year-old continental flood basalts of the Central Atlantic Magmatic Province. Science 284, 616–618.
Marzoli, A., Bertrand, H., Knight, K.B., Cirilli, S., Buratti, N., Verati, C., Nomade, S., Renne, P.R., Youbi, N., Martini, R., Allenbach, K., Neuwerth, R., Rapaille, C., Zaninetti, L., Bellieni, G., 2004. Synchrony of the Central Atlantic magmatic province and the Triassic-Jurassic boundary climatic and biotic crisis. Geology 32, 973–976.
Marzoli, A., Bertrand, H., Knight, K., Cirilli, S., Nomade, S., Renne, P., Vérati, C., Youbi, N., Martini, R., Bellieni, G., 2008. Comments on Synchrony between the Central Atlantic magmatic province and the Triassic–Jurassic mass-extinction event? by Whiteside et al. 2007. Palaeogeogr. Palaeoclimatol. Palaeoecol. 262, 189–193.
Marzoli, A., Jourdan, F., Puffer, J.H., Cuppone, T., Tanner, L.H., Weems, R.E., Bertrand, H., Cirilli, S., Bellieni, G., De Min, A., 2011. Timing and duration of the Central Atlantic magmatic province in the Newark and Culpeper basins, eastern U.S. A. Lithos 122, 175–188.
Marzoli, A., Callegaro, S., Dal Corso, J., Davies, J.H.F.L., Chiaradia, M., Youbi, N., Bertrand, H., Reisberg, L., Merle, R., Jourdan, F., 2018. The Central Atlantic Magmatic Province (CAMP): A review, The Late Triassic World. Springer, Cham.
Marzoli, A., Bertrand, H., Youbi, N., Callegaro, S., Merle, R., Reisberg, L., Chiaradia, M., Brownlee, S., Jourdan, F., Zanetti, A., Davies, J.H.F.L., Cuppone, T., Mahmoudi, A., Medina, F., Renne, P.R., Bellieni, G., Crivellari, S., El Hachimi, H., Bensalah, M.K., Meyzen, C.M., Tegner, C., 2019. The Central Atlantic Magmatic Province (CAMP) in Morocco. J. Petrol. 60, 945–996. https://doi.org/10.1093/petrology/egz021.
McElwain, J.C., Beerling, D.J., Woodward, F.I., 1999. Fossil plants and global warming at the Triassic-Jurassic boundary. Science 285, 1386–1390.
McElwain, J.C., Popa, M.E., Hesselbo, S.P., Haworth, M., Surlyk, F., 2007. Macroecological responses of terrestrial vegetation to climatic and atmospheric change across the Triassic/Jurassic boundary in East Greenland. Paleobiology 33, 547–573.
McHone, J.G., 2000. Non-plume magmatism and rifting during the opening of the central Atlantic Ocean. Tectonophysics 316, 287–296.
McHone, J.G., 2003. Volatile emissions from Ventral Atlantic Magmatic Province basalts: mass assumptions and environmental consequences. In: Hames, W.E., McHone, J.G., Renne, P.R., Ruppel, C. (Eds.), The Central Atlantic magmatic province: insights from fragments of Pangaea. Am. Geophys. Union, Geophysical Monographs 136, 241–254.
Medina, F., 1995. Syn- and postrift evolution of the El Jadida-Agadir basin (Morocco): constraints for the rifting model of the Central Atlantic. Can. J. Earth Sci. 32, 1273–1291.
Merle, R., Marzoli, A., Bertrand, H., Reisberg, L., Verati, C., Zimmermann, C., Chiaradia, M., Bellieni, G., Ernesto, M., 2011. Ar^{40}/Ar^{39} ages and Sr-Nd-Pb-Os geochemistry of CAMP tholeiites from Western Maranhao basin (NE Brazil). Lithos 122, 137–151.
Merle, R., Marzoli, A., Reisberg, L., Bertrand, H., Nemchin, A., Chiaradia, M., Callegaro, S., Jourdan, F., Bellieni, G., Kontak, D., Puffer, J., McHone, J.G., 2014. Sr, Nd, Pb and Os Isotope systematics of CAMP tholeiites from Eastern North America (ENA): Evidence of a subduction-enriched mantle source. J. Petrol 55, 133–180.
Nabbefeld, B., Grice, K., Twitchett, R., Summons, R.E., Hays, L., Böttcher, M.E., Asif, M., 2010. An integrated biomarker, isotopic and palaeoenvironmental study through the Late Permian event at Lusitaniadalen. Spitsbergen. Earth Planet. Sci. Lett. 291, 84–96.
Newton, R., Bottrell, S., 2007. Stable isotopes of carbon and sulphur as indicators of environmental change: past and present. J. Geol. Soc. London 164, 691–708.
Nicoll, R., Foster, C.B., 1994. Late Triassic conodont and palynomorph biostratigraphy and conodont thermal maturation, North West Shelf. Australia. AGSO J. Austral. geol. geophys. 15, 101–118.
Nomade, S., Knight, K.B., Beutel, E., Renne, P.R., Vérati, C., Féraud, G., Marzoli, A., Youbi, N., Bertrand, H., 2007. Chronology of the Central Atlantic Magmatic Province: implications for the Central Atlantic rifting processes and the Triassic–Jurassic biotic crisis. Palaeogeogr. Palaeoclimatol. Palaeoecol. 244, 326–344.
O'Leary, M.H., 1988. Carbon isotopes in photosynthesis. Bioscience 38, 328–336.
Olsen, P.E., Kent, D.V., Sues, H.-D., Koeberl, C., Huber, H., Montanari, A., Rainforth, E.C., Fowell, S.J., Szajna, M.J., Hartline, B.W., 2002. Ascent of dinosaurs linked to an iridium anomaly at the Triassic-Jurassic Boundary. Science 296, 1305–1307.
Olsen, P.E., Kent, D.V., Et-Touhami, M., Puffer, J.H., 2003. Cyclo-, magneto-, and bio-stratigraphic constraints on the dura-tion of the CAMP event and its relationship to the Triassic–Jurassic boundary. In: Hames, W.E., McHone, J.G., Renne, P.R., Ruppel, C. (Eds.), The Central Atlantic Magmatic Province: Insights From Fragments of Pangea. Geophysical Monograph Series 136. : American Geophysical Union, Washington, DC, pp. 7–32.
Oppenheimer, C., Scaillet, B., Martin, R.S., 2011. Sulfur degassing from volcanoes: Source conditions, surveillance, plume chemistry and Earth system impacts. Rev. Mineral. Geochem. 73, 363–421. https://doi.org/10.2138/rmg.2011.73.13.
Outridge, P.M., Mason, R.P., Wang, F., Guerrero, S., Heimbürger-Boavida, L.E., 2018. Updated global and oceanic mercury budgets for the United Nations global mercury assessment 2018. Environ. Sci. Technol. 52, 11466–11477.
Page, K.N., Clémence, M.E., Bloos, G., 2010. The Tilmanni Chronozone in NW Europe: Re-correlating the base of the Jurassic System. Earth Sci. Front. 17, 8–9 special issue.
Pálfy, J., Zajzon, N., 2012. Environmental changes across the Triassic–Jurassic boundary and coeval volcanism inferred from elemental geochemistry and mineralogy in the Kendlbachgraben section (Northern Calcareous Alps, Austria). Earth Planet. Sci. Lett. 335–336, 121–134.
Pálfy, J., Mortensen, J.K., Carter, E.S., Smith, P.L., Friedman, R.M., Tipper, H.W., 2000. Timing the end-Triassic mass extinction: First on land, then in the sea? Geology 28, 39–42.
Pálfy, J., Demény, A., Haas, J., Hetényi, M., Orchard, M., Veto, I., 2001. Carbon isotope anomaly and other geochemical changes at the Triassic-Jurassic boundary from a marine section in Hungary. Geology 29, 1047–1050.
Pálfy, J., Demény, A., Haas, J., Carter, E.S., Görög, Á., Halász, D., Oravecz-Scheffer, A., Hetényi, M., Márton, E., Orchard, M.J., Ozsvárt, P., Vető, I., Zajzon, N., 2007. Triassic–Jurassic boundary events inferred from integrated stratigraphy of the Csővár section, Hungary. Palaeogeogr. Palaeoclimatol. Palaeoecol. 244, 11–33.
Panfili, G., Cirilli, S., Dal Corso, J., Bertrand, H., Medina, F., Youbi, N., Marzoli, A., 2019. New biostratigraphic constraints show rapid emplacement of the Central Atlantic Magmatic Province (CAMP) during the end-Triassic mass extinction interval. Global Planet. Change 172, 60–68.

Paris, G., Donnadieu, Y., Beaumont, V., Fluteau, F., Goddéris, Y., 2012. Modelling the consequences on late Triassic environment of intense pulse-like degassing during the Central Atlantic magmatic province using the GEOCLIM model. Climate Past Discuss. 8, 2075–2110.
Paris, G., Donnadieu, Y., Beaumont, V., Fluteau, F., Goddéris, Y., 2016. Geochemical consequences of intense pulse-like degassing during the onset of the central Atlantic Magmatic Province. Palaeogeogr. Palaeoclimatol. Palaeoecol. 441, 74–82.
Peace, A.L., Phethean, J.J.J., Franke, D., Foulger, G.R., Schiffer, C., Welford, J.K., McHone, G., Rocchi, S., Schnabel, M., Doré, A.G., 2020. A review of Pangaea dispersal and Large Igneous Provinces – In search of a causative mechanism. Earth Sci. Rev. 206, 102902. https://doi.org/10.1016/j.earscirev.2019.102902.
Percival, L.M.E., Ruhl, M., Hesselbo, S.P., Jenkyns, H.C., Mather, T.A., Whiteside, J.H., 2017. Mercury evidence for pulsed volcanism during the end-Triassic mass extinction. Proc. Natl. Acad. Sci. 114, 7929–7934.
Petersen, H.I., Lindström, S., 2012. Synchronous wildfire activity rise and mire deforestation at the Triassic-Jurassic boundary. PLoS One 7, e47236.
Pienkowski, G., Niedzwiedzki, G., Waksmunska, M., 2011. Sedimentological, palynological and geochemical studies of the terrestrial Triassic–Jurassic boundary in northwestern Poland. Geol. Mag. 149, 308–332.
Pienkowski, G., Niedzwiedzki, G., Branski, P., 2014. Climatic reversals related to the Central Atlantic magmatic province caused the end-Triassic biotic crisis – Evidence from continental strata in Poland. Geol. Soc. Amer. Spec. Pap. 505, 264–287.
Poulsen, N.E., Riding, J.B., 2003. The Jurassic dinoflagellate cyst zonation of Subboreal Northwest Europe. Geol. Surv. Denmark Greenland Bull. 1, 115–144.
Preto, N., Kustatscher, E., Wignall, P.B., 2010. Triassic climates - State of the art and perspectives. Palaeogeogr. Palaeoclimatol. Palaeoecol. 290, 1–10.
Racki, G., Rakocinski, M., Marynowski, L., Wignall, P.B., 2018. Mercury enrichments and the Frasnian-Famennian biotic crisis: A volcanic trigger proved? Geology 46, 543–546.
Radley, Jonathan D., 2008. Discussion on palaeoecology of the Late Triassic extinction event in the SW UK Journal. Journal of the Geological Society 165(5), 319–333. https://doi.org/10.1144/0016-76492008-014.
Rampino, M.R., Self, S., Stothers, R.B., 1988. Volcanic winters. Annu. Rev. Earth Planet. Sci. 16, 73–99.
Rigo, M., Mazza, M., Karádi, V., Nicora, A., 2018. New Upper Triassic Conodont Biozonation of the Tethyan Realm. In: Tanner, L. (Ed.), The Late Triassic World. Topics in Geobiology, 46. Springer, Cham.
Robock, A., 2000. Volcanic eruptions and climate. Rev. Geophys. 38, 191–219. https://doi.org/10.1029/1998RG000054.
Robock, A., 2002. Pinatubo eruption - The climatic aftermath. Science 295, 1242–1244.
Ross, P.-S., Ukstins Peate, T.I., McClintock, M.K., Xu, Y.G., Skilling, I.P., White, J.D.L., Houghton, B.F., 2005. Mafic volcaniclastic deposits in flood basalt provinces: A review. J.Volcanol. Geotherm. Res. 145, 281–314.
Ruhl, M., Kürschner, W.M., 2011. Multiple phases of carbon cycle disturbance from large igneous province formation at the Triassic-Jurassic transition. Geology 39, 431–434.
Ruhl, M., Veld, H., Kürschner, W.M., 2010. Sedimentary organic matter characterization of the Triassic–Jurassic boundary GSSP at Kuhjoch (Austria). Earth Planet. Sci. Lett. 292, 17–26.
Ruhl, M., Bonis, N.R., Reichart, G.-J., Sinninghe Damsté, J.S., Kürschner, W.M., 2011. Atmospheric carbon injection linked to end-Triassic mass extinction. Science 333, 430–434.
Ruiz-Martinez, V.C., Torsvik, T.H., van Hinsbergen, D.J.J., Gaina, C., 2012. Earth at 200 Ma: Global palaeogeography refined from CAMP palaeomagnetic data. Earth Planet. Sci. Lett. 331, 67–79.
Sanei, H., Grasby, S.E., Beauchamp, B., 2012. Latest Permian mercury anomalies. Geology 40, 63–66.
Surlyk, F., 2003. The Jurassic of East Greenland: a sedimentary record of thermal subsidence, onset and culmination of rifting. GEUS Bulletin 1, 657–722. https://doi.org/10.34194/geusb.v1.4674.
Saunders, A.D., England, R.W., Reichow, M.K., White, R.V., 2005. A mantle plume origin for the Siberian Traps: uplift and extension in the West Siberian Basin, Russia. Lithos 79, 407–424.
Schaller, M.F., Wright, J., Kent, D., 2011. Atmospheric PCO_2 Perturbations Associated with the Central Atlantic Magmatic Province. Science 331, 1404–1409.
Schaller, M.F., Wright, J.D., Kent, D.V., Olsen, P.E., 2012. Rapid emplacement of the Central Atlantic magmatic province as a net sink for CO_2. Earth Planet. Sci. Lett. 323–324, 27–39. https://doi.org/10.1016/jepsl.2011.12.028.
Schaller, M.F., Wright, J.D., Kent, D.V., 2016. A 30 Myr record of Late Triassic atmospheric pCO_2 variations reflects a fundamental control of the carbon cycle by changes in continental weathering. GSA Bull. 127, 661–671.
Schaltegger, U., Guex, J., Bartolini, A., Schoene, B., Ovtcharova, M., 2008. Precise U-Pb age constraints for end-Triassic mass extinction, its correlation to volcanism and Hettangian post-extinction recovery. Earth Planet. Sci. Lett. 267, 266–275.
Schmidt, A., Skeffington, R.A., Thordarson, T., Self, S., Forster, P.M., Rap, A., Ridgwell, A., Fowler, D., Wilson, M., Mann, G.W., Wignall, P.B., Carslaw, K.S., 2016. Selective environmental stress from sulphur emitted by continental flood basalt eruptions. Nat. Geosci. 9, 77–82.
Schneebeli-Hermann, E., Looser, N., Hochuli, P.A., Furrer, H., Reisdorf, A.G., Wetzel, A., Bernasconi, S.M., 2017. Palynology of Triassic–Jurassic boundary sections in northern Switzerland. Swiss J. Geosci. 111, 99–115.
Schobben, M., Gravendyck, J., Mangels, F., Struck, U., Bussert, R., Kürschner, W.M., Korn, D., Sander, P.M., Aberhan, M., 2019. A comparative study of total organic carbon-$\delta^{13}C$ signatures in the Triassic–Jurassic transitional beds of the Central European Basin and western Tethys shelf seas. Newslett. Stratigr. 52, 461–486.
Schoene, B., Guex, J., Bartolini, A., Schaltegger, U., Blackburn, T.J., 2010. Correlating the end-Triassic mass extinction and flood basalt volcanism at the 100 ka level. Geology 38, 387–390.
Schoepfer, S.D., Algeo, T.J., Ward, P.D., Williford,K.H., Haggart, J.W., 2016. Testing the limits in a greenhouse ocean: Did low nitrogen availability limit marine productivity during the end-Triassic mass extinction? Earth Planet. Sci. Lett. 451, 138–148.
van de Schootbrugge, B., Tremolada, F., Rosenthal, Y., Bailey, T.R., Feist-Burkhardt, S., Brinkhuis, H., Pross, J., Kent, D.V., Falkowski, P.G., 2007. End-Triassic calcification crisis and blooms of organic-walled disaster species. Palaeogeogr. Palaeoclimatol. Palaeoecol. 244, 126–141.
van de Schootbrugge, B., Payne, J.L., Tomasovych, A., Pross, J., Fiebig, J., Benbrahim, M., Föllmi, K.B., Quan, T.M., 2008. Carbon cycle perturbation and stabilization in the wake of the Triassic-Jurassic boundary mass-extinction event. Geochem. Geophys. Geosyst. 9, Q04028.
van de Schootbrugge, B., Quan, T.M., Lindstrom, S., Puttmann, W., Heunisch, C., Pross, J., Fiebig, J., Petschick, R., Rohling, H.G., Richoz, S., Rosenthal, Y., Falkowski, P.G., 2009. Floral changes across the Triassic/Jurassic boundary linked to flood basalt volcanism. Nat. Geosci. 2, 589–594.
van de Schootbrugge, B., Bachan, A., Suan, G., Richoz, S., Payne, J.L., 2013. Microbes, mud and methane: Cause and consequence of recurrent early Jurassic anoxia following the end-Triassic mass extinction. Palaeontology 56, 685–709.
van de Schootbrugge, B., Weijst, C.M.H., Hollaar, T., Vecoli, M., Strother, P.K., Kuhlmann, N., Thein, J., Visscher, H., van Konijnenburg-van Cittert, H., Schobben, M., Sluijs, A., Lindström, S., 2020. Catastrophic soil loss associated with end-Triassic deforestation. Earth Sci. Rev. 210, 103332.
Self, S., Widdowson, M., Thordarson, T., Jay, A.E., 2006. Volatile fluxes during flood basalt eruptions and potential effects on the global environment: A Deccan perspective. Earth Planet. Sci. Lett. 248, 518–532.
Self, S., Blake, S., Sharma, K., Widdowson, M., Sephton, S., 2008. Sulfur and chlorine in Late Cretaceous Deccan magmas and eruptive gas release. Science 319, 1654–1657.
Self, S., Schmidt, A., Mather, T.A., 2014. Emplacement characteristics, time scales, and volcanic gas release rates of continental flood basalt eruptions on Earth. Geol. Soc. Amer. Spec. Pap. 505, 319–337.
Sibik, S., Edmonds, M., Mclennan, J., Svensen, H., 2015. Magmas erupted during the main pulse of Siberian Traps volcanism were volatile-poor. J. Petrol. 56, 2089–2116.
Simms, M.J., 2003. Uniquely extensive seismite from the latest Triassic of the United Kingdom: Evidence for bolide impact? Geology 31, 557–560.
Simms, M.J., 2007. Uniquely extensive soft-sediment deformation in the Rhaetian of the UK : evidence for earthquake or impact ? Palaeogeogr. Palaeoclimatol. Palaeoecol. 244, 407–423.
Song, Y., Algeo, T.J., Wu, W., Luo, G., Li, L., Wang, Y., Xie, S., 2020. Distribution of pyrolytic PAHs across the Triassic-Jurassic boundary in the Sichuan Basin, southwestern China: Evidence of wildfire outside the Central Atlantic Magmatic Province. Earth Sci. Rev. 201, 102970. https://doi.org/10.1016/j.earscirev.2019.102970.
Steinthorsdottir, M., Jeram, A.J., McElwain, J.C., 2011. Extremely elevated CO2 concentrations at the Triassic/Jurassic boundary. Palaeogeogr. Palaeoclimatol. Palaeoecol. 308, 418–432.
Steinthorsdottir, M., Elliott-Kingston, C., Bacon, K.L., 2018. Cuticle surfaces of fossil plants as a potential proxy for volcanic SO_2 emissions: observations from the Triassic-Jurassic transition of East Greenland. Palaeobiodiversity Palaeoenvironments 98, 49–69.
Svensen, H., Planke, S., Malthe-Sorenssen, A., Jamtveit, B., Myklebust, R., Eidem, T.R., Rey, S.S., 2004. Release of methane from a volcanic basin as a mechanism for initial Eocene global warming. Nature 429, 542–545.
Svensen, H., Planke, S., Chevallier, L., Malthe-Sorenssen, A., Corfu, F., Jamtveit, B., 2007. Hydrothermal venting of greenhouse gases triggering Early Jurassic global warming. Earth Planet. Sci. Lett. 256, 554–566.
Svensen, H., Planke, S., Polozov, A.G., Schmidbauer, N., Corfu, F., Podladchikov, Y.Y., Jamtveit, B., 2009. Siberian gas venting and the end-Permian environmental crisis. Earth Planet. Sci. Lett. 277, 490–500.
Svensen, H.H., Planke, S., Neumann, E.-R., Aarnes, I., Marsh, J.S., Polteau, S., Harstad, C. H., Chevallier, L., 2015. Sub-volcanic intrusions and the link to global climatic and environmental changes. In: Breitkreuz, C., Rocchi, S. (Eds.), Physical Geology of Shallow Magmatic Systems. Advances in Volcanology (An Official Book Series of the International Association of Volcanology and Chemistry of the Earth's Interior). Springer, Cham.
Svensen, H.H., Torsvik, T., Callegaro, S., Augland, L., Hatlen Heimdal, T., Jerram, D., Planke, S., Pereira, E., 2017. Gondwana Large Igneous Provinces: Plate reconstructions, volcanic basins and sill volumes. Geol. Soc., London, Spec. Publ. 463. SP463.7. 10.1144/SP463.7.
Swift, A., 1989. First records of conodonts from the Late Triassic of Britain. Palaeontology 32, 325–333.
Swift, A., 1999. Stratigraphy (including biostratigraphy). In: Swift, A., Martill, D.M. (Eds.), Fossils of the Rhaetian Penarth Group. The Palaeontological Association, pp. 15–30.
Tanner, L.H., Kyte, F.T., 2005. Anomalous iridium enrichment in sediments at the Triassic–Jurassic boundary, Blomidon Formation, Fundy basin. Can. Earth Planet. Sci. Lett. 240, 634–641.
Tanner, L.H., Lucas, S.G., Chapman, M.G., 2004. Assessing the record and causes of Late Triassic extinctions. Earth-Science Reviews 65, 103–139.
Tanner, L.H., Kyte, F.T., Walker, A.E., 2008. Multiple Ir anomalies in uppermost Triassic to Jurassic-age strata of the Blomidon Formation, Fundy basin, eastern Canada. Earth Planet. Sci. Lett. 274, 103–111.
Tanner, L.H., Kyte, F.T., Richoz, S., Krystyn, L., 2016. Distribution of iridium and associated geochemistry across the Triassic–Jurassic boundary in sections at Kuhjoch

and Kendlbach, Northern Calcareous Alps, Austria. Palaeogeogr. Palaeoclimatol. Palaeoecol. 449, 13–26.
Tegner, C., Michelis, S.A.T., McDonald, I., Brown, E.L., Youbi, N., Callegaro, S., Lindström, S., Marzoli, A., 2020a. Mantle Dynamics of the Central Atlantic Magmatic Province (CAMP): Constraints from Platinum Group, Gold and Lithophile Elements in Flood Basalts of Morocco. J. Petrol. 60, 1621–1652. https://doi.org/10.1093/petrology/egz041.
Tegner, C., Marzoli, A., McDonald, I., Youbi, N., Lindström, S., 2020b. Platinum-group elements link the end-Triassic mass extinction and the Central Atlantic Magmatic Province. Sci. Rep. 10 (1), 3482. https://doi.org/10.1038/s41598-020-60483-8.
Thibodeau, A.M., Ritterbush, K., Yager, J.A., West, A.J., Ibarra, Y., Bottjer, D.J., Berelson, W.M., Bergquist, B.A., Corsetti, F.A., 2016. Mercury anomalies and the timing of biotic recovery following the end-Triassic mass extinction. Nat. Commun. 7, 11147.
Thordarson, T., Self, S., 1996. Sulfur, chlorine and flourine degassing and atmospheric loading by the Roza eruption, Columbia River Basalr group, Washington. USA. J. Volcanol. Geotherm. Res. 74, 49–73.
Thordarson, T., Self, S., 2003. Atmospheric and environmental effects of the 1783-1784 Laki eruption: A review and reassessment. J. Geophys. Res.-Atmospheres 108 (D1).
Van Veen, P.M., 1995. Time calibration of Triassic/Jurassic microfloral turnover, eastern North America–comment. Tectonophysics 245, 93–95.
Verati, C., Bertrand, H., Féraud, G., 2005. The farthest record of the Central Atlantic Magmatic Province into West Africa craton: precise $^{40}Ar/^{39}Ar$ dating and geochemistry of Taoudenni basin intrusives (northern Mali). Earth Planet. Sci. Lett. 235, 391–407.
Vérati, C., Rapaille, C., Féraud, G., Marzoli, A., Bertrand, H., Youbi, N., 2007. 40Ar/39Ar ages and duration of the Central Atlantic Magmatic Province volcanism in Morocco and Portugal and its relation to the Triassic-Jurassic boundary. Palaeogeogr. Palaeoclimatol. Palaeoecol. 244, 308–325.
Visscher, H., Looy, C.V., Collinson, M.E., Brinkhuis, H., Cittert, J., Kurschner, W.M., Sephton, M.A., 2004. Environmental mutagenesis during the end-Permian ecological crisis. Proc. Natl. Acad. Sci. 101, 12952–12956.
Von Glasow, R., Bobrowski, N., Kern, C., 2009. The effects of volcanic eruptions on atmospheric chemistry. Chem. Geol. 263, 131–142.
Wanderley Filho, J.R., Travassos, W.A.S., Alves, D.B., 2006. O diabásio nas bacias paleozóicas amazônicasherói ou vilão. The diabase in the Amazonian Paleozoic basins: hero or villain? Boletim de Geociências da Petrobrás 14, 177–184.
Ward, P.D., Haggart, J.W., Carter, E.S., Wilbur, D., Tipper, H.W., Evans, T., 2001. Sudden productivity collapse associated with the Triassic–Jurassic boundary mass extinction. Science 292, 1148–1151.
Ward, P.D., Garrison, G.H., Haggart, J.W., Kring, D.A., Beattie, M.J., 2004. Isotopic evidence bearing on Late Triassic extinction events, Queen Charlotte Islands, British Columbia, and implications for the duration and cause of the Triassic/Jurassic mass extinction. Earth Planet. Sci. Lett. 224, 589–600.
Ward, P.D., Garrison, G.H., Williford, K.H., Kring, D., Goodwin, D., Beattie, M., McRoberts, C., 2007. The organic carbon isotopic and paleontological record across the Triassic–Jurassic boundary at the candidate GSSP section at Ferguson Hill, Muller Canyon, Nevada, USA. Palaeogeogr. Palaeoclimatol. Palaeoecol. 244, 279–287.
Weedon, G., Jenkyns, H., Page, K., 2018. Combined sea-level and climate controls on limestone formation, hiatuses and ammonite preservation in the Blue Lias Formation, South Britain (uppermost Triassic – Lower Jurassic). Geological Magazine 155(5), 1117–1149. https://doi.org/10.1017/S001675681600128X.
Weems, R.E., Tanner, L.H., Lucas, S.G., 2016. Synthesis and revision of the lithostratigraphic groups and formations in the Upper Permian?–Lower Jurassic Newark Supergroup of eastern North America. Stratigraphy 13, 111–153.
White, J.D.L., Bryan, S.E., Rossi, P.-S., Self, S., Thordarson, T., 2009. Physical volcanology of continental large igneous provinces: update and review. In: Thordarson, T., Self, S., Larsen, G., Rowland, S.K., Hoskuldsson, A. (Eds.), Studies in Volcanology: The Legacy of George Walker. Special Publications of IAVCEI, 2. Geological Society, London, pp. 291–321.
Whiteside, J.H., Olsen, P.E., Kent, D.V., Fowell, S.J., Et-Touhami, M., 2007. Synchrony between the Central Atlantic magmatic province and the Triassic–Jurassic mass-extinction event? Palaeogeogr. Palaeoclimatol. Palaeoecol. 244, 345–367.
Whiteside, J.H., Olsen, P.E., Kent, D.V., Fowell, S.J., Et-Touhami, M., 2008. Synchrony between the Central Atlantic magmatic province and the Triassic–Jurassic mass-extinction event? Reply to comment of Marzoli et al., 2008. Palaeogeogr. Palaeoclimatol. Palaeoecol. 262, 194–198.
Whiteside, J.H., Olsen, P.E., Eglinton, T., Brookfield, M.E., Sambrotto, R.N., 2010. Compound-specific carbon isotopes from Earth's largest flood basalt eruptions directly linked to the end-Triassic mass extinction. Proc. Natl. Acad. Sci. 107, 6721–6725.
Wignall, P.B., 2001. Large igneous provinces and mass extinctions. Earth Sci. Rev. 53, 1–33.
Wignall, P.B., Bond, D.P.G., 2008. The end-Triassic and Early Jurassic mass extinction records in the British Isles. Proc. Geol. Assoc. 119, 73–84.
Williford, K.H., Ward, P.D., Garrison, G.H., Buick, R., 2007. An extended organic carbon-isotope record across the Triassic–Jurassic boundary in the Queen Charlotte Islands, British Columbia, Canada. Palaeogeogr. Palaeoclimatol. Palaeoecol. 244, 290–296.
Williford, K.H., Grice, K., Holman, A., McElwain, J.C., 2014. An organic record of terrestrial ecosystem collapse and recovery at the Triassic–Jurassic boundary in East Greenland. Geochim. Cosmochim. Acta 127, 251–263.
Woodward, F.I., 1987. Stomatal numbers are sensitive to increases in CO_2 from preindustrial levels. Nature 327, 617–618.
Woollam, R., Riding, J.B., 1983. Dinoflagellate cyst zonation of the English Jurassic. Institute of Geological Sciences Report, 1–44, 83/2, 42 p.
Wotzlaw, J.F., Guex, J., Bartolini, A., Gallet, Y., Krystyn, L., McRoberts, C.A., Taylor, D., Schoene, B., Schaltegger, U., 2014. Towards accurate numerical calibration of the Late Triassic: High-precision U-Pb geochronology constraints on the duration of the Rhaetian. Geology 42, 571–574.
Yager, J.A., West, A.J., Corsetti, F.A., Berelson, W.M., Rollins, N.E., Rosas, S., Bottjer, D. J., 2017. Duration of and decoupling between carbon isotope excursions during the end-Triassic mass extinction and Central Atlantic Magmatic Province emplacement. Earth Planet. Sci. Lett. 473, 227–236.
Yapp, C.J., Poths, H., 1996. Carbon isotopes in continental weathering environments and variations in ancient atmospheric CO_2 pressure. Earth Planet. Sci. Lett. 137, 71–82.
Youbi, N., Martins, L., Munhá, J.M., Ibouh, H., Madeira, J., Aït Chayeb, E.H., El Boukhari, A., 2003. The Late Triassic-Early Jurassic Volcanism of Morocco and Portugal in the framework of the Central Atlantic Magmatic Province. In: Hame, W. E., McHone, J.M., Renne, P.R., Ruppel, C. (Eds.), The Central Atlantic Magmatic Province: Insights From Fragments of Pangea, 136, pp. 179–207. AGU Geophysical Monographs Series.
Zhang, Y., Ren, Z.-Y., Xu, Y.-G., 2013. Sulfur in olivine-hosted melt inclusions from the Emeishan picrites: Implications for S degassing and its impact on environment. J. Geophys. Research Solid Earth 118, 4063–4070.